

MATERIALS CHARACTERIZATION AND ANALYSIS COLLECTION

C. Richard Brundle, *Editor*



Spectroscopic Ellipsometry *Practical Application to Thin Film Characterization*

**Harland G. Tompkins
James N. Hilfiker**



**MOMENTUM PRESS
ENGINEERING**

SPECTROSCOPIC ELLIPSOMETRY

SPECTROSCOPIC ELLIPSOMETRY

**PRACTICAL APPLICATION
TO THIN FILM CHARACTERIZATION**

**HARLAND G. TOMPKINS
AND JAMES N. HILFIKER**



**MOMENTUM PRESS
ENGINEERING**

MOMENTUM PRESS, LLC, NEW YORK

Spectroscopic Ellipsometry: Practical Application to Thin Film Characterization

Copyright © Momentum Press®, LLC, 2016.

All rights reserved. No part of this publication may be reproduced, stored in a retrieval system, or transmitted in any form or by any means—electronic, mechanical, photocopy, recording, or any other—except for brief quotations, not to exceed 400 words, without the prior permission of the publisher.

First published by Momentum Press®, LLC
222 East 46th Street, New York, NY 10017
www.momentumpress.net

ISBN-13: 978-1-60650-727-8 (print)
ISBN-13: 978-1-60650-728-5 (e-book)

Momentum Press Materials Characterization and Analysis Collection

Collection ISSN: 2377-4347 (print)
Collection ISSN: 2377-4355 (electronic)

Cover and interior design by Exeter Premedia Services Private Ltd.,
Chennai, India

10 9 8 7 6 5 4 3 2 1

Printed in the United States of America

To our wives

*Rose Ann Tompkins
Lisa Hilfiker*

ABSTRACT

Ellipsometry is an experimental technique for determining the thickness and optical properties of thin films. It is ideally suited for films ranging in thickness from subnanometer to several microns. Spectroscopic measurements have greatly expanded the capabilities of this technique and introduced its use into all areas where thin films are found: semiconductor devices, flat panel and mobile displays, optical coating stacks, biological and medical coatings, protective layers, and more. While several scholarly books exist on the topic, this book provides a good introduction to the basic theory of the technique and its common applications. It follows in the footsteps of two previous books written by one of the authors with important updates to emphasize modern instrumentation and applications. The target audience is not the ellipsometry scholar, but process engineers and students of materials science who are experts in their own fields and wish to use ellipsometry to measure thin film properties without becoming an expert in ellipsometry itself.

KEYWORDS

Cauchy equation, dispersion equations, ellipsometry, optical constants, polarized light, refractive index, thin film thickness

CONTENTS

LIST OF FIGURES	xiii
LIST OF TABLES	xxv
PREFACE	xxvii
ACKNOWLEDGMENTS	xxix
1 PERSPECTIVE, PREVIOUS WORKS, AND PURPOSE OF THIS VOLUME	1
1.1 Historical Aspects	1
1.2 Focus of This Book and Target Audience	1
1.3 Overview of Topics	2
2 BASIC PHYSICAL PHENOMENA	5
2.1 The Electromagnetic Wave	5
2.2 Interactions Between the Electromagnetic Wave and Matter	10
2.3 Laws of Reflection and Refraction	14
2.4 Polarized Light	14
2.5 The Reflection and Transmission of Light	18
2.6 Measurement Quantities	26
3 SPECTROSCOPIC ELLIPSOMETRY COMPONENTS AND INSTRUMENTATION	31
3.1 Components of a Spectroscopic Ellipsometer	31
3.2 Spectroscopic Ellipsometers	45
4 GENERAL DATA FEATURES	57
4.1 Spectra for Substrates	58
4.2 Spectra for Films on a Substrate	65
5 REPRESENTING OPTICAL FUNCTIONS	71
5.1 Tabulated List	71
5.2 Dispersion Equations	73

5.3	The Cauchy Equation—A Dispersion Equation for Transparent Regions	75
5.4	Oscillator Models	79
5.5	B-Spline	84
6	OPTICAL DATA ANALYSIS	89
6.1	Direct Calculation: Pseudo-Optical Constants	89
6.2	Data Analysis—The Problem	91
6.3	Data Analysis—The Approach	92
7	TRANSPARENT THIN FILMS	101
7.1	Data Features of Transparent Films	102
7.2	Fitting a Transparent Film with Known Index	104
7.3	Fitting a Transparent Film with an Unknown Index	105
7.4	Example: Dielectric SiN_x Film on Si	108
7.5	Example: Dielectric SiO_2 Film on Glass	110
8	ROUGHNESS	113
8.1	Macroscopic Roughness	113
8.2	Microscopic Roughness	114
8.3	Effective Medium Approximations	116
8.4	Rough Film Example	116
9	VERY THIN FILMS	119
9.1	Determining Thickness with Known Optical Functions	119
9.2	Determining Optical Constants of a Very Thin Film	120
9.3	Distinguishing One Film Material from Another	123
10	THIN FILMS WITH ABSORBING SPECTRAL REGIONS	127
10.1	Selecting the Transparent Wavelength Region	129
10.2	Models for the Absorbing Region	131
10.3	Example: Amorphous Si on Glass, Using the Oscillator Method	134
10.4	Example: Photoresist on Si, Using the B-Spline Method	137

11	METALLIC FILMS	139
11.1	Challenge of Absorbing Films	139
11.2	Strategies for Absorbing Films	139
12	MULTILAYER THIN FILM STACKS	145
12.1	Multilayer Strategies	146
12.2	Example: Two Layer Organic Stack, Using “Divide and Conquer”	148
12.3	Example: High-Low Optical Stack, Using “Coupling”	149
	REFERENCES	151
	INDEX	155

LIST OF FIGURES

Figure 2.1.	Christiaan Huygens proposed, in 1673, that light was a wave.	6
Figure 2.2.	(a) Thomas Young, (b) Augustin-Jean Fresnel, and (c) David Brewster developed the concept of light waves in the early 1800s.	6
Figure 2.3.	In 1864, James Clerk Maxwell developed the theory which showed that light was an electromagnetic wave.	7
Figure 2.4.	Light is shown as an electromagnetic wave. Both the electric field (E) and the magnetic field (B) are perpendicular to each other and to the direction of wave propagation.	7
Figure 2.5.	(a) Constructive and (b) destructive interference.	9
Figure 2.6.	A light beam is shown interacting with an interface between air and a material with a complex index of refraction \tilde{N}_2 .	10
Figure 2.7.	A light beam enters an absorbing material at position $z = 0$. Not considering losses due to reflection at each interface, the intensity decreases exponentially as a function of the distance into the material.	12
Figure 2.8.	Two orthogonal light waves of the same frequency are traveling in the same direction (shown offset for clarity). Because the two waves have equal amplitude and are in-phase, the resultant electric field is linearly polarized at an orientation of 45° between the x - and y -axes.	16
Figure 2.9.	Combining two linearly polarized light beams with the same frequency, which are a quarter-wavelength out of phase and have the same amplitude produce circularly polarized light.	17

- Figure 2.10. The plane of incidence contains the incoming beam and the normal to the surface. The component of the electric field parallel to the plane of incidence is denoted as E_p , and is called the *p*-wave. The component perpendicular to the plane of incidence is denoted as E_s , and is called the *s*-wave. 19
- Figure 2.11. (a) Fresnel reflection coefficients, and (b) the reflectance, plotted versus the angle of incidence for light incident from air onto a dielectric such as TiO_2 , with $n = 2.2$ and $k = 0$ at a wavelength of 632 nm. At the Brewster angle, all of the reflected light is polarized with the electric vector perpendicular to the plane of incidence. 21
- Figure 2.12. The reflectance, plotted versus the angle of incidence, for a metal such as Ta with $n = 1.72$ and $k = 2.09$ at a wavelength of 632 nm. 23
- Figure 2.13. Phase shift, as a function of angle-of-incidence for a transparent material ($k = 0$) and for materials with successively larger values of k . The optical constants have been adjusted such that the principal angle is the same for all of the materials. 24
- Figure 2.14. Reflections and transmissions for two interfaces. The resultant reflected beam is made up of the initially reflected beam and the infinite series of beams, which are transmitted from the second medium back into the first medium. 25
- Figure 2.15. Matrix representation of a multilayer stack. 26
- Figure 2.16. Ellipsometry measurement is shown with incident linearly polarized light oriented with both *p*- and *s*-components. The interaction with the sample leads to different amplitudes and phase for the reflected *p*- and *s*-polarizations, producing elliptically polarized light. 28
- Figure 3.1. Light passes through the PSG to create a known polarization that reflects from the sample surface at a specified angle of incidence. The light reflects to the PSD which determines the polarization change caused through interaction with the sample. 32
- Figure 3.2. Wavelength range is shown for common spectroscopic ellipsometry (SE) sources and detectors. 33
- Figure 3.3. Colors can be dispersed in different directions by (a) refraction through a prism, or (b) scattering from a diffraction grating. 35

Figure 3.4.	(a) A monochromator is used to isolate a single wavelength of light, while (b) a spectrometer is used to image the refracted light directly onto a detector array for simultaneous collection of all wavelengths.	36
Figure 3.5.	Polarization change can occur upon (a) reflection from a surface, (b) total internal reflection, which maintains the light intensity, and (c) refraction into a birefringent material. The <i>p</i> - and <i>s</i> -light components are represented by arrows and circles, respectively.	38
Figure 3.6.	Demonstration of retardance caused by light traveling through anisotropic material with different indexes of refraction along the <i>x</i> - and <i>y</i> -directions.	39
Figure 3.7.	Diattenuation of a light beam is shown due to travel through a linearly dichroic material with stronger extinction coefficient along the <i>y</i> -direction.	40
Figure 3.8.	Basics of polarizer operation.	41
Figure 3.9.	Two examples of crystal polarizers, which use anisotropic prisms with optical axes denoted by black arrows to separate the ordinary and extraordinary beams via refraction as shown in (a) a Rochon prism, or total internal reflection as shown in (b) a Glan–Foucault prism.	41
Figure 3.10.	Linearly polarized light passes through a compensator to become circularly polarized light.	42
Figure 3.11.	Three different compensators are compared. A single-element compensator (a) shows a large amount of variation in total phase retardation. The wavelength dependence is reduced by stacking two compensator elements (b) at different orientations. A total internal reflection compensator (c) has the flattest wavelength dependence.	43
Figure 3.12.	The polarization changes from linear to elliptical due to multiple total-internal-reflections within this rhombohedral prism.	43
Figure 3.13.	Linearly polarized light is modulated upon travel through a photoelastic modulator, where the compression and expansion (gray arrows) of the crystal quartz are resonating at 50 kHz to 100 kHz to produce the opposite effect in the amorphous fused quartz section, with the goal of producing enough strain-birefringence to retard the transmitted light.	45

Figure 3.14.	Angle dependence of ellipsometric Ψ and Δ calculated at 633 nm wavelength for different Si_3N_4 coating thicknesses on Si substrate.	46
Figure 3.15.	Image of (a) ex situ spectroscopic ellipsometer and (b) in situ spectroscopic ellipsometer attached to a vacuum process chamber.	47
Figure 3.16.	The modulating time-signal can be transformed into the unique frequency signal components, which are available to determine the SE data parameters. The SE data parameters represent the change in polarization, which is then used to determine sample properties, such as film thickness and refractive index.	48
Figure 3.17.	An RAE operation is reviewed. Light reaching the sample is linearly polarized, but reflects at a distinct elliptical polarization that passes through the rotating analyzer. This leads to a time-varying detected signal consisting of a DC and 2ω frequency terms (both cosine and sine).	50
Figure 3.18.	Basic RCE configuration.	52
Figure 4.1.	Ellipsometry spectra (Ψ and Δ) for a 75° measurement of a thin-film coated substrate.	58
Figure 4.2.	A “substrate” consists of a single interface, where only light reflecting from the surface will reach the detector.	58
Figure 4.3.	The values of Ψ and Δ for a dielectric substrate of N-BK7 glass with 1.3 nm of surface roughness. Three angles-of-incidence are shown.	60
Figure 4.4.	The values of the index of refraction, n , for a dielectric, N-BK7 glass.	60
Figure 4.5.	The values of Ψ and Δ for a cobalt substrate.	62
Figure 4.6.	The values of the optical functions for cobalt.	62
Figure 4.7.	The values of Ψ and Δ for a typical semiconductor substrate, silicon.	64
Figure 4.8.	The values of the optical functions for a typical semiconductor, silicon.	64
Figure 4.9.	Reflection of light within a thin transparent film on substrate.	65
Figure 4.10.	The Ψ spectrum for a transparent film on a substrate. For this particular example, we show a single-crystal silicon substrate with a 1 μm thermal oxide film. Also shown is the spectrum for the bare substrate. The peaks and valleys correspond to wavelengths where the detected light from the thin film exhibits constructive and destructive interference.	66

Figure 4.11.	Destructive and constructive interference from within a thin film. Different wavelengths will produce different effects, depending on how the final light components “align” in-phase or out-of-phase as they recombine traveling to the detector.	66
Figure 4.12.	The Ψ spectrum for a series of SiO_2 coatings on crystalline Si with different film thicknesses. As the thickness increases, so do the number of interference features within the measurement wavelength range.	67
Figure 4.13.	Comparison of the index of refraction for the thin film and glass substrate. This small index difference leads to smaller amplitude data fluctuations.	67
Figure 4.14.	Ψ and Δ spectra for a coating on BK7 glass substrate. The coating has a slightly higher index of refraction than the substrate. This leads to interference oscillations as compared to the data from the bare substrate (also shown). Note the interference features for Ψ have one edge along the bare substrate curves—high or low edge depends on the angle of incidence. The Δ interference features fluctuate around the central curve of the bare substrate.	68
Figure 4.15.	Ψ and Δ spectra from a semiabsorbing film show the interference features of a transparent film over the spectrum above 600 nm. However, absorption within the film prevents interference at shorter wavelengths. Thus, the data curves appear like an absorbing substrate at these wavelengths, as only light from the film surface reaches the detector.	69
Figure 5.1.	The optical functions for polyimide are shown with both normal and anomalous dispersion regions.	74
Figure 5.2.	The optical function for n is shown as described by the Cauchy equation.	76
Figure 5.3.	The optical function for n is shown for several dielectric materials as described by the Cauchy equation.	77
Figure 5.4.	The optical functions for a silicon nitride film, described using the Cauchy equation for n with Urbach absorption to describe k .	78
Figure 5.5.	A mechanical oscillator, which is a forced harmonic oscillator with damping, is shown.	79
Figure 5.6.	General shape for a Gaussian oscillator is shown. The imaginary dielectric function (ϵ_2) is described by the center energy, amplitude, and broadening of the resonant	

absorption. The real dielectric function is produced from KK transformation of the ϵ_2 curve, along with an offset added to ϵ_1 .	80
Figure 5.7. ϵ_2 versus photon energy plotted for a Gaussian oscillator and a Lorentz oscillator.	81
Figure 5.8. A Tauc-Lorentz oscillator describing the optical functions of Ta_2O_5 is shown.	81
Figure 5.9. Optical functions for a material with three separate absorptions described by Gaussian oscillators. Each absorption “bump” has a corresponding “wiggle” in ϵ_1 . The general shape is determined from the KK transform, with an additional ϵ_1 offset (shown for two different values).	83
Figure 5.10. The optical functions, n and k , are shown versus wavelength for a Gaussian oscillator.	84
Figure 5.11. A b-spline curve is described by a series of nodes that adjust the amplitude of individual basis functions which are summed to form the final curve.	85
Figure 5.12. A b-spline is shown representing the optical functions for PCBM.	86
Figure 5.13. A KK consistent b-spline is shown representing the optical functions for PCBM.	87
Figure 6.1. With ellipsometry, it is important to consider the methods to bridge from experimental measurements to desired sample quantities.	90
Figure 6.2. Ψ and Δ spectra were measured from an opaque metal film at three angles of incidence. These spectra are directly transformed to show pseudo-dielectric function curves corresponding with each angle. Because light is reflected from a single interface, the pseudo-dielectric function curves from the three angles overlie each other.	91
Figure 6.3. Ψ and Δ spectra from a multilayer SOI sample, along with the direct transformation to pseudo-dielectric functions. The pseudo-dielectric functions separate at longer wavelengths where light is detected from multiple interfaces within the thin film stack.	92
Figure 6.4. Demonstration of the “Inverse” problem, where sample properties cannot be directly calculated from measured ellipsometric quantities, but the ellipsometric quantities can be calculated for any given sample structure.	92

- Figure 6.5. The typical flow for SE data analysis involves: (1) Measure the SE data, (2) describe sample with a model, (3) fit the experimental data and model-calculations by varying unknown model properties, and (4) evaluate results. 93
- Figure 6.6. A model representing the measured sample with both fixed values (known properties) and fit parameters (unknown properties). 94
- Figure 6.7. The curve generated from an initial thickness guess of 700 nm has a shape similar to the experimental data curve but is offset toward shorter wavelengths. An iterative data analysis algorithm searches for a minimum MSE value by adjusting the thickness guess. A few iterations are shown along with the final thickness result of 749.18 nm, which lies on top of the experimental data. 96
- Figure 6.8. The MSE profile for the fit from Figure 6.7 versus thickness is shown. The initial guess has an MSE over 500. The slope of the MSE curve at this point shows that a thicker film will produce a lower MSE. The fit iterations progress toward the minimum MSE, which is reached for a thickness of 749.18 nm. 96
- Figure 6.9. An MSE plot versus film thickness shows both the “best fit” MSE minimum (black circle) and many “local minima” that may stop a standard regression algorithm from proceeding but would not result in the best-fit result. 97
- Figure 6.10. The MSE profile versus the fit parameter (in this case, film thickness) verifies how sensitive the data analysis will be to the fit parameter of interest. If the MSE rises quickly from the minimum value as the fit parameter varies, then the result has high sensitivity (e.g., Model #1). If the MSE stays nearly the same value around the minimum, it shows that other answers give similar results, which calls into question the uniqueness and sensitivity of the final answer (e.g., Model #2). 99
- Figure 7.1. The indexes for various inorganic films are shown in their transparent spectral regions. 102
- Figure 7.2. As film thickness increases, the interference features shift toward longer wavelengths. This is a result of longer path lengths within the film. 103
- Figure 7.3. As the film index increases, the interference features shift toward longer wavelengths and with reduced

Ψ peak amplitudes. This is a result of reduced phase velocity and reduced optical contrast between film and substrate.	103
Figure 7.4. The measured Ψ spectrum for a thermal oxide on silicon is shown along with simulated data for a film thickness of 150 nm.	104
Figure 7.5. Advanced procedure is shown for fitting thickness and index of transparent thin film using the Cauchy dispersion relation.	106
Figure 7.6. The index for this film on silicon can be estimated between 1.75 and 2.00 based on Ψ peak height.	107
Figure 7.7. With estimated film index of 1.9, the thickness is adjusted to 148 nm to match the interference feature position.	108
Figure 7.8. Data fits to both Ψ and Δ using a Cauchy dispersion relation for the SiN_x thin film.	109
Figure 7.9. Cauchy index is shown for SiN_x .	110
Figure 7.10. Index variation is shown for films on fused silica.	111
Figure 7.11. Data fit for SiO_2 coating on glass substrate. While Ψ curves are well matched with a single-layer model, the tilt in Δ spectra is only matched with the inclusion of a thin surface roughness layer.	112
Figure 7.12. The index is shown for the glass substrate, our SiO_2 film as described by a 3-term Cauchy relation and the surface roughness layer as described by a 50-50 effective medium approximation.	112
Figure 8.1. A representation of macroscopic roughness. Note that the wavelength of the light is much shorter than the roughness dimensions.	114
Figure 8.2. A representation of microscopic roughness is shown. Note that the wavelength of the light is much longer than the roughness dimensions.	115
Figure 8.3. (A) A bulk material which has microscopic roughness. (B) A model of the material shown in (A) where the roughness is modeled as a thin layer whose index of refraction is intermediate between that of the bulk material and empty space.	115
Figure 8.4. Experimental Ψ from a niobium oxide layer on BK7 glass, along with two model fits—one without roughness and the second with roughness. The MSE for the model-fit without roughness is 1.5; while the MSE	

reduces to 0.6 with the addition of a 30 Å roughness layer modeled using a 50-50 EMA approach.	117
Figure 9.1. Ellipsometry spectra are graphed for film-free silicon and for oxide on silicon. Plots are shown for 20 Å, 40 Å, 60 Å, 80 Å, and 100 Å oxide films at a 75° angle-of-incidence.	120
Figure 9.2. The first part of the Ψ - Δ trajectories for a single wavelength for transparent films on silicon with index of refraction of the films as indicated. These trajectories are for an angle-of-incidence of 70° and a wavelength of 632.8 nm.	121
Figure 9.3. Ψ - Δ trajectories are plotted for the first 500 Å of a film with index of 2.0 at a 70° angle of incidence. Each open circle represents 100 Å increments along the trajectories.	122
Figure 9.4. The first part of the Ψ - Δ trajectories for a single wavelength for transparent films on silicon with index of refraction of the films as indicated. These trajectories are for an angle-of-incidence of 70° and a wavelength of 200 nm.	123
Figure 9.5. Experimental data along with modeled data for a thermal oxide on silicon, modeled with a tabulated list for the thermal oxide. The resulting thickness was 96.5 Å and the MSE was 1.85.	124
Figure 9.6. The same data as shown in Figure 9.5, modeled as a silicon nitride film, using a tabulated list for LPCVD Si_3N_4 . The resulting thickness is 76.6 Å and the MSE is 22.1.	124
Figure 9.7. A native oxide film on silicon, modeled as SiO_2 , with tabular values for the index of refraction. The thickness value was determined to be 17 Å with an MSE of 2.4.	125
Figure 9.8. The same data as shown in Figure 9.7, modeled as a silicon nitride film, using a tabulated list for LPCVD Si_3N_4 . The resulting thickness is 13.6 Å and the MSE is 3.82.	125
Figure 10.1. Example materials, which are transparent at longer wavelengths, but absorbing at shorter wavelengths, are graphed.	128
Figure 10.2. Ellipsometry spectra from a film that is transparent above and absorbing below 800 nm.	128
Figure 10.3. The general procedure for data analysis of a thin film with absorbing spectral regions is shown.	129

Figure 10.4.	Graph of the transparent and absorbing spectral regions for an amorphous semiconductor film on a germanium substrate.	130
Figure 10.5.	Visualizing the transparent and absorbing spectral regions for this organic layer on silicon is more complicated as small absorptions may not completely dampen the interference features.	130
Figure 10.6.	Optical functions from the Cauchy fit and Direct fit are shown for a 99 nm SiON film on a Si substrate.	132
Figure 10.7.	General procedure for oscillator modeling is shown.	133
Figure 10.8.	Data and fits are shown for an a-Si film on glass.	136
Figure 10.9.	Optical functions for a-Si as determined using a T-L oscillator function.	136
Figure 10.10.	Data and fits are shown for a photoresist on Si.	137
Figure 10.11.	Optical functions are shown for the photoresist film.	138
Figure 10.12.	KK consistent B-spline model results are plotted for the photoresist.	138
Figure 11.1.	The basic challenge of absorbing films is that the number of unknown sample properties outweighs the number of measured data.	140
Figure 11.2.	Comparison of methods for metal films is shown. Methods are successful if they provide a distinct MSE minimum for one thickness. The data are from different samples, which explains the different resulting thickness values.	141
Figure 11.3.	SE + T can be used to provide a unique solution for thickness and optical constants when the metal is deposited on a transparent substrate.	142
Figure 11.4.	Interference enhancement method adds a thick transparent film below the metal to change the overall interaction of light with the metal layer for different angles of incidence. This can break the correlation and provide unique thickness and optical constants for the metal film.	143
Figure 11.5.	Multisample analysis, whether from multiple samples of varying thickness or directly from a dynamic measurement during film growth, can provide additional sample information to help solve for optical constants and each thickness.	143

Figure 12.1.	Measured spectra and model-generated fit from a four-layer optical coating stack consisting of high and low index dielectric layers.	146
Figure 12.2.	“Divide and conquer” approach to multilayer characterization is illustrated where the optical constants are first determined from single-layer films.	147
Figure 12.3.	“Consecutive layers” approach to multilayers works by measuring each new layer as it is added to the overall stack.	147
Figure 12.4.	Consecutive films with the same thickness are simplified by using the same optical constants for each layer of the same material and assuming that the thickness for repeated layers that were designed and deposited is the same.	147
Figure 12.5.	Optical functions for an antireflection coating and a photoresist, which are measured as a stack.	148
Figure 12.6.	Optical functions for a high-index and a low-index film, which are used to construct a 37-layer optical coating stack.	149
Figure 12.7.	Measured spectra and corresponding model fits are shown from a 37-layer optical coating stack consisting of repeated high-index and low-index films.	150

LIST OF TABLES

Table 5.1.	Example of a tabulated list to represent the optical functions of GaAs	72
Table 5.2.	Cauchy coefficients associated with each index curve shown in Figure 5.3	77
Table 5.3.	Cauchy and Urbach parameter values related to the optical functions plotted in Figure 5.4	78
Table 10.1.	Comparison is given between different fit methods for films that absorb in some spectral regions	135
Table 11.1.	Methods for absorbing films are listed based on their primary goal	140

PREFACE

Ellipsometry is an experimental technique for determining the thickness and optical properties of thin films ranging in thickness from submonolayer coverage to several micrometers thick. Elliptically polarized light is used as a probe to determine these properties. Many different wavelengths of light are used, hence the term “Spectroscopic.” This provides the optical properties in the ultraviolet, visible, and infrared spectral range. The ellipsometric quantities measured are delta, the phase shift of the component of light in the plane of incidence compared to the component perpendicular to the plane of incidence, and psi, the tangent of which equals the ratio of the amplitudes of the electric fields in those two directions. The quantities of interest are film thickness and spectral optical functions. In order to determine these, it is necessary to do a regression analysis to determine the best fit of the proposed values of thickness and optical functions to the aforementioned measured ellipsometric values.

In this book, we discuss the physical properties of polarized light, how the ellipsometric values are measured, and how we transform these ellipsometric values to values of interest, that is, the thickness and optical functions.

The target audience for this book are process engineers who are experts in their respective fields and who want to understand how their ellipsometer does what it does. Graduate students and advanced undergraduates in a scientific or engineering field will also benefit from reading this work.

ACKNOWLEDGMENTS

The authors wish to express their gratitude to C. R. Brundle for the opportunity to write this text as part of his book series covering various characterization methods.

We also wish to personally thank Professor John A. Woollam for his continued support and his dedication to the development, exploration, and education of spectroscopic ellipsometry and its applications.

CHAPTER 1

PERSPECTIVE, PREVIOUS WORKS, AND PURPOSE OF THIS VOLUME

1.1 HISTORICAL ASPECTS

Ellipsometry is an experimental technique for determining the thickness and optical properties of thin films. The name “ellipsometry” comes from the fact that the technique uses elliptically polarized light as a probe in order to determine the thickness of thin films and the optical properties of the film material. Originally, ellipsometry was practiced using one wavelength. That practice is now called “single-wavelength ellipsometry.” Starting in the 1990s, many wavelengths from the ultraviolet (UV) to the near infrared (NIR) spectral range were used and this practice is called “spectroscopic ellipsometry” or simply “SE.” The primary strength of SE is the ability to analyze multiple layers and determine the optical constant dispersion (variation with wavelength). From the optical dispersion, additional material properties can be deduced. Examples include the degree of crystallinity of annealed amorphous silicon and the aluminum fraction in $\text{Al}_x\text{Ga}_{1-x}\text{As}$.

1.2 FOCUS OF THIS BOOK AND TARGET AUDIENCE

There are several scholarly books on SE [1–9] for those interested in leading-edge technology and researching further in the field. However, there has always been a need for a preliminary introduction to ellipsometry for the nonellipsometry expert. The first such work was introduced in 1993—

“A User’s Guide to Ellipsometry” by H.G. Tompkins [3], which covered the subject of single-wavelength ellipsometry. This was followed in 1999 by the publication of “Spectroscopic Ellipsometry and Reflectometry: A User’s Guide” by H.G. Tompkins and W.A. McGahan [4]. The target audience for these books was not the ellipsometry scholars, but process engineers, who were experts in their own field (e.g., a thin-film deposition engineer) and who wanted to use ellipsometry to measure the properties of their films without having to become an expert in ellipsometry itself. These books were also a perfect starting-point for materials-science students, where ellipsometry is only one of many tools used to study thin film properties. While very well received, the natural evolution of the field, particularly SE instrumentation, has left the most recent book somewhat out of date.

The focus of the previous book was on rotating-analyzer instruments, which had no compensator and often used monochromators to scan through select wavelengths. This was the prevailing type of instrument used at that time. Rotating-analyzer ellipsometers, with a phase-shifting element, are still used, primarily in academia. However, the rotating-compensator instrument, with fast charge-coupled device (CCD)-detection, has become the prevailing ellipsometer type used in both industry and academia. Whereas the monochromator-based rotating-analyzer instrument took 5 to 10 minutes to collect a spectrum at one angle, the newer CCD-based detection allows spectra to be collected in seconds. This has greatly expanded the use of SE for applications requiring high-speed, such as real-time dynamic measurements or large-area uniformity maps.

It seems reasonable that a new book be written emphasizing the faster ellipsometer technology. Accordingly, the purpose of the present work is to give a brief summary of the SE technique, as currently practiced, directed toward the casual user who is an expert in his or her own field (e.g., a process engineer), who wants to use an ellipsometer but does not feel the need to become an expert in ellipsometry. This is in keeping with the intent of the previous books by one of the authors.

1.3 OVERVIEW OF TOPICS

The usual methods for determining thickness (calipers, micrometers, yard sticks, etc.) are ineffective for films thinner than about one micrometer. On the other hand, microelectronic devices, optical coating components, and so on often have layers that are significantly thinner (e.g., down to monolayer thicknesses). Interferometry methods (where intensity is the

measured quantity) are ineffective below thicknesses of several thousand angstroms. The ellipsometry technique is useful for film thicknesses of several micrometers down to submonolayer coverages.

The probe for ellipsometry is a polarized light beam. The sample of interest is illuminated by a light beam of known polarization; the light beam is reflected by the sample and is directed back into the instrument. The ellipsometer measures what the sample did to the polarization state of the reflected light beam. The entities that are measured by the ellipsometer involve the mutually perpendicular components (called the p-waves and the s-waves) of the probing beam. The entities are the ratio of the amplitudes (giving us the quantity called “psi”) and the phase shift (giving us the quantity called “delta”) of the mutually perpendicular components. Ψ and Δ are measured for various wavelengths of light, hence the term “spectroscopic” in the technique name.

Software is used to convert the ellipsometric quantities Ψ and Δ into the ultimate quantities of interest such as film thickness and optical functions of the film (and substrate). The methods that provide sample information from the measured ellipsometric quantities will be the focus throughout the second half of this book.

The general format of this book will be as follows. We start with the physics of light and interaction between light and matter in Chapter 2. This chapter will also define the basic measurement quantities of interest. In Chapter 3, we describe the primary components of any spectroscopic ellipsometer, along with example optical configurations for the instrumentation currently available. In Chapter 4, we discuss the SE data features from common sample types including bare substrates and thin film coatings. As we consider a wide spectral range, we also need methods for representing the optical functions of each material. In Chapter 5, we introduce common dispersion relationships used for both transparent and absorbing optical functions.

In Chapter 6, we move to the processes and applications used to determine material properties such as film thickness and index of refraction. Chapter 7 is dedicated to the most common application of ellipsometry—the measure of film thickness and index from a transparent layer on a known substrate. This is followed by chapters introducing roughness (Chapter 8) and very thin films (Chapter 9). We then describe films which absorb over a specific spectral region (Chapter 10) or over all wavelengths (Chapter 11). Finally, we introduce the basic approaches to consider multilayer characterization in Chapter 12.

We provide references which consist of books on ellipsometry [1–9], the SE conference proceedings [10–15], works on optical properties

[16–21], instrumentation [22–25], optics and polarized light [26–29], and specific papers on SE methods and applications [30–37]. Throughout, we introduce methods that can be applied irrespective of the instrument and software at your disposal.

CHAPTER 2

BASIC PHYSICAL PHENOMENA

Ellipsometry uses polarized light as a probe of thin films on a substrate. In this chapter, we discuss the physical phenomena of light and how it interacts with the sample of interest to provide film thickness and optical properties.

2.1 THE ELECTROMAGNETIC WAVE

In much of the historical understanding, the concept of light and sight were convoluted. From Greek antiquity to the 19th century, light was thought to be a stream of particles going either from the object being observed to the eye or vice versa [38]. Christiaan Huygens (Figure 2.1), in 1673, proposed that light was actually a wave [39].

This concept was developed extensively in the early 1800s by Thomas Young, Augustin-Jean Fresnel, David Brewster (Figure 2.2), and others, although it was not known what actual material was waving.

In 1864, in a paper presented before the Royal Society, James Clerk Maxwell (Figure 2.3) proposed a theory which required the light wave vibrations to be strictly transverse (perpendicular to the propagation direction) and provided a definite connection between light and electricity. The results of this theory were expressed as four equations which are known as *Maxwell's Equations*.

The quantity which was waving was not an actual material, but instead was both an electric field (E) and magnetic field (B). The vector fields, E and B , are perpendicular to each other and both are perpendicular to the direction of propagation, as shown in Figure 2.4.

It is generally accepted that the human eye reacts to the electric vibration. The two vibrations are not independent and specification of the electric field vector completely determines the magnetic field vector. For these reasons, and for simplicity, we consider only the electric field vibration.



Figure 2.1. Christiaan Huygens proposed, in 1673, that light was a wave.

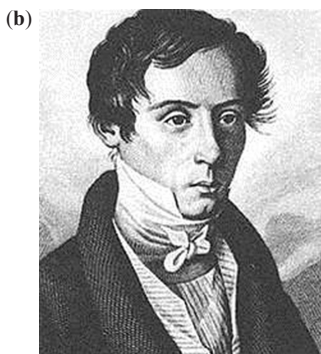
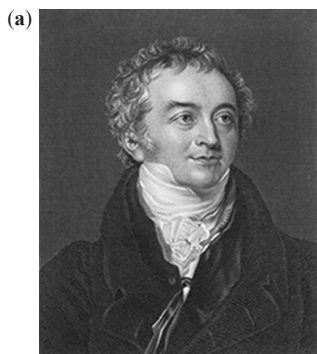


Figure 2.2. (a) Thomas Young, (b) Augustin-Jean Fresnel, and (c) David Brewster developed the concept of light waves in the early 1800s.



Figure 2.3. In 1864, James Clerk Maxwell developed the theory which showed that light was an electromagnetic wave.

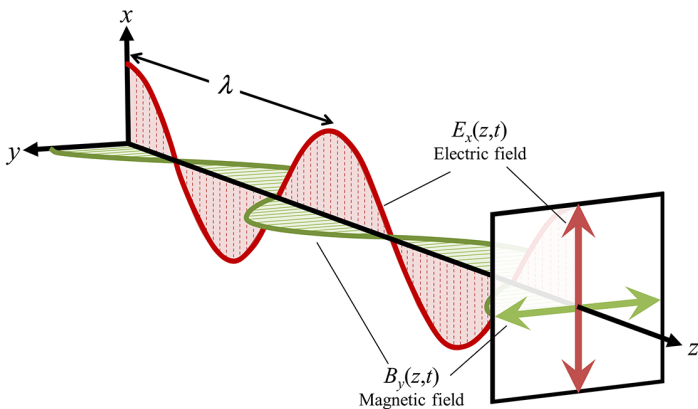


Figure 2.4. Light is shown as an electromagnetic wave. Both the electric field (E) and the magnetic field (B) are perpendicular to each other and to the direction of wave propagation.

The equation for an electromagnetic plane wave can be expressed several ways. It describes the electric field as a function of both position and time. If we consider motion in one dimension (z), with the electric field oscillating only within the x -plane, the solution to the wave equation can be expressed as

$$E_x(z,t) = E_0 \sin\left(-\frac{2\pi}{\lambda}(z-vt) + \xi\right) \quad (2.1)$$

where E is the electric field strength at any time or place, E_0 is the maximum field strength or wave “amplitude,” z is the distance along the direction of travel, t is the time, v is the phase velocity, λ is the wavelength, and ξ is an arbitrary phase angle (which will allow us to offset one wave from another when we combine waves).

Although light waves can occur in several different forms (e.g., spherical, plane, etc.), we shall deal exclusively with plane waves.

2.1.1 WAVELENGTH, FREQUENCY, AND PHOTON ENERGY

Light is often described by its wavelength, frequency, or photon energy. The wavelength, λ , is the distance between two consecutive peaks of the electric field, as shown in Figure 2.4. Wavelength is specified for the electric field in free space*, where phase velocity is equal to the speed of light, c . The wave frequency, f , refers to how often the electric field vibrates per unit time. These terms are related by the following:

$$f = \frac{v}{\lambda} \quad (2.2)$$

Both phase velocity and wavelength are altered when electric fields travel through materials. However, the frequency remains constant.

Typical ellipsometry measurements use light from the ultraviolet ($\lambda \sim 200$ nm) to the near infrared ($\lambda \sim 2000$ nm). This is equivalent to frequencies of $\sim 1.5 \times 10^{15} - 1.5 \times 10^{14}$ oscillations per second (Hz), respectively.

Because the oscillations are at extremely high frequencies, we cannot directly measure the electric field. Instead, we measure the flux of energy of the radiation. The quantity of energy being transferred across a unit area which is perpendicular to the propagation direction is called the “intensity” or “irradiance” of the wave (here denoted as I). The intensity is proportional to the square of the wave amplitude, that is,

$$I \propto E_0^2 \quad (2.3)$$

While light can be described as an electromagnetic wave, it also behaves as a collection of quanta, called photons. Each photon carries a specific amount of energy, referred to as photon energy (E_{photon}), which

* Throughout this book, we will refer to the wavelength for light in free space.

is related to the frequency. Higher frequencies provide larger photon energies. The wavelength is inversely related to both the frequency and photon energy, as shown in Equation 2.4. Thus, short wavelengths carry more energy than long wavelengths. Our wavelength range from 200 nm to 2000 nm has photon energies of ~ 6.2 eV to 0.62 eV, respectively.

$$E_{\text{photon}} = hf = \frac{hc}{\lambda}, \text{ where } h \text{ is Planck's constant} \quad (2.4)$$

2.1.2 INTERFERENCE

We now consider the combination of multiple electromagnetic waves of the same frequency propagating along the same direction. Under certain conditions, the combination of waves leads to interference, which is the algebraic sum of the electric fields at each position. Interference will not occur if the electric fields are orthogonal. However, when electric fields are oriented along the same direction, they will interfere. The resultant electric field amplitude of the combined wave can be enlarged (constructive interference) or reduced (destructive interference).

Constructive interference occurs when each electric field is displaced in the same direction, as shown in Figure 2.5a. This occurs when the

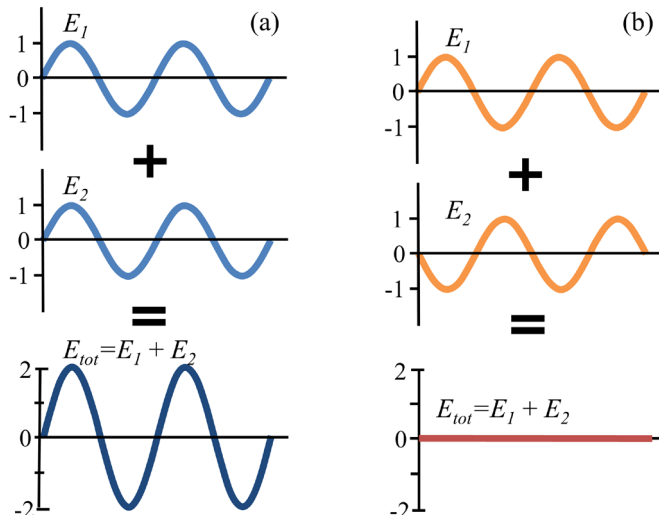


Figure 2.5. (a) Constructive and (b) destructive interference.

waves are in-phase, that is, their phase difference is near 0° . Destructive interference occurs when each electric field is displaced in opposite directions, as shown in Figure 2.5b. This occurs when the waves are out-of-phase, that is, their phase difference is close to 180° .

2.2 INTERACTIONS BETWEEN THE ELECTROMAGNETIC WAVE AND MATTER

In this section, we describe the relationship between materials and light. The material properties of interest are referred to as “optical properties” or “optical constants”. Because they vary with the wavelength, they are also referred to as optical functions. Two common descriptions for the optical constants of a material are the complex refractive index and the complex dielectric function.

2.2.1 COMPLEX REFRACTIVE INDEX

When light interacts with different materials, several phenomena occur. Each can be described by considering the optical properties of the material. First, the wave can change directions. Figure 2.6 depicts a plane wave light beam arriving at an interface between air and another material. Some of the light is reflected back into the first medium (air) and does not enter the second medium. The light entering the second medium travels in a new direction, which is covered in a later section on light refraction.

Second, the phase velocity of the light wave can be altered. This is represented by the three parallel-lines in Figure 2.6 that represent

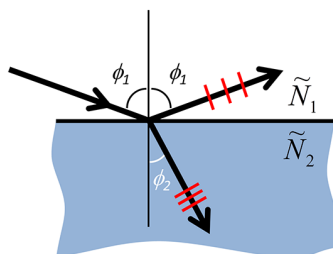


Figure 2.6. A light beam is shown interacting with an interface between air and a material with a complex index of refraction \tilde{N}_2 .

corresponding wavelengths. The phase velocity is faster (and thus the wavelength longer) in the first medium than the second. Third, the light wave can change amplitude. This occurs either by division of the light wave (some part of it reflects and the remaining part transmits) or from the loss of energy when traveling through an absorbing material. Each of these phenomena can be described by considering the complex refractive index of the material.

The complex refractive index, \tilde{N} , is composed of both a real and imaginary component:

$$\tilde{N} = n \pm ik \quad (2.5)$$

where n is the “index of refraction” or simply “index,” k is the “extinction coefficient,” and i is the imaginary number. Whether we use the plus or the minus sign depends on how one sets up their mathematical universe.

The index of a dielectric material, such as glass, is the inverse of the ratio of the phase velocity of light in the material to the speed of light in free space (c), that is,

$$n = \frac{c}{v} \quad (2.6)$$

In silicon nitride, where $n \approx 2$, the phase velocity of light is half that of light in free space.

The extinction coefficient is a measure of how rapidly the intensity decreases as light passes through the material. To better understand the extinction coefficient, let us consider first the “absorption coefficient” which is denoted by α .

As depicted in Figure 2.7, the light beam approaches the absorbing material from the left along the z -axis. Some intensity loss occurs upon reflection at the air and material interface. We denote I_0 as the intensity just inside the material. The intensity decrease in the absorbing material is given by:

$$\frac{dI(z)}{dz} = -\alpha I(z) \quad (2.7)$$

The solution to this equation is

$$I(z) = I_0 e^{-\alpha z} \quad (2.8)$$

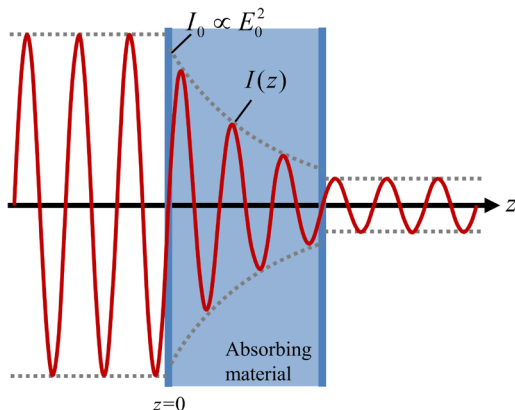


Figure 2.7. A light beam enters an absorbing material at position $z = 0$. Not considering losses due to reflection at each interface, the intensity decreases exponentially as a function of the distance into the material.

Loss of light due to reflection or scattering does not contribute to the magnitude of α , which is only dependent on intensity loss due to absorption.

This is the familiar negative exponential function that decreases but never quite reaches zero. The extinction coefficient, k , is related to the absorption coefficient and is defined as

$$k = \left(\frac{\lambda}{4\pi} \right) \alpha \quad (2.9)$$

Note the unit for the absorption coefficient, α , is cm^{-1} . Since α is multiplied by the wavelength, λ , with unit cm, the extinction coefficient, k , is unitless, as is the index, n .

For the negative exponential curve described by Equation 2.8, we can identify the “Characteristic Depth” (sometimes called Penetration Depth), where the intensity drops to $1/e$ or approximately 37 percent of the original value. This occurs when

$$\alpha z = 1 \quad (2.10)$$

We denote the value of z at this point as the Characteristic Depth, C_p

$$C_p = \frac{1}{\alpha} \quad (2.11)$$

or, using Equation 2.9,

$$C_p = \lambda / 4\pi k \quad (2.12)$$

Absorbing films can be considered opaque when thickness is greater than 6 times the characteristic depth.

While the refractive index and extinction coefficient are often referred to as the “optical constants” of a material, neither n nor k are constant. Rather, they are functions of the frequency of the light wave (i.e., they are wavelength-dependent). They also vary with temperature of the material. We will consider the wavelength-dependence of optical properties in Chapter 5.

2.2.2 COMPLEX DIELECTRIC FUNCTION

The complex dielectric function is an alternate description for the optical properties of a material. Whereas n and k describe how a light wave is affected by a material, the dielectric function describes how the material is affected by the light wave. There are four equations, called the “constitutive” or “material” equations, which describe the response of a material to electromagnetic radiation. For nonconductive, nonmagnetic materials, the equation of interest relates the electric displacement, D , to the electric field, E , as:

$$D = \epsilon_0 \tilde{\epsilon} E \quad (2.13)$$

where ϵ_0 is the permittivity in vacuum, and $\tilde{\epsilon}$ is the dielectric constant for the material. The dielectric constant will also vary with the light wave frequency or wavelength, so it is commonly referred to as the dielectric function. The dielectric function can be complex. The real component, denoted by ϵ_1 , is the electric polarizability and describes how the electric field may distort the charge distribution within a material. The imaginary component, denoted by ϵ_2 , describes the absorption properties of the material. The “complex dielectric function”, then, is

$$\tilde{\epsilon} = \epsilon_1 \pm i\epsilon_2 \quad (2.14)$$

The relationship between the complex dielectric function and the complex index of refraction is

$$\tilde{\epsilon} = \tilde{N}^2 \quad (2.15)$$

2.3 LAWS OF REFLECTION AND REFRACTION

When a light beam interacts with a surface, as suggested by Figure 2.6, some of the light is reflected and some is transmitted into the material. It was known by the ancients (Euclid, 300 BC) that the angle of reflection is equal to the angle of incidence, that is,

$$\phi_i = \phi_r \quad (2.16)$$

In Figure 2.6, both angles are listed as ϕ_1 . The law of refraction is somewhat more involved and is called “Snell’s Law” after Willebrord Snellius, who discovered the principle in 1621. Snell’s law, in its most general form is

$$\tilde{N}_1 \sin \phi_1 = \tilde{N}_2 \sin \phi_2 \quad (2.17)$$

where subscripts indicate the two materials per Figure 2.6. When dealing with a dielectric material, that is, $k=0$, the law simplifies to the more familiar

$$n_1 \sin \phi_1 = n_2 \sin \phi_2 \quad (2.18)$$

All terms in Equation 2.18 are real numbers. For Equation 2.17, generally $k=0$ for the ambient, hence \tilde{N}_1 is real, and the sine function for the first medium is a real number (as we would expect). If \tilde{N}_2 is a complex number (k_2 is nonzero), then the sine function in the second medium is a complex function rather than the familiar function (opposite side over the hypotenuse). There is a corresponding complex cosine function such that

$$\sin^2 \phi_2 + \cos^2 \phi_2 = 1 \quad (2.19)$$

We shall see later that Fresnel’s equations use the complex cosine function. Along with Snell’s law, Equation 2.19 can be used to compute the complex cosine.

2.4 POLARIZED LIGHT

The polarization of a light beam describes the shape of the electric field as viewed by looking along the direction of propagation. In this section, we will discuss the properties of unpolarized and polarized light.

2.4.1 POLARIZATION

The electric field orientation for a single photon occurs along a single plane. As mentioned in Section 2.1.2, the superposition of multiple electric fields propagating in the same direction can lead to interference when electric fields are aligned. Alternately, orthogonal electric fields travel together without interference. The shape of the resultant electric field as it passes a stationary observer is referred to as polarization.

2.4.2 UNPOLARIZED LIGHT

“Unpolarized” light has photons in random orientations. The electric field of a single photon from the light source is oriented in a given direction. The electric field of the next photon will be oriented in a different direction, and in general, photons are emitted with electric fields all oriented in different directions. The most common unpolarized source of light is sunlight. However, the orientation of the electric field is altered upon reflection, refraction, and scattering. The indirect sunlight that reaches an observer has a preferred electric field orientation. This is generally called “partially polarized” light to describe the electric field with a preferred orientation that is not well-defined.

2.4.3 LINEARLY POLARIZED LIGHT

In Figure 2.8, we depict the electric field strength for two light beams with the same frequency and the same amplitude traveling along the same path (we show them offset for clarity). One is polarized in the vertical direction and one is polarized in the horizontal direction. Each individual wave is considered linearly polarized, because the electric field would appear along a single line when observed along the propagation direction. In this case, note specifically that the maximum, minimum, and zero points of the vertical wave coincide with those of the horizontal wave, that is, the waves are *in-phase*. Because the two waves are orthogonal, they do not interfere. The vector sum of the components of the two waves are added at each point in space, resulting in a linear wave which is polarized at 45° to the vertical, as shown in Figure 2.8. If the two waves remain in-phase but the amplitudes are not equal, the result would be a linearly polarized wave at an angle different from 45° . Specifically, when two linearly polarized

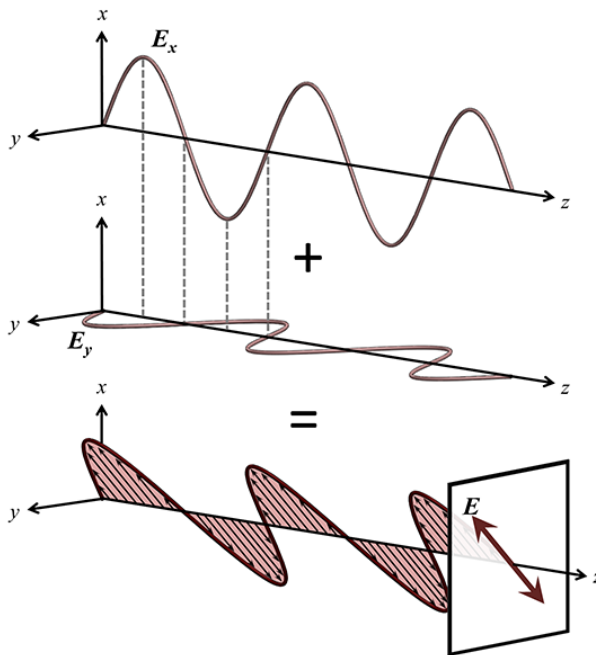


Figure 2.8. Two orthogonal light waves of the same frequency are traveling in the same direction (shown offset for clarity). Because the two waves have equal amplitude and are in-phase, the resultant electric field is linearly polarized at an orientation of 45° between the x - and y -axes.

waves with the same frequency are combined in-phase, the resultant wave is linearly polarized.

2.4.4 CIRCULARLY POLARIZED LIGHT

In Figure 2.9, we again depict two light beams with the same frequency and amplitude traveling along the same path. Again, one is polarized vertically and the other horizontally. In this case, however, the maximum, zero, and minimum of the electric field strength of the horizontal wave have been displaced from that of the vertical wave: the two waves are *out of phase* by a quarter wave or by 90° . When the two waves are combined, the tips of the arrows of the resultant wave do not move back and forth in a plane as in the previous illustration. Instead, the electric field moves in a manner which, viewed end-on, describes a circle. This is referred to as

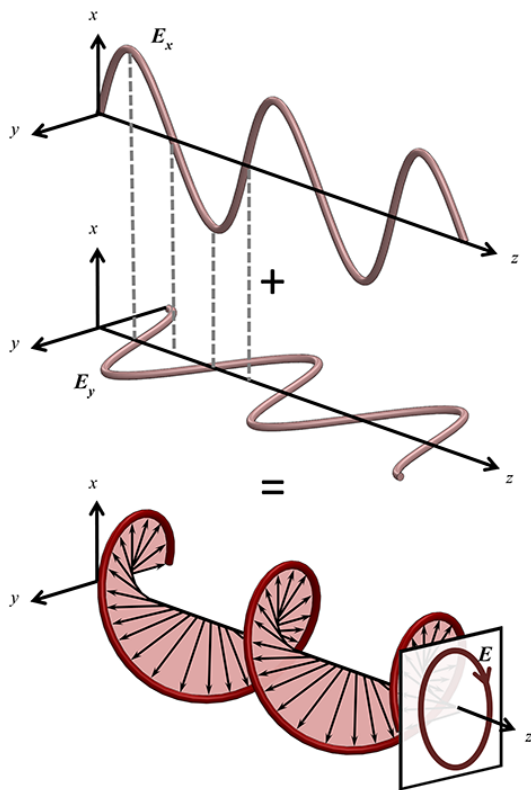


Figure 2.9. Combining two linearly polarized light beams with the same frequency, which are a quarter-wavelength out of phase and have the same amplitude produce circularly polarized light.

circularly polarized light and only occurs when the two linearly polarized waves with the same frequency have the same amplitude and a phase difference of 90° .

2.4.5 ELLIPTICALLY POLARIZED LIGHT

Had the phase shift been anything other than 90° or had the amplitudes not been equal, the electric field, viewed end-on, would have appeared to be moving on an ellipse, and this is referred to as elliptically polarized light. Specifically, when two linearly polarized waves with the same frequency are combined out of phase, the resultant wave is elliptically polarized.

Elliptically polarized light is used in ellipsometry, and in fact, is the reason for the name ellipsometry. Elliptically polarized light is generated when linearly polarized light reflects from a surface under certain conditions. The change in polarization depends on the surface (optical constants, presence of films, etc.). Ellipsometry measures this polarization change to determine sample properties of interest.

2.5 THE REFLECTION AND TRANSMISSION OF LIGHT

We saw earlier that light is separated into reflected and transmitted components when incident upon an interface between different materials. In this section, we will consider the details of this interaction and how it depends on the angle of incidence and polarization of the electric field.

2.5.1 ORIENTATION

The reflection and transmission of light at an interface is subject to the light polarization. There are two orientations where linearly polarized light is maintained along the same plane.* We use these two orientations to establish our coordinate system.

Figure 2.10 shows schematically a light beam reflecting from the surface. The incident beam and the normal to the surface define a plane which is perpendicular to the surface and this is called the “plane of incidence.” Note that if the reflection is specular, the outgoing beam is also in the plane of incidence.

As indicated in Figure 2.10, the angle of incidence is defined between the light beam and the normal to the surface.

The effect of the reflection depends on the polarization state of the incoming light and the angle-of-incidence. In Figure 2.10, we show the amplitude of the electric field which is vibrating in the plane of incidence as E_p and the amplitude of the electric field which is vibrating perpendicular to the plane of incidence as E_s . The respective waves are referred to as *p*-waves and *s*-waves. The subscripts “*p*” and “*s*” stand for the German words for parallel (“parallel”) and perpendicular (“senkrecht”), referring to the orientation relative to the plane of incidence.

* This applies to isotropic materials, where the optical properties are the same for all directions.

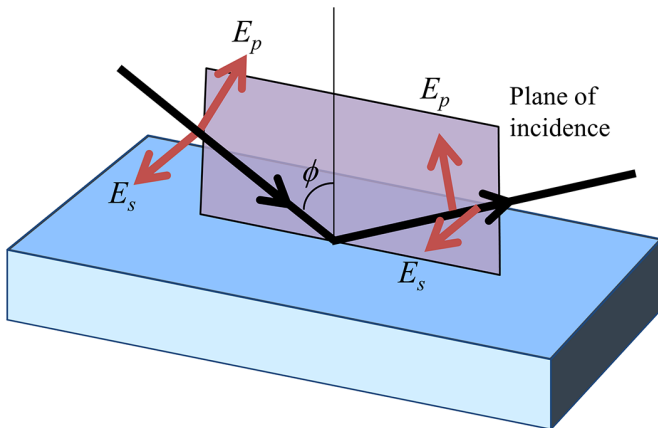


Figure 2.10. The plane of incidence contains the incoming beam and the normal to the surface. The component of the electric field parallel to the plane of incidence is denoted as E_p , and is called the *p*-wave. The component perpendicular to the plane of incidence is denoted as E_s , and is called the *s*-wave.

2.5.2 THE EQUATIONS OF FRESNEL

Boundary conditions describe the reflected and transmitted electromagnetic waves across an interface. These conditions, developed from Maxwell's equations, maintain that tangential E -fields and normal B -fields must be continuous across the interface. The solution to these conditions leads to a description of the change in amplitude and phase at the interface. The ratios of the reflected and transmitted electric field components to the incident field components are referred to as the "Fresnel coefficients" of reflection or transmission from a single interface. The boundary conditions lead to different equations for *s*-waves and *p*-waves, as their field components are oriented along different planes.

Consider a single interface between the first medium and the second medium, where each is described optically by their respective complex refractive indices, \tilde{N}_1 and \tilde{N}_2 . When the beam is incident from the first medium onto the second one, the Fresnel reflection coefficients for *p*-waves and *s*-waves are given by

$$r_{p,12} = \frac{E_p^{refl}}{E_p^{inc}} = \frac{\tilde{N}_2 \cos \phi_1 - \tilde{N}_1 \cos \phi_2}{\tilde{N}_2 \cos \phi_1 + \tilde{N}_1 \cos \phi_2} \quad (2.20a)$$

$$r_{s,12} = \frac{E_s^{refl}}{E_s^{inc}} = \frac{\tilde{N}_1 \cos \phi_1 - \tilde{N}_2 \cos \phi_2}{\tilde{N}_1 \cos \phi_1 + \tilde{N}_2 \cos \phi_2} \quad (2.20b)$$

with angles of incidence and refraction as ϕ_1 and ϕ_2 (related by Snell's law). The corresponding Fresnel transmission coefficients are

$$t_{p,12} = \frac{E_p^{tran}}{E_p^{inc}} = \frac{2\tilde{N}_1 \cos \phi_1}{\tilde{N}_1 \cos \phi_2 + \tilde{N}_2 \cos \phi_1} \quad (2.21.a)$$

$$t_{s,12} = \frac{E_s^{tran}}{E_s^{inc}} = \frac{2\tilde{N}_1 \cos \phi_1}{\tilde{N}_1 \cos \phi_1 + \tilde{N}_2 \cos \phi_2} \quad (2.21b)$$

As intensity is related to the square of the amplitude of the electric-field, we can determine the ratio of reflected and transmitted intensity to the incident intensity, as:

$$\mathfrak{R}_p = \frac{|E_p^{refl}|^2}{|E_p^{inc}|^2} = |r_p|^2 \quad (2.22a)$$

$$\mathfrak{R}_s = \frac{|E_s^{refl}|^2}{|E_s^{inc}|^2} = |r_s|^2 \quad (2.22b)$$

$$T_p = \frac{|E_p^{tran}|^2}{|E_p^{inc}|^2} = |t_p|^2 \quad (2.22c)$$

$$T_s = \frac{|E_s^{tran}|^2}{|E_s^{inc}|^2} = |t_s|^2 \quad (2.22d)$$

These are referred to as the polarized reflectance and transmittance.

2.5.3 THE BREWSTER ANGLE

The equations of Fresnel contain several complex numbers. If both materials are transparent (i.e., $k = 0$), however, all of the terms in the previous Fresnel

equations are real numbers. Figure 2.11a shows a plot of both Fresnel coefficients as a function of the angles of incidence, for a dielectric material such as TiO_2 . This material has $n = 2.2$ and $k = 0$ at a wavelength of 632 nm.

At normal incidence, r_p and r_s have equal magnitudes, but opposite signs. This is due to our definition of positive directions for the p - and s -electric fields of incident and reflected beams. For a single interface, the reflectance is simply the square of the Fresnel reflection coefficient. Figure 2.11b shows the reflectance, \mathfrak{R} , also plotted versus the angle of incidence. At normal incidence, cosine terms are equal to +1, the index for air is unity, and we have

$$r_{p,12} = \frac{n_2 - 1}{n_2 + 1} \quad (2.23a)$$

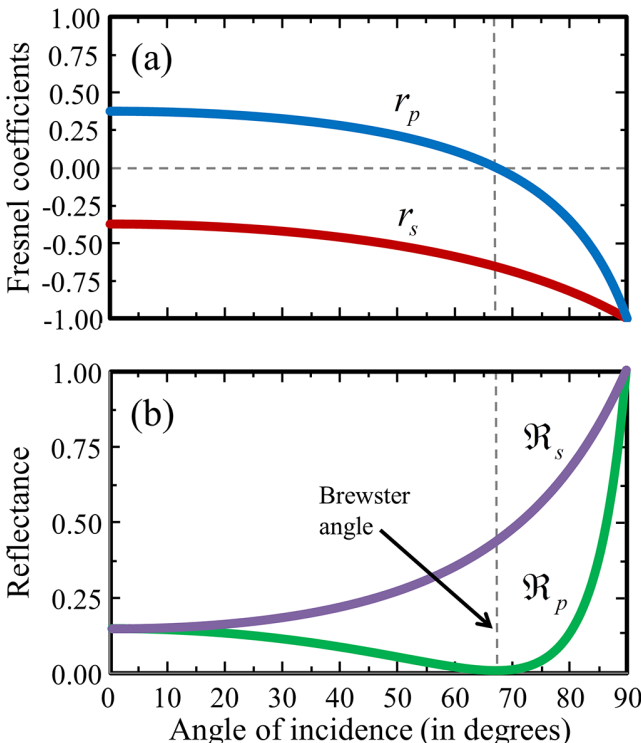


Figure 2.11. (a) Fresnel reflection coefficients, and (b) the reflectance, plotted versus the angle of incidence for light incident from air onto a dielectric such as TiO_2 , with $n = 2.2$ and $k = 0$ at a wavelength of 632 nm. At the Brewster angle, all of the reflected light is polarized with the electric vector perpendicular to the plane of incidence.

$$r_{s,12} = \frac{1-n_2}{1+n_2} \quad (2.23b)$$

$$\Re_p = \Re_s = \left(\frac{n_2 - 1}{n_2 + 1} \right)^2 \quad (2.23c)$$

The reflectance of the two waves must be equal at normal incidence since the plane of incidence is no longer uniquely defined.

For oblique angles, we see that r_s is always negative and nonzero whereas r_p is positive for angles near-normal, passes through zero, and is negative for near-grazing angles of incidence. This can be rationalized algebraically [3] from the relationship $n_2 > n_1$ and $\cos \phi_1 > 0$.

At the angle of incidence where r_p crosses zero, the reflectance \Re_p is also zero, hence all of the reflected light is polarized with the electric field perpendicular to the plane of incidence, that is, s -waves. This is shown in Figure 2.11b as the “Brewster angle.” This phenomenon was discovered by David Brewster in the early 1800s. This angle is also known as the “Polarizing Angle” and sometimes the “Principal Angle.”

Two significant ramifications of the Brewster angle are that at that angle, designated as ϕ_B ,

$$\tan \phi_B = \frac{n_2}{n_1} \quad (2.24)$$

and

$$\cos \phi_2 = \sin \phi_1 \quad (2.25)$$

Equation 2.25 implies that the angle between the reflected beam and the transmitted beam is a right angle. One additional feature of the Brewster angle for transparent materials is that the phase of the p -wave on reflection shifts abruptly from zero to 180° . No such shift occurs for the s -wave.

The Brewster angle is a function of the index of refraction, and as indicated earlier, the index of refraction is a function of wavelength. Hence, the Brewster angle is a function of wavelength. The term “Brewster wavelength” is sometimes used with a single angle-of-incidence. This is simply the wavelength where the value of the index of refraction matches the Brewster condition for that angle-of-incidence.

The concept of the Brewster angle or polarizing angle is used routinely by photographers for objects that are under water. The light coming from

the underwater object (e.g., fish or alligators) is often significantly less than the light reflected from the top surface of the water and the reflected light will obscure the underwater object. If the angle of incidence of the reflected light is roughly equal to the Brewster angle, a polarizer adjusted to the correct azimuth will remove the surface reflection, which is purely *s*-polarized, allowing the camera to capture the light from the underwater object.

When the reflecting surface is not transparent, that is, k is nonzero, the situation becomes more complicated. The Fresnel reflection coefficients are now complex numbers and the concepts of “greater than zero” and “less than zero” have no meaning. Normally, there is no situation where both the real and imaginary parts of the complex number are zero; hence there is no analogous version for Figure 2.11a for metals or semiconductors. The reflectance values, \Re_p and \Re_s , are real numbers, however, and can be plotted, as indicated in Figure 2.12, for Tantalum. Although \Re_p does not go to zero, it does go through a minimum at an angle that is called the principal angle.

For a transparent material, the phase difference between the *p*-wave and *s*-wave abruptly changes from 180° to zero when increasing through the Brewster angle, as shown in Figure 2.13. For absorbing materials, the phase difference shifts gradually, rather than abruptly, again as shown in Figure 2.13. For metals, as for all other materials, the phase difference passes through 90° at the principal angle.

It might be noted that high reflectance is obtained when the index of the substrate is significantly different from that of the ambient. This

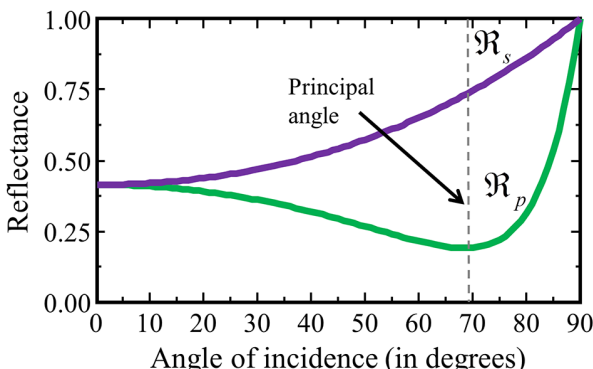


Figure 2.12. The reflectance, plotted versus the angle of incidence, for a metal such as Ta with $n = 1.72$ and $k = 2.09$ at a wavelength of 632 nm.

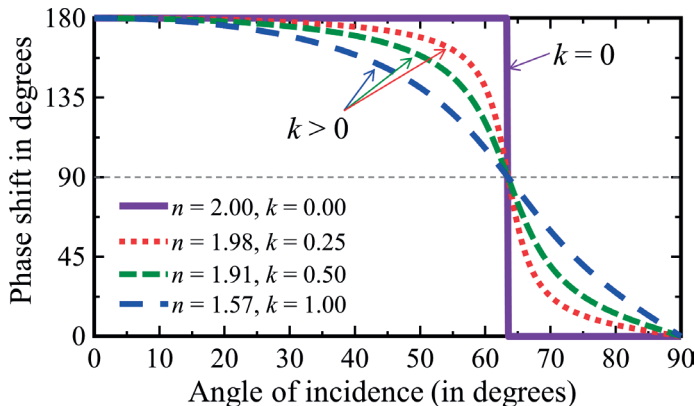


Figure 2.13. Phase shift, as a function of angle-of-incidence for a transparent material ($k = 0$) and for materials with successively larger values of k . The optical constants have been adjusted such that the principal angle is the same for all of the materials.

can occur when n_2 is significantly different from 1.0 or when k_2 is large (significantly different from zero).

2.5.4 REFLECTIONS WITH FILMS

For reflection ellipsometry, when only one interface is present (i.e., the sample is a substrate), the light which is reflected is often measured and used. The light which passes through the interface (i.e., is transmitted) can normally be ignored. However, this is not the case when more than one interface is present (i.e., with a film). As suggested by Figure 2.14, the resultant reflected wave returning to the first medium will consist of light which is initially reflected from the first interface as well as light which is transmitted by the first interface, reflected from the second interface, and then transmitted by the first interface going in the reverse direction, and so on. Each successive transmission back into the first medium is smaller than the last, and the infinite series of partial waves makes up the resultant reflected wave.

From a macroscopic point of view, the quantities of interest are the amplitude of the incoming wave and the amplitude of the resultant outgoing wave. For the ellipsometry technique, we are interested in the phase and amplitude relationships between the p -wave and the s -wave.

The ratio of the *amplitude* of the outgoing resultant wave to the *amplitude* of the incoming wave is defined as the “Total Reflection

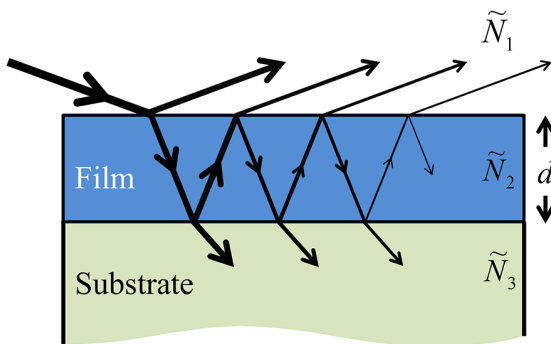


Figure 2.14. Reflections and transmissions for two interfaces. The resultant reflected beam is made up of the initially reflected beam and the infinite series of beams, which are transmitted from the second medium back into the first medium.

Coefficient" and is analogous to the Fresnel reflection coefficients for a single interface. For a single film (two interfaces) this is

$$R_p = \frac{r_{p,12} + r_{p,23}e^{-i2\beta}}{1 + r_{p,12}r_{p,23}e^{-i2\beta}} \quad (2.26a)$$

$$R_s = \frac{r_{s,12} + r_{s,23}e^{-i2\beta}}{1 + r_{s,12}r_{s,23}e^{-i2\beta}} \quad (2.26b)$$

where

$$\beta = 2\pi \left(\frac{d}{\lambda} \right) \tilde{N}_2 \cos \phi_2 \quad (2.27)$$

These equations are derived in Tompkins and McGahan [4].

When $k \neq 0$, the Fresnel coefficient, \tilde{N}_2 , and $\cos \phi_2$ (and hence, β) are complex numbers. When $k = 0$, these numbers are real. In general, except for very special circumstances, R_p and R_s are complex numbers. β is the phase change in the wave, as it moves from the top of the film to the bottom of the film. Hence, 2β is the phase difference between the part of the wave reflecting from the top surface and the part of the wave which has traversed the film twice (in and out).

2.5.5 STACK CALCULATIONS

We now consider the interaction of light with more than one layer on a substrate. Each additional interface gives rise to reflection and transmission and it soon becomes cumbersome to track all the wave components traveling within each layer.

Matrix methods provide an elegant representation of each layer and simplify the math involved [1, 40]. In one such approach, each thin film is represented by two matrices—one for the interface and another for the bulk of the film. Figure 2.15 shows such a multilayer stack and how the math is constructed using 2×2 layer (L) and 2×2 interface (I) matrixes. Matrix multiplication leads to a single transfer matrix that describes the outgoing to the incoming p - and s -electric fields.

2.6 MEASUREMENT QUANTITIES

2.6.1 REFLECTANCE AND TRANSMITTANCE

The reflectance is defined as the ratio of the *intensities* of the outgoing wave to the incoming wave. The total reflection coefficients, R_p and R_s , are defined as the ratio of *amplitudes* of the outgoing wave to the incoming wave. Hence, the reflectance is the square of the magnitude of the total reflection coefficient, that is,

$$\Re_p = |R_p|^2 \quad (2.28a)$$

$$\Re_s = |R_s|^2 \quad (2.28b)$$

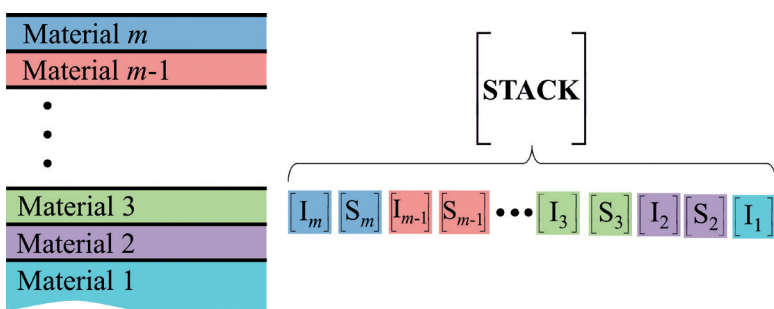


Figure 2.15. Matrix representation of a multilayer stack.

Similar equations can be shown for the transmitted intensity (transmittance). The reflectance and transmittance are very common measurement quantities from devices such as spectrophotometers. Measurements are often at normal incidence (0°), such that the polarization state is of no concern. Even when measurements are performed at oblique angles, it is common to use unpolarized light as this simplifies the instrumentation required. An unpolarized reflectance or transmittance measurement will be equivalent to the average of the *p*- and *s*-polarized values.

2.6.2 DELTA AND PSI

In Figure 2.10, we showed the *p*-waves and *s*-waves reflecting from a surface. When each reflects, there is a possible phase shift for the *p*-waves and *s*-waves, and the shift is not necessarily the same for each. Let us denote the phase difference between the *p*-wave and the *s*-wave before the reflection as δ_1 and the phase difference after the reflection as δ_2 . We define the parameter Δ , called “delta” as

$$\Delta = \delta_1 - \delta_2. \quad (2.29)$$

Δ , then, is the phase shift induced by the reflection and this value can be from -180° to $+180^\circ$ (or alternatively, from 0° to 360°).

In addition to a phase shift, the reflection will also induce an amplitude reduction for both the *p*-wave and *s*-wave, and again, it will not necessarily be the same for each. The total reflection coefficient for the *p*-wave (R_p) and *s*-wave (R_s) was previously defined as the ratio of the outgoing wave amplitude to the incoming amplitude and, in general, this is a complex number. We define the quantity Ψ , called “psi,” such that

$$\tan \Psi = \frac{|R_p|}{|R_s|} \quad (2.30)$$

Ψ is the angle whose tangent is the ratio of the magnitudes of the total reflection coefficients, and its value can range from 0° to 90° . The effect of Ψ and Δ is such that linearly polarized light will be altered to elliptically polarized light upon reflection from the surface of a sample, as shown in Figure 2.16.

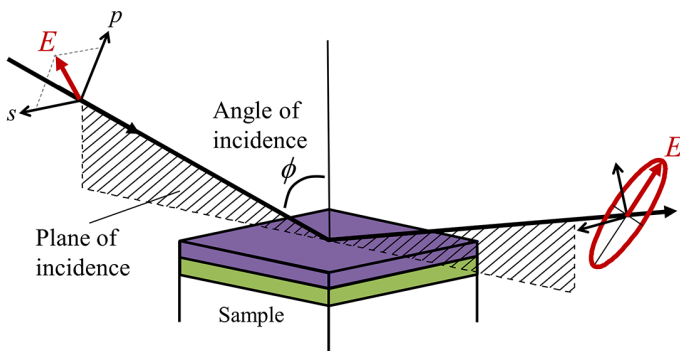


Figure 2.16. Ellipsometry measurement is shown with incident linearly polarized light oriented with both p - and s -components. The interaction with the sample leads to different amplitudes and phase for the reflected p - and s -polarizations, producing elliptically polarized light.

2.6.3 FUNDAMENTAL EQUATION OF ELLIPSOMETRY

As discussed, $\tan \Psi$ is defined as the ratio of the magnitudes of the total reflection coefficients, and is hence a real number. Let us define a complex number ρ (rho) to be the complex ratio of the total reflection coefficients, that is,

$$\rho = \frac{R_p}{R_s} \quad (2.31)$$

The fundamental equation of ellipsometry [1] then is

$$\rho = \tan \Psi e^{i\Delta} = \frac{R_p}{R_s} \quad (2.32)$$

Then $\tan \Psi$ is the magnitude of ρ and the exponential function is the phase of ρ . The quantities Ψ and Δ (sometimes only $\cos \Delta$) are measured by ellipsometers. These are properties of our probing light beam. The information about our sample is contained in the total reflection coefficients, and hence in ρ . It should be noted that assuming our instrument is operating correctly, the measured quantities Δ and Ψ are always correct. We deduce the quantities such as thickness and optical constants from regression analysis. Whether these quantities are correct or not depends on

our model assumptions. As an example, incorrect values of n and k can be deduced if we assume that our material is a substrate when in fact we have a thin layer of one material on top of a substrate of another material. This simply makes the point that the quantities that ellipsometers measure are Δ and Ψ . Quantities such as thickness and optical constants are calculated quantities based on an assumed model.

2.6.4 N , C , AND S

There are many ways to represent the polarization change that is measured by an ellipsometer. Ψ and Δ have become ubiquitous due to their early adoption in null-ellipsometers. In these early single-wavelength instruments, the optical elements were oriented until the detected light vanished (was null). Ψ and Δ were directly related to optical readings from these early devices used predominately before 1990. In Chapter 3, we will discuss the operation of modern ellipsometers, which do not measure Ψ and Δ directly. Rather, they collect a modulated intensity that can be related to the polarization change. The actual values most directly related to the instrumentally measured intensities are referred to as N , C , and S and are given in relation to Ψ and Δ as:

$$N = \cos(2\Psi) \quad (2.33a)$$

$$C = \sin(2\Psi)\cos(\Delta) \quad (2.33b)$$

$$S = \sin(2\Psi)\sin(\Delta) \quad (2.33c)$$

By their nature, each of these three parameters is bounded between -1 and $+1$. Determination of all three parameters is equivalent to measurement of the full range of Ψ and Δ values. As we will see in the next chapter, early rotating-analyzer ellipsometer configurations were limited to a measure of N and C , which reduced the range of Δ to 180° , rather than the full 360° .

2.6.5 JONES AND MUELLER MATRICES

The ellipsometry measurement can be represented by a set of linear equations to describe the interaction of p -waves and s -waves with the sample. The Jones vector notation treats polarized light as two complex numbers (amplitude and phase) describing the p - and s -electric fields.

A 2×2 Jones matrix is then used to describe the sample, or any optical element that may alter the polarization. For an isotropic sample, there is no cross-polarization between p - and s -waves. In other words, p -polarized light will remain p -polarized and s -polarized light will remain s -polarized. However, they will undergo their own amplitude reduction and phase change. This is represented by a sample Jones matrix (in different forms), as:

$$\begin{bmatrix} E_p \\ E_s \end{bmatrix}_{out} = \begin{bmatrix} r_p & 0 \\ 0 & r_s \end{bmatrix} \begin{bmatrix} E_p \\ E_s \end{bmatrix}_{in} = r_s \begin{bmatrix} \tan(\Psi)e^{i\Delta} & 0 \\ 0 & 1 \end{bmatrix} \begin{bmatrix} E_p \\ E_s \end{bmatrix}_{in} = r_s \begin{bmatrix} \rho & 0 \\ 0 & 1 \end{bmatrix} \begin{bmatrix} E_p \\ E_s \end{bmatrix}_{in} \quad (2.34)$$

The Jones description is limited to polarized light and is not able to describe partially polarized or unpolarized light. For these important cases, the sample (or optical element) can be described using the Stokes–Mueller representation. Here, each light beam is described by four real intensities making up a Stokes vector, while a 4×4 Mueller matrix describes the transformation of light. For the Stokes–Mueller description, an isotropic sample will have off-diagonal 2×2 blocks that are zero (because of no cross-polarization between p - and s -waves), as:

$$\begin{bmatrix} S_0 \\ S_1 \\ S_2 \\ S_3 \end{bmatrix}_{out} = m_{11} \begin{bmatrix} 1 & -N & 0 & 0 \\ -N & 1 & 0 & 0 \\ 0 & 0 & C & S \\ 0 & 0 & -S & C \end{bmatrix} \begin{bmatrix} S_0 \\ S_1 \\ S_2 \\ S_3 \end{bmatrix}_{in} \quad (2.35)$$

where N , C , and S are the ellipsometric parameters discussed in the prior section and m_{11} is the reflected intensity for unpolarized light. Note the importance of N , C , and S when considering the Mueller-matrix for an isotropic sample. The full implications of these mathematical descriptions are beyond the scope of this book, but can be found in Humlcek [40] and Jellison [41].

CHAPTER 3

SPECTROSCOPIC ELLIPSOMETRY COMPONENTS AND INSTRUMENTATION

In this chapter, we review the key components of any spectroscopic ellipsometer. Many are essential, such as a light source, a detector, and a method to separate wavelengths. Of equal significance are optical elements to control and detect light polarization—typically polarizers, compensators, or phase modulators (PMs). With these basic components, a variety of ellipsometry configurations are achieved. We review the most common: rotating analyzer or polarizer, rotating compensator, and phase modulation ellipsometers.

3.1 COMPONENTS OF A SPECTROSCOPIC ELLIPSOMETER

We start with a review of the individual components within an ellipsometer. These components can be divided into two categories, depending on whether they manipulate the light polarization. Every ellipsometer must have a source of light and a method to detect that light. In addition, spectroscopic ellipsometers must have a means to discriminate the different wavelengths. While these are essential, they could also be used to construct a simple photometric instrument to detect reflected or transmitted intensity.

The essence of an ellipsometer is the measure of polarization. Thus, optical elements are required to manipulate the light polarization—both forming a known polarization before the sample and detecting the resulting polarization after the sample. We introduce the key polarizing optics used by spectroscopic ellipsometers. There may be additional optical elements, such as lenses, mirrors, and pinholes, within the ellipsometer

to guide the measurement beam. However, we restrict discussion to the optical elements required to make the ellipsometry measurement.

3.1.1 POLARIZATION STATE GENERATOR AND DETECTOR

One key difference between spectroscopic ellipsometers and other optical instruments is the measure of polarization. Photometric tools, such as reflectometers, simply measure the light intensity—in this case, reflected from the sample surface. This makes ellipsometry unique and introduces important system requirements. Specifically, ellipsometry needs both a means of creating and then measuring light polarization.

Ellipsometer instrumentation can be split into two primary sections, separated by the sample. The optical elements before the sample have the general role of producing a known polarization state for the light that is to interact with the sample, and are thus referred to collectively as the polarization state generator (PSG). The polarization generated within this section does not have to be linear and can even vary with time—but it should be “known.” The polarized light interacts with the sample (reflection or transmission), which produces a change to the initial polarization. The change in polarization needs to be determined in order to access the sample properties that caused this change. Thus, the optical components after the sample function to detect the new “unknown” polarization state. They are referred to collectively as the polarization state detector (PSD). The basic ellipsometry components are shown in Figure 3.1.

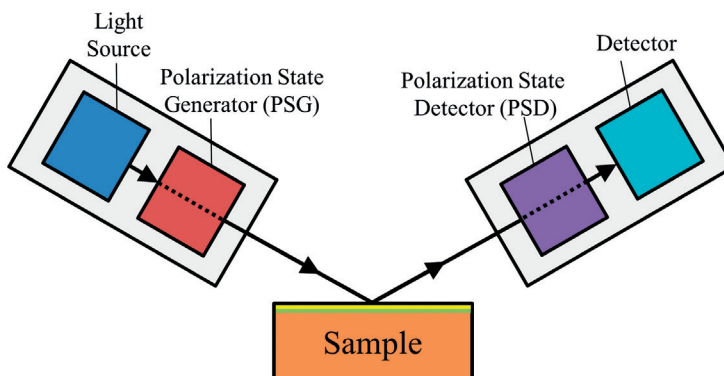


Figure 3.1. Light passes through the PSG to create a known polarization that reflects from the sample surface at a specified angle of incidence. The light reflects to the PSD which determines the polarization change caused through interaction with the sample.

3.1.2 SOURCES

Spectroscopic Ellipsometers require a light source that covers a broad range of wavelengths. Thus, we will not discuss laser or light emitting diode sources, as their spectral output is confined to a single or narrow range of wavelengths. Lamps are the most common spectroscopic light sources. Arc-lamps, such as Xenon and Deuterium lamps, operate by exciting molecules within a plasma of ionized gas that emits light when returning to their initial state. Incandescent lamps, such as quartz-tungsten-halogen (QTH), operate by passing electricity through a material (filament) to increase the temperature to the point where it radiates light. A similar physical process is used by SiC globars, which produce infrared blackbody radiation by heating the SiC material.

Figure 3.2 shows the approximate wavelength coverage for various lamps. As shown, Deuterium lamps produce light at ultraviolet wavelengths below about 400 nm. Xenon lamps can produce light from 185 nm to 2000 nm. Halogen lamps radiate wavelengths above 350 nm extending into the near infrared. Silicon carbide globars cover mid-infrared wavelengths.

The output of each lamp can vary widely within their useable wavelength range. For ellipsometry, it is important that light is available at all measured wavelengths and that any intensity fluctuations are on a different time-scale from the measurement cycle. For example, if an

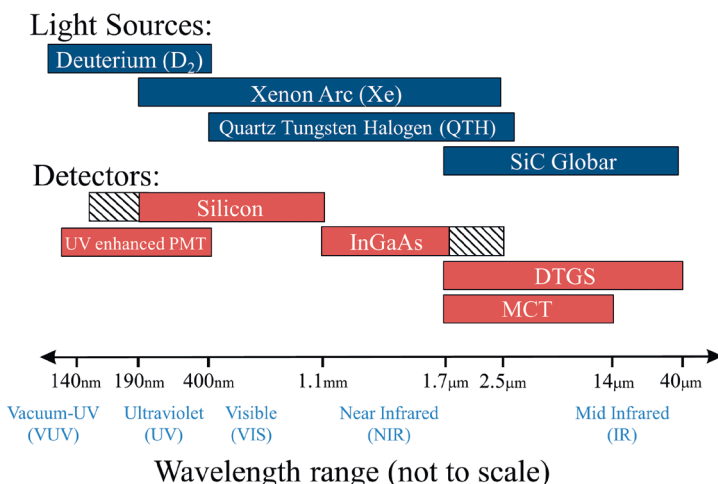


Figure 3.2. Wavelength range is shown for common spectroscopic ellipsometry (SE) sources and detectors.

ellipsometer requires 1/10th of a second to complete a measurement cycle, the light source should be stable within that time-frame.

3.1.3 DETECTORS

The electric field oscillates too quickly to measure directly, so the polarization state is determined from the irradiance (intensity). Thus, every ellipsometer contains a detector to convert the electromagnetic field to a measurable property. This is generally done with a photodiode detector or detector array. Photodetection works by converting the electromagnetic wave into a voltage or current that scales with the amount of light. The type of photodetector and detector material depends on wavelength range. The operational wavelengths of semiconductor detectors are related to the material bandgap. Bandgap energy is defined by the minimum photon energy of light that can excite an electronic transition within the material and is inversely related to light wavelength, as:

$$E_{gap} = \frac{1,240}{\lambda_{nm}} \quad (3.1)$$

Detection occurs at wavelengths shorter than calculated from Equation 3.1 and smaller bandgap energies allow detection of longer wavelengths.

The most common photodetector material is silicon, which can detect ultraviolet and visible wavelengths. Silicon has a bandgap of 1.1eV, so the upper detection wavelength is about 1100 nm. Photodetectors using InGaAs ternary alloys have a lower bandgap near 0.5 to 0.7 eV, depending on composition and strain. This allows operation at near infrared wavelengths up to 1700 nm to 2500 nm. Mid-infrared detectors, such as mercury-cadmium-tellurium (MCT) ternary alloys and deuterated triglycine sulfate (DTGS), have even smaller bandgaps. Figure 3.2 illustrates the useful detection wavelength range for a few common detector materials.

Another type of detector found in spectroscopic ellipsometers is the photomultiplier tube (PMT). It uses a photosensitive material called the photocathode, which will release electrons when struck by photons (light). The released electrons are accelerated through a series of dynodes, which release additional electrons. In this manner, the number of electrons related to the initial photon flux is multiplied before the final signal detection. PMT detectors are useful for very low light levels. The useful wavelength range of the PMT is primarily related to the photocathode material [42].

While photodiodes refer to a single detection element, many ellipsometers use photodetector arrays. This allows simultaneous collection

of light over many separate detector elements (pixels). While a few ellipsometers use the array to collect spatial image from the measurement spot at a single wavelength (imaging ellipsometry), it is more common to use the array to detect different wavelengths on each pixel. This is further described in the following section.

3.1.4 SPECTROMETERS, MONOCHROMATORS, AND INTERFEROMETERS

Spectroscopic ellipsometers must have a method to separate the wavelengths during measurement. Wavelength separation is most commonly achieved by refracting light through a prism or scattering light from a grating. Prisms refract different colors at different angles, as shown in Figure 3.3a. Their applicable wavelength range is limited to the transparent region of the prism material, but they maintain most of the light intensity when not absorbing. Gratings scatter different colors at different angles from a structured surface that has repeated features of size similar to the wavelength of light as shown in Figure 3.3b. As shown, some light can be specularly reflected (reflection angle equal to incident angle) and there can be multiple orders of scattered light in multiple directions. Thus, gratings are not as efficient as prisms, as the light is divided into different reflections. Gratings also have limited wavelength range, but this range can be shifted by using different feature sizes to scatter different wavelengths. Modern spectroscopic ellipsometers commonly combine multiple dispersive elements to cover wider-and-wider wavelength ranges.

While the grating or prism is the wavelength-dispersing optical element, they are integrated into an optical device such as a monochromator or spectrometer. The monochromator converts spectroscopic light to

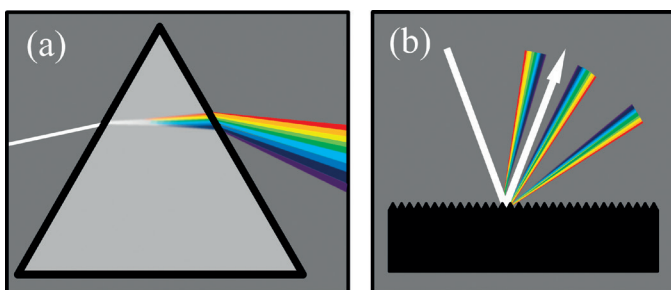


Figure 3.3. Colors can be dispersed in different directions by (a) refraction through a prism, or (b) scattering from a diffraction grating.

a single wavelength, by isolating a narrow spatial section of the wavelength-dispersed light. Figure 3.4a shows light passing through a single-chamber monochromator where white light is first collimated onto the grating to achieve the wavelength dispersion and then a single wavelength is focused onto the exit slit. The slit allows only a narrow spectral region of the beam to pass through—essentially limiting the outgoing light to a single, narrow wavelength range. While not as narrow as a laser-wavelength, the bandwidth of the outgoing light can be controlled by closing or opening the slit. Thus, bandwidth can be tailored depending on application requirements. It is not always preferred to have the narrowest wavelength, as this also greatly reduces measurement signal intensity. The monochromator is used in ellipsometers that have a single photodiode or PMT detection system. Spectroscopic ellipsometers that utilize a monochromator are inherently slow since they measure only one wavelength at any given time. However, monochromators offer inherent advantages: (i) the measurement can be optimized at each individual wavelength, and (ii) the monochromator can be situated before the sample to avoid illuminating photosensitive sample surfaces (such as photolithographic films) with intense spectroscopic light. The first advantage not only includes modifying the slit width to optimize intensity versus bandwidth but also the possibility to switch between different dispersive gratings that are optimized for different wavelength ranges.

A dispersive spectrometer is commonly used in ellipsometers that have a detector array. The broadband light is dispersed such that different wavelengths are imaged onto the detector array. Thus, each individual detecting element collects a different color. This is demonstrated in Figure 3.4b where white light (all colors) in the spectrometer is dispersed

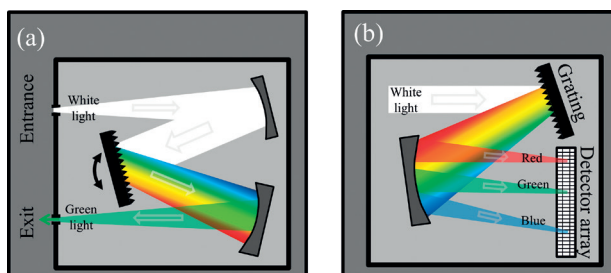


Figure 3.4. (a) A monochromator is used to isolate a single wavelength of light, while (b) a spectrometer is used to image the refracted light directly onto a detector array for simultaneous collection of all wavelengths.

from a grating before being collected at the detector array. While we show only 3 colors, in reality an entire spread of wavelengths is imaged across the detector array. In this manner, spectrometers can detect many different wavelengths at the same time. This significantly increases the spectroscopic measurement speed such that a thousand wavelengths can be simultaneously detected. One drawback is that dispersive spectrometers cover a limited wavelength range. Several methods are often used to divide the beam and use multiple spectrometers to stitch different wavelength ranges together.

Infrared ellipsometers generally utilize Fourier transform infrared (FTIR) spectroscopy for wavelength separation. FTIR uses a Michelson Interferometer where a scanning mirror changes the interferometer path length to modulate the light beam. Different wavelengths are modulated at different rates. A Fourier transform of the interferogram produces the intensity spectrum to measure all wavelengths simultaneously. FTIR uses the entire light beam for measurement, can cover much wider wavelength ranges than dispersive spectrometers, and wavelength resolution can be optimized for the application.

3.1.5 MANIPULATING POLARIZATION

The ellipsometry measurement is essentially a measure of polarization. Thus, there are critical components within all ellipsometers to either create or detect the polarization. Before discussing the most common polarizing optical components, we review how polarization can be manipulated.

Polarization is formed through the interaction of light and materials. The interaction can include reflection, refraction, transmission, or absorption. The optical constants (n, k) of each material establish these optical interactions. We need to first differentiate between isotropic and anisotropic optical properties. The former have the same optical constants in all directions. The latter refer to materials that have different optical constants depending on the orientation of the electric field in the material. Optically anisotropic materials are also called birefringent materials. Their distinct optical axes are commonly referred to as the ordinary and the extraordinary directions. We consider the interactions that may affect light polarization, keeping in mind the distinction between isotropic and anisotropic materials.

Reflection: Reflection from a surface can produce a polarization change. For isotropic materials, this relies on the difference between the p - and s -electric field interactions at the interface. Reflection at normal incidence reduces intensity but does not change polarization. Reflec-

tion at oblique angles (Figure 3.5a) produces different amplitudes and phases for reflected and transmitted *p*- and *s*-electric fields. Thus, any light reflecting at an oblique angle that contains electric fields in both planes will experience a polarization change. In Figure 3.5, this is represented by showing the phases of the *p*- and *s*-waves as arrows and circles, respectively. If the incoming light is linearly polarized along only the *p*- or *s*-plane, the reflected light remains linearly polarized in the same plane. Reflection at the Brewster angle from transparent substrates produces a special effect where only the linearly polarized light along the *s*-direction is reflected, regardless of the incoming polarization.

Anisotropic materials also produce a polarization change upon reflection. In addition, it is possible to produce cross-polarization between the *p*- and *s*-components. Thus, linearly polarized *p*- or *s*-light reflected from anisotropic materials can experience a polarization change, depending on the alignment of the anisotropic optical axes with respect to the plane of incidence.

Total internal reflection: The amount of light that is reflected from a surface depends on the angle of incidence, the electric field direction, and the change in optical constants across the interface. For the special case where light is incident at an interface from a higher index to a lower index, there is total internal reflection at angles equal to or above the critical angle (θ_c):

$$\theta_c = \sin^{-1} \left(\frac{n_t}{n_i} \right) \quad (2.2)$$

where n_t and n_i are the indexes for transmitted and incident materials, respectively. This effect is beneficial in optics as light intensity is maintained and yet a polarization change can occur. Figure 3.5b shows

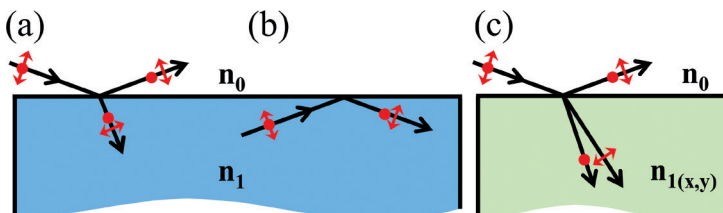


Figure 3.5. Polarization change can occur upon (a) reflection from a surface, (b) total internal reflection, which maintains the light intensity, and (c) refraction into a birefringent material. The *p*- and *s*-light components are represented by arrows and circles, respectively.

this effect going from the higher index of n_1 to the lower index of n_0 . All of the light is reflected back into the material, yet a polarization change occurs, as represented by the shift between p - and s -reflected components.

Refraction: The refracted light at an interface can also experience a polarization change (Figure 3.5a). In addition, the refracted angle is different from the incoming incident angle—changing the direction of the light. For anisotropic materials, an interesting effect can be observed where the p - and s -polarizations refract at different angles (Figure 3.5c). For this reason, anisotropic materials are also called birefringent (two refractions) materials.

Transmission and absorption: Polarization is not affected by travel through an isotropic material. However, the polarization can change when traveling through anisotropic materials due to two different effects. First, the polarization can be modified due to different phase velocities that occur as a result of different indexes of refraction. Second, the polarization can be modified due to different amounts of absorption when the anisotropic material has different extinction coefficients.

Figure 3.6 shows light traveling through an anisotropic material. The different indexes of refraction along the x - and y -directions lead to different phase velocities for electric fields along these directions. Consider linearly polarized light, where x - and y -electric fields are in-phase, traveling into the material. The electric field that experiences the lower index of refraction will have a faster phase velocity. For this reason, the lower index of refraction is along what is referred to as the “fast-axis” of the material. The total phase delay between the x - and y -electric fields due to travel through the anisotropic material is referred to as retardance (δ).

Figure 3.7 shows light traveling through an anisotropic material that has different extinction coefficients along the x - and y -directions. This

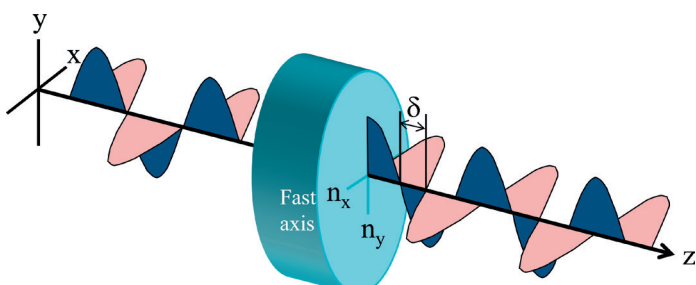


Figure 3.6. Demonstration of retardance caused by light traveling through anisotropic material with different indexes of refraction along the x - and y -directions.

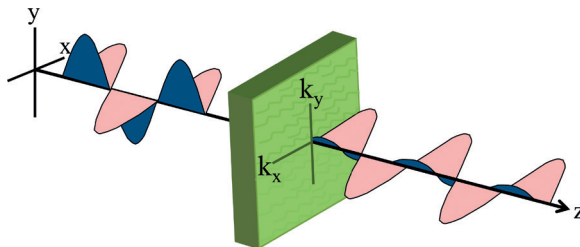


Figure 3.7. Diattenuation of a light beam is shown due to travel through a linearly dichroic material with stronger extinction coefficient along the y-direction.

is referred to as a linearly dichroic material because it absorbs different amounts of light along orthogonal linear polarizations. The amplitude is diminished along the y -direction due to a larger extinction coefficient along this direction. The effect of reducing light intensity between orthogonal directions is also called diattenuation. Figure 3.7 demonstrates linear diattenuation from a linearly dichroic material. Some materials differentiate between left- and right-circularly polarized light and are thus called circularly dichroic. They can produce circular diattenuation, which reduces the amplitude of right and left circular polarizations by different amounts.

Now that we have reviewed the common methods to change polarization, we will see how they are utilized within the polarizing optical elements of a spectroscopic ellipsometer.

3.1.6 POLARIZERS

Polarizers are a common optical element found in almost every spectroscopic ellipsometer. Their basic function is to change any polarization into linearly polarized light. This is demonstrated in Figure 3.8 where unpolarized light enters a polarizer. The extinction axis of the polarizer blocks that direction of light, allowing only the orthogonal, linearly polarized component to transmit through the polarizer.

Polarizers isolate the linear polarization via some of the phenomena discussed in Section 3.1.5. Polarizers can reflect light at the Brewster angle to isolate only the s-reflected component. Polarizers can use diattenuation through a dichroic material, such as a thin film Polaroid sheet or wire-grid (which is used to polarize mid-infrared wavelengths). However, the most common method used by polarizers is to send light through birefringence crystal prisms. Many polarizer designs exist such as Wollaston, Nicol,

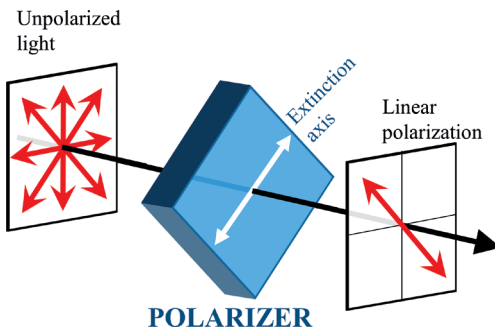


Figure 3.8. Basics of polarizer operation.

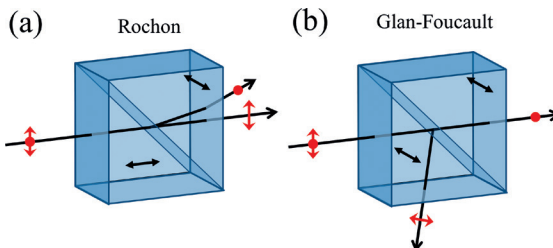


Figure 3.9. Two examples of crystal polarizers, which use anisotropic prisms with optical axes denoted by black arrows to separate the ordinary and extraordinary beams via refraction as shown in (a) a Rochon prism, or total internal reflection as shown in (b) a Glan–Foucault prism.

Glan–Taylor, and Glan–Thompson prisms, to name a few. Each design works by separating the beam direction within anisotropic prisms through refraction or total internal reflection. Figure 3.9 shows two different crystal polarizers. The Rochon polarizer (Figure 3.9a) transmits the ordinary ray, while refracting the extraordinary ray. The Glan–Foucault polarizer (Figure 3.9b) transmits the extraordinary ray, while reflecting the ordinary ray. In either case, a linear polarization can be isolated from its orthogonal direction for use within the ellipsometer.

The polarizer quality is judged by how close to linearly polarized the exiting light has become. This is often specified by the extinction ratio, which compares the intensity of the desired direction to the intensity of the orthogonal, unwanted direction. An extinction ratio of 100,000 to 1 is considered excellent. Lower quality polarizers may still be used, especially for special wavelength regions, but require special corrections to calculate accurate data.

3.1.7 COMPENSATORS

Compensators are another common optical element used within an ellipsometer to manipulate polarization. Compensators delay the phase between orthogonal electric field orientations. Compensators are also referred to as waveplates or retarders because they delay (or retard) the wave along one direction relative to another. A compensator can retard the wave by any specified phase and this amount is typically wavelength dependent. When the compensator is designed to impart 90° or 180° of total phase retardation at the designed wavelength, it is referred to as a Quarter Waveplate (QWP) or Half Waveplate (HWP), respectively.

The primary function of a compensator is to change the polarization state of the light. When the retardance is 90° ($1/4$ of the wavelength), the compensator, or QWP, can change linearly polarized light into circularly polarized light and vice versa. A HWP can rotate the polarization direction—changing linear horizontal polarization to linear vertical polarization, for example. A HWP can also change left-circular polarized light to right-circular polarized light, and vice versa.

The phase compensation can be achieved via reflection or more commonly via transmission through an anisotropic material. Figure 3.10 illustrates a compensator with 90° of retardance, which changes the linear polarization to circular polarization. This requires alignment of the compensator fast axis such that equal amounts of linearly polar-

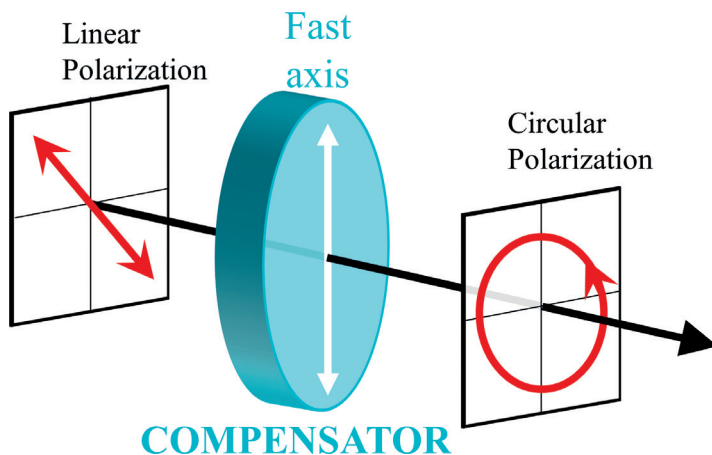


Figure 3.10. Linearly polarized light passes through a compensator to become circularly polarized light.

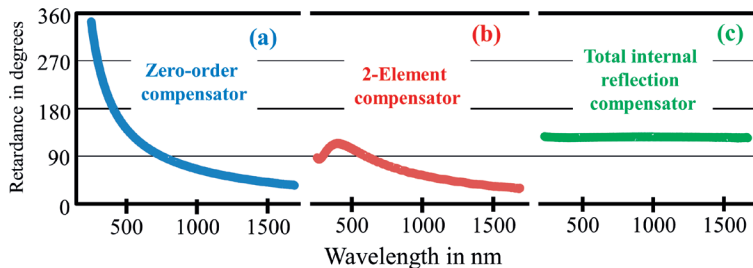


Figure 3.11. Three different compensators are compared. A single-element compensator (a) shows a large amount of variation in total phase retardation. The wavelength dependence is reduced by stacking two compensator elements (b) at different orientations. A total internal reflection compensator (c) has the flattest wavelength dependence.

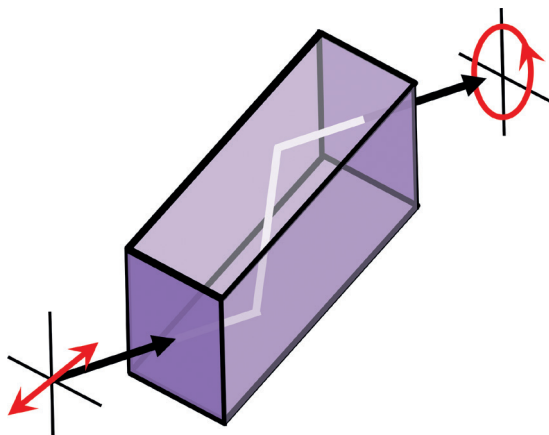


Figure 3.12. The polarization changes from linear to elliptical due to multiple total-internal-reflections within this rhombohedral prism.

ized light components travel along both the fast and slow axes of the compensator. The main drawback to compensators that use transmission through anisotropic media is that they have strong wavelength dependence, as shown in Figure 3.11a. Using multiple compensators that are rotated relative to each other is one way to modify the wavelength dependence, as shown in Figure 3.11b. Total Internal Reflection (TIR) can be a useful method to produce phase retardance. This has the benefit of transmitting most of the light and providing flat wavelength

dependence for the phase retardance, as shown in Figure 3.11c. The TIR compensator works by passing light through one or more prisms, as shown in Figure 3.12 for a rhombohedral prism. The light experiences a polarization change at each oblique reflection, adding to the total amount of retardance.

The total amount of phase compensation (retardance) does not have to equal 90° or 180° . For example, the TIR compensator of Figure 3.11c was designed to introduce 130° of phase retardance versus wavelength, as optimized for this specific ellipsometer design.

3.1.8 PHASE MODULATORS

A PM is similar to a compensator. It also functions to delay the phase between orthogonal directions. While compensators provide a fixed amount of retardance, PMs vary the retardation versus time. To do this, the optical anisotropy that produces the compensation is varied either through stress or alignment. In the case of crystal photoelastic modulators (PEM), a time-varying stress in the crystal produces time-varying compensation for transmitted light. Another approach is to use liquid crystals to modulate the light. Applying an electric field can align the liquid crystal that provides a different anisotropy and thus different amounts of phase compensation.

Figure 3.13 shows basic operation of a PEM, where linearly polarized light enters the device and exits with time-dependent modulated polarization. The compression and expansion within the crystal quartz (as shown with gray arrows) is electrically stimulated at a resonant frequency—typically around 50 kHz to 100 kHz. This leads to the opposite expansion or compression in the fused quartz side. The fused quartz is amorphous and would not alter the polarization, but the compression or expansion produces slight anisotropy which is the basis for the phase compensation. In Figure 3.13 a total phase compensation of $\pm 90^\circ$ occurs, so the exiting light modulates between right and left circular polarizations. The total amount of compensation depends on the device properties and applied voltage. It does not have to be 90° and there are good reasons to choose a different value in actual ellipsometry applications [24].

While PMs and compensators perform a similar function, the phase can be changed very quickly within a PEM. To change the retardance from a compensator requires it be rotated. We will show how both are involved in SE designs.

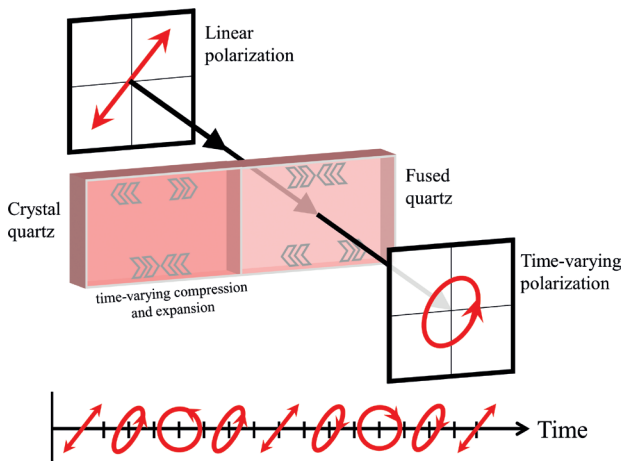


Figure 3.13. Linearly polarized light is modulated upon travel through a photoelastic modulator, where the compression and expansion (gray arrows) of the crystal quartz are resonating at 50 kHz to 100 kHz to produce the opposite effect in the amorphous fused quartz section, with the goal of producing enough strain-birefringence to retard the transmitted light.

3.2 SPECTROSCOPIC ELLIPSOMETERS

In this section, we describe how the optical components from the previous section come together in different ellipsometer configurations.

3.2.1 MEASUREMENT ANGLE

Ellipsometry measurements require interaction of a polarized light beam with a sample surface at a specified angle of incidence. It is important to precisely know or determine the measurement angle, as it is an integral part of the equations leading to film thickness and refractive index. Angle errors can lead directly to errors in determined material properties, such as thin film index.

For the majority of ellipsometry measurements, the angle of incidence is oblique to the sample surface near the Brewster angle (Section 2.5.3). Too much emphasis is often placed on the Brewster angle. Modern ellipsometers can accurately determine material properties using a wide range of angles. The choice is based more on data variation, which is largest near the Brewster angle for very thin films.

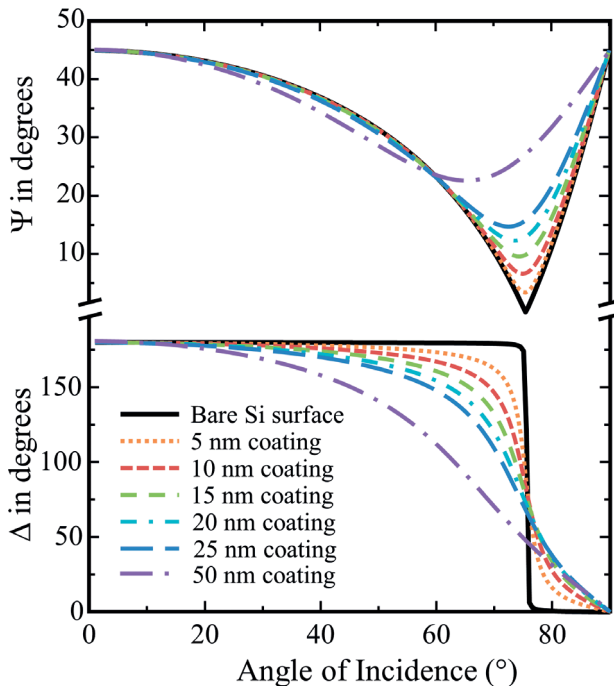


Figure 3.14. Angle dependence of ellipsometric Ψ and Δ calculated at 633 nm wavelength for different Si_3N_4 coating thicknesses on Si substrate.

Thus, the Brewster angle is still an appropriate indicator of approximate measurement angles.

In Figure 3.14, the angle dependence of Ψ and Δ is shown for a series of thin silicon nitride films on silicon substrate. The Brewster angle for bare silicon is 75° for 633 nm wavelength. Data variation is largest near the Brewster angle but spreads over a wider angle range as thickness increases.

Because silicon is a very common substrate, 75° has become one of the most common ellipsometry angles. The Brewster angle depends on the refractive index and with glass substrates is closer to 55° . Thus, a general angle range for ellipsometry lies between 50° and 80° for thin film measurements.

3.2.1.1 Ex Situ

Ex situ refers to table-top instruments where the sample is measured away from the thin film processing. It is beneficial to have an accurate and

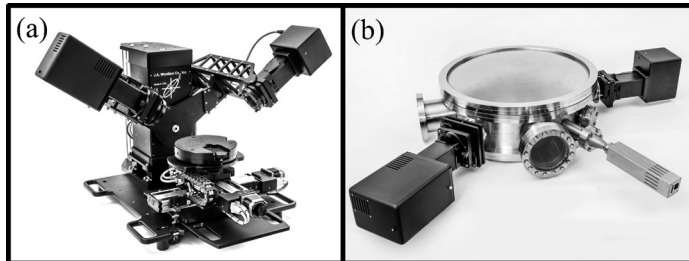


Figure 3.15. Image of (a) ex situ spectroscopic ellipsometer and (b) in situ spectroscopic ellipsometer attached to a vacuum process chamber.

reproducible method to position the sample at a known angle of incidence. Many stages provide sample tip and tilt with feedback positioning sensors to reproduce beam alignment from sample-to-sample.

Ex situ instruments can be configured for a single angle or, with mechanical adjustment, for varied angles. In either case, the angles generally lie between 50° and 80° . A representative ex situ ellipsometer is shown in Figure 3.15a.

3.2.1.2 *In Situ*

In situ refers to measurements of a sample “in the original position.” The sample is often undergoing some processing step and is still in the same location for the in situ measurement. In situ measurements can be performed before, during, and after processing, which allows characterization of properties not available during ex situ measurements. For example, in situ measurements can determine growth or etch rates, monitor surface development (roughness or oxidation), and provide real-time feedback control [37].

For vacuum processes, the ellipsometer is external to the chamber and light enters through windows to interact with the sample surface. In situ ellipsometry is often restricted to a single angle of incidence and the angle choice can be dictated by chamber geometry.

In Figure 3.15b, we show a spectroscopic ellipsometer attached to a process chamber, where source and receiver are attached to separate window ports. For in situ measurements, the angle depends on the construction geometry of the chamber and may not be specified exactly. The angle of incidence is determined by measuring a well-characterized sample, such as a thermal SiO_2 film on silicon. The optical properties of the silicon substrate and the thermal oxide film have been carefully

determined [43], which leaves two unknown properties—oxide thickness and angle of incidence. This method can provide a unique angle determination. If the equipment geometry is not changed, the predetermined measurement angle can be used for subsequent measurements.

3.2.2 MEASUREMENT CAPABILITIES

As we compare different ellipsometer instrumentation, we will consider key measurement aspects including speed, accuracy, sensitivity, and capabilities.

Measurement speed will be judged by how quickly a single, spectroscopic measurement can be achieved. Each configuration operates by adjusting optical elements placed before or after the sample. In this manner, the polarization is modulated with time, either by rotating an optical element (polarizer, compensator) or varying the phase (PEM, Liquid Crystal). The time-varying signal can be transformed to corresponding, independent frequency components, as shown in Figure 3.16. These contain the maximum information available to determine the SE data parameters, such as Ψ and Δ , or NCS. As we will see in future chapters, the Ψ and Δ data are then used to determine sample properties of interest, such as film thickness and optical constants.

Measurement accuracy depends on our ability to know the polarization state of light before the sample and measure the new polarization state after the sample. This requires calculation (also known as calibration) of the optical effects in both the PSG and PSD. Polarizers are generally easier to calibrate because their behavior is typically independent of wavelength. We primarily need to determine their orientation relative to the sample

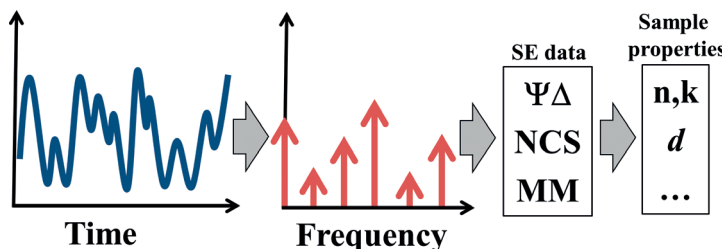


Figure 3.16. The modulating time-signal can be transformed into the unique frequency signal components, which are available to determine the SE data parameters. The SE data parameters represent the change in polarization, which is then used to determine sample properties, such as film thickness and refractive index.

plane of incidence to understand their optical effects. Compensators and PMs are more difficult to calibrate accurately as their optical effects depend not only on orientation but are also wavelength-dependent and, in the case of PEMs, drive-voltage dependent. Once we calibrate the effects of all optics, our measurement accuracy relies on the stability of this calibration.

The ellipsometer capabilities relate to the type of data the ellipsometer can collect. The primary goal of any ellipsometer is to collect Ψ and Δ . The possible parameter range of Ψ and Δ is 90° and 360° , respectively. Recall from Section 2.6.4 that Ψ and Δ can also be represented by three parameters: *NCS*. If all three *NCS* parameters are determined, then the full parameter ranges of Ψ and Δ are also known. In addition, a measure of *NCS* can be used to estimate the “percent depolarization.” This simply informs whether the detected light is partially polarized due to either sample or instrumentation during the measurement. In an ideal situation, the light would remain polarized and the percent depolarization would be zero.

3.2.3 ROTATING POLARIZER OR ANALYZER ELLIPSOMETRY

A common early SE configuration consisted solely of polarizers in the PSG and PSD. One polarizer is held at a fixed position while the other is rotated. If the rotating polarizer is before or after the sample, the configuration is called a Rotating Polarizer Ellipsometer (RPE) or Rotating Analyzer Ellipsometer (RAE), respectively. Measurement speed is limited by the motor rotation frequency, ω which is typically 10 to 30 Hz. An entire spectrum can be collected, using a diode array, in a fraction of a second. Longer averaging of a few seconds is typical to reduce noise.

Figure 3.17 is an overview of an RAE operation. Light from the source is polarized in the PSG by a linear polarizer oriented to provide both *p*- and *s*-electric fields. The light reflects from the sample, changing the polarization to generally an elliptical state. The elliptically polarized light travels through the rotating analyzer to the detector. The detected signal modulates as the analyzer rotates, with maximum and minimum intensities occurring when the analyzer is aligned with long and short ellipse axes, respectively. The maximum and minimum values occur twice per rotation, leading to a 2ω frequency signal for RAE and RPE ellipsometers. The detected signal for an RAE can be written as:

$$I_{RAE} \propto 1 - N \cos(2\mathbf{P}) + (\cos(2\mathbf{P}) - N) \cos(2\mathbf{A}) + C \sin(2\mathbf{P}) \sin(2\mathbf{A}) \quad (3.3)$$

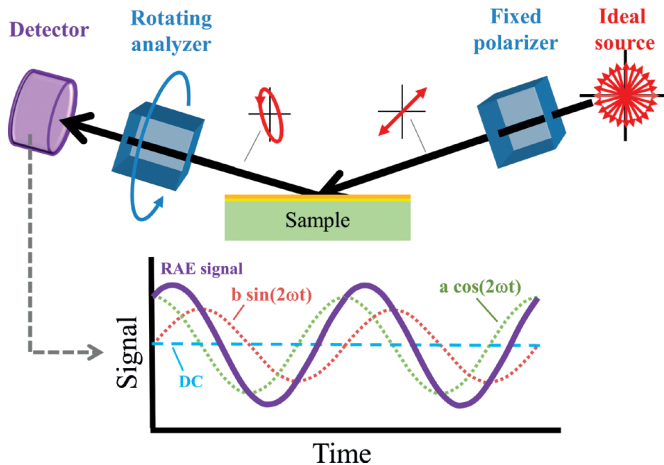


Figure 3.17. An RAE operation is reviewed. Light reaching the sample is linearly polarized, but reflects at a distinct elliptical polarization that passes through the rotating analyzer. This leads to a time-varying detected signal consisting of a DC and 2ω frequency terms (both cosine and sine).

where N and C are SE data values, \mathbf{P} is the fixed polarizer angle, and \mathbf{A} is the angle of the rotating analyzer. The RAE signal can be divided into a DC term (common offset from zero at all rotations) and both 2ω cosine and 2ω sine terms, as shown in Figure 3.17.

To avoid measuring absolute signal values, the frequency terms (a, b) are normalized to the DC term. The two remaining ratios are referred to as normalized Fourier coefficients (NFCs). For RAE and RPE, the normalized cosine and sine terms are referred to as α and β , respectively, as shown here for RAE configuration:

$$\alpha = \frac{a}{DC} = \frac{\cos(2\mathbf{P}) - N}{1 - N \cos(2\mathbf{P})} \quad (3.4a)$$

$$\beta = \frac{b}{DC} = \frac{C \sin(2\mathbf{P})}{1 - N \cos(2\mathbf{P})} \quad (3.4b)$$

Fixing the input polarizer at 45° , these equations simplify to:

$$\alpha = -N \quad (3.5a)$$

$$\beta = C \quad (3.5b)$$

Thus, the signal from an RAE ellipsometer can directly access N and C . However, there is no measurement of the S parameter. This is equivalent to stating that the measured Δ range is limited to 0° to 180° rather than the full 360° .

RAE and RPE designs were very popular for early spectroscopic ellipsometers because of their simplicity. These configurations are highly sensitive to Ψ and Δ when the reflected light is close to being circularly polarized. Because light arriving at the sample is linearly polarized, Δ must be 90° to convert the light to circularly polarized and achieve the high-sensitivity region of an RAE or RPE ellipsometer. This caused emphasis on measurements at the Brewster angle where Δ goes through a 90° phase change. However, an appropriate Ψ value from the sample is also required to achieve circularly polarized light.

The biggest limitation of RAE and RPE is related to their lack of a compensating element. This prevents measurement of S , which in turn prevents measurement of the full range of Δ and prevents measurement of percent depolarization. More significantly, RAE and RPE instruments suffer from greatly reduced sensitivity for Δ values near 0° or 180° . Modern ellipsometers overcome this deficiency by adding a compensating element into the PSG or PSD, as we describe in subsequent sections.

3.2.4 ROTATING COMPENSATOR ELLIPSOMETRY

Spectroscopic ellipsometers using rotating compensator ellipsometry (RCE) were developed in the mid-1990s [32]. A key enabling factor was developing compensators that provided adequate retardance over a wide wavelength range. The compensators are not used by themselves, as they have no effect on unpolarized light. Rather, they are used in combination with a polarizer. The compensator can be situated either before or after the sample. To differentiate between these two configurations, we refer to the order of polarization-altering components: Polarizer-Compensator-Sample-Analyzer (PCSA) or Polarizer-Sample-Compensator-Analyzer (PSCA). Measurement speed is again limited by motor rotation speeds, with entire spectra accessible in a fraction of a second.

The rotation of the compensator next to the fixed polarizer introduces both 2ω and 4ω frequencies into the detected signal. Normalizing to the DC term produces four possible NFCs.

Figure 3.18 shows the components of a representative PCSA ellipsometer configuration. The light is polarized and then enters the rotating compensator. The polarization exiting the compensator varies with time as the compensator orientation changes with respect to the linear polarization. For the special case of a QWP, the light will modulate between left-circular and right-circular polarizations. When the

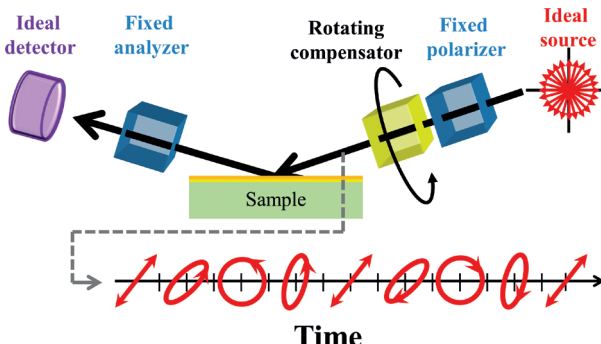


Figure 3.18. Basic RCE configuration.

compensator axes align with the polarizer axes, no polarization change occurs and linearly polarized light passes through to the sample. The compensator is continuously rotating so the light polarization after the compensator is continuously changing its shape from linear to circular with elliptical states in between, as shown in Figure 3.18. Regardless of the incident polarization state, it is altered by the sample, such that the reflected light is also modulating versus time but with a different variation of polarizations. The fixed analyzer passes only electric fields aligned with the analyzer orientation. In general, the detected signal is modulated with DC, 2ω and 4ω variations.

The signal intensity for an RCE ellipsometer is more complex than with the RAE or RPE designs of the previous section. However, the intensity can be simplified by choosing fixed polarizer and analyzer orientations. With $\mathbf{P} = 0^\circ$ and $\mathbf{A} = 45^\circ$, the PCSA intensity becomes:

$$I_{RCE} \propto 1 - \frac{1}{2}(1 + \cos(\delta))N + S \sin(\delta) \sin(2C) - \frac{1}{2}(1 - \cos(\delta))N \cos(4C) + \frac{1}{2}(1 - \cos(\delta))C \sin(4C) \quad (3.6)$$

where δ is the compensator retardance and C is the rotating compensator orientation. Our choice of polarizer and analyzer orientations reduced the number of Fourier coefficients, as the cosine ($2C$) term is zero and no longer appears. The NFCs of Equation 3.6 can be written in terms of the cosines (a_2, a_4) and sines (β_2, β_4) of the modulating compensator frequency:

$$\alpha_2 = 0 \quad (3.7a)$$

$$\beta_2 \propto S \sin(\delta) \quad (3.7b)$$

$$\alpha_4 \propto N(1 - \cos(\delta)) \quad (3.7c)$$

$$\beta_4 \propto C(1 - \cos(\delta)) \quad (3.7d)$$

With an ideal QWP where $\delta = 90^\circ$, the equations further simplify to:

$$\alpha_2 = 0 \quad (3.8a)$$

$$\beta_2 \propto S \quad (3.8b)$$

$$\alpha_4 \propto N \quad (3.8c)$$

$$\beta_4 \propto C \quad (3.8d)$$

It is clear that RCE ellipsometers can measure N , C , and S . In fact, in this configuration, the three SE Data Parameters are determined from three independent NFCs.

There are many advantages to including a compensating element within the ellipsometer, as the compensator overcomes the primary limitations of the RAE and RPE. With a compensator, the full ranges of Ψ and Δ can be measured. In addition, percent depolarization can be measured from isotropic samples. Finally, the rotating compensator provides sensitivity to any value of Ψ or Δ .

A thorough treatment of RCE can be found in Collins et al. [23].

3.2.5 DUAL ROTATING INSTRUMENTS

It can be beneficial to rotate more than one optical element simultaneously. Rotating multiple optical elements produces a larger number of NFCs. Care must be taken when choosing the separate optical rotation frequencies, such that any new frequencies, which are naturally generated (sums and differences of the base frequencies), are not overlapping. The extra

frequencies contain the same inherent information as when one element is continuously rotated and the second element is stepped to multiple positions. However, continuous rotation of both optical elements improves measurement speed. Now, the total measurement time is related to a single optical cycle, which is the completion of a certain number of rotations for each optic. Thus, a dual rotating element SE is slower than a single rotating element SE, but with additional measurement information. Considering the two instrument configurations we have previously listed, dual rotating instruments could be constructed by the following: (i) rotating both polarizer and analyzer, (ii) rotating compensator on one side of sample while rotating polarizer on the opposite side of the sample, and (iii) rotating compensators on both sides of the sample.

Each case leads to more NFCs, which contain sample information. In the case of dual rotating compensators, there are potentially 24 NFCs. These can be used to significantly overdetermine Ψ and Δ or even determine all 16 normalized Mueller matrix elements for advanced samples (Section 2.6.5).

3.2.6 PHASE MODULATION ELLIPSOMETRY

Phase modulation ellipsometry (PME) has many similarities to RCE. Both have an optical element that provides phase retardance. The main difference is how each varies the amount of compensation versus time. The RCE rotates the compensator orientation, while PME varies optical anisotropy with a fixed optical orientation.

Just like a compensator, the PM must be used in combination with a polarizer. To achieve the largest range of modulation, the PM is typically rotated 45° from the polarizer axis. The PM can be situated before or after the sample, leading to two common configurations, which we will denote by the order of polarization-altering components: Polarizer-Phase Modulator-Sample-Analyzer (P-PM-S-A) or Polarizer-Sample-Phase Modulator-Analyzer (P-S-PM-A).

The signal from a PME is very complex and will not be detailed here. A full account can be found in Jellison [24].

The implementation of a single PEM can measure either N and S or C and S, but not all three simultaneously. To determine all three simultaneously requires movement of the PEM axis and a second measurement or additional PEM in the optical path. Thus, a single measurement with PME does not measure the full range of Ψ and Δ and can't provide percent depolarization.

PME is often used for very fast SE data measurements with the measurement signal around 50 to 100 kHz. However, this speed advantage comes with a disadvantage—it makes the device incompatible with modern linear detector arrays such as charge-coupled device detectors. To collect parallel wavelengths with this type of ellipsometer requires parallel detection from different detectors with their own lock-in circuitry. This has been demonstrated by collecting approximately 50 different wavelengths, but does not come close to achieving over 1,000 wavelengths common in rotating element ellipsometers. Thus, the speed advantage has the caveat of limited wavelengths.

Another important consideration with PME systems is the stability of the calibration. The calibration is inherently more difficult, as the PM is not only wavelength-dependent but also dependent on drive voltage and sensitive to temperature variations. For this reason, accurate measurement may require frequent calibration.

CHAPTER 4

GENERAL DATA FEATURES

In this chapter, we illustrate the appearance of Ψ and Δ data collected with a spectroscopic ellipsometer. We show general data features from dielectric, semiconductor, and metal substrates. We then demonstrate the effect of thin films on a substrate, specifically how thickness affects the spectra.

A spectroscopic ellipsometry spectra is shown in Figure 4.1. The measurement includes two data curves, Ψ and Δ , which describe the polarization change. Curves are shown from a single angle of incidence; however, it is common to measure multiple angles and each will have Ψ and Δ curves.

The general range of Ψ is between 0° and 90° , while Δ covers a 360° total range. Because we do not collect absolute phase, the minimum Δ value on the graph can be arbitrarily selected. Here we have graphed the curves with 0° as the Δ minimum. The sharp step at 410 nm is actually a graphing artifact when Δ exceeds the maximum and enters the graph at the minimum range. If we select a different minimum value for Δ , it will change where this “step” appears.

While Ψ and Δ curves are interesting, they do not typically hold quantitative information about sample properties. Film thickness and optical constants are determined via regression analysis, which will be covered in Chapter 6. However, a basic overview of the spectral features from typical substrates and single-layer coatings is helpful to build an intuitive understanding of the measured sample. A cursory glance at the data should inform whether our sample is a bare substrate or has a thin film coating. If the substrate has a single-layer coating, we can deduce the general film properties. Is it a thin or thick layer? Is it transparent or absorbing? The spectroscopic ellipsometry spectra suggest the answers to these questions.

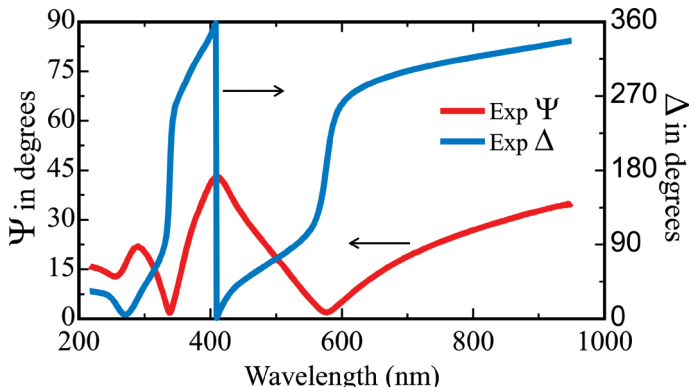


Figure 4.1. Ellipsometry spectra (Ψ and Δ) for a 75° measurement of a thin-film coated substrate.

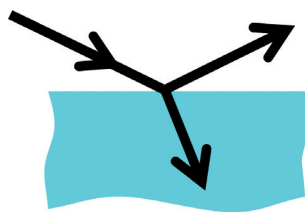


Figure 4.2. A “substrate” consists of a single interface, where only light reflecting from the surface will reach the detector.

4.1 SPECTRA FOR SUBSTRATES

For substrates, we consider a single surface reflection from the material without any surface coatings, as shown in Figure 4.2. We also consider the substrate to be infinitely thick. This latter condition is met whenever the light entering the material does not return to the detector. This can be accomplished in a number of ways. First, there can be adequate physical separation between the surface reflection and any additional beams from the backside of the substrate (e.g., a 5 mm thick optical flat). The light can also be scattered from a rough surface, such as the backside of a

single-side polished semiconductor substrate. Finally, the light can be strongly absorbed within the substrate. This final case is met by metals which are only 100 to 200 nm thick. Thus, when referring to a metal substrate, we may actually be measuring a thin film of the metal. Because we only detect the top-reflection from the metal surface, it is effectively our substrate.

Interestingly for substrates in general (transparent and absorbing), the data range reduces to $\Psi \leq 45^\circ$ and Δ between 0° and 180° . The Ψ range is evident from Figures 2.11 and 2.12, where the reflectance of *s*-waves is always greater than that of *p*-waves. From the definition of the tangent of Ψ (Equation 2.30) we see that, for substrates, $\tan \Psi \leq 1$, and hence, $\Psi \leq 45^\circ$. The Δ range for substrates is demonstrated in Figure 2.13.

4.1.1 DIELECTRIC SUBSTRATES

We consider dielectric materials to be essentially transparent over our spectroscopic ellipsometry (SE) measurement wavelength range. With $k = 0$, the SE data simplify with Ψ tracking the index and Δ equal to either 0° or 180° . As an example of a dielectric substrate, we consider Schott N-BK7®, a common glass. In Figure 4.3, we show the values of Ψ and Δ for three angles-of-incidence. Each of the Ψ curves is relatively flat and smooth, with mild curvature at shortest wavelengths. This is due to the glass index, which is also relatively smooth and flat across this spectral range. The refractive index for the N-BK7 substrate is shown in Figure 4.4. The slight variation of the index, n , which increases toward shorter wavelength, is called “normal” dispersion (Section 5.2.1). This is common to all dielectric materials.

The extinction coefficient, k , is zero throughout the entire spectral range of interest. For a “pure” substrate (no surface coating), the value of Δ would be exactly 0° or 180° . Pure substrates are rarely seen in nature. The deviation of Δ from ideal values can be attributed to a very thin surface layer. To match the data, the N-BK7 was modeled with a 1.3 nm roughness layer on the interface that consists of half air and half glass (Chapter 8). With this surface, we note that for an angle-of-incidence of 51° , the value of Δ is almost 180° and for an angle-of-incidence of 63° the value of Δ is almost 0° .

The Brewster angle for bare substrates occurs when Δ crosses 90° and Ψ goes through a minimum. For the angle-of-incidence of 57° , Δ changes gradually from near 180° to near 0° , passing 90° at about 366 nm. This is to say that for $\lambda \approx 366$ nm, the middle angle, 57° , is the Brewster angle.

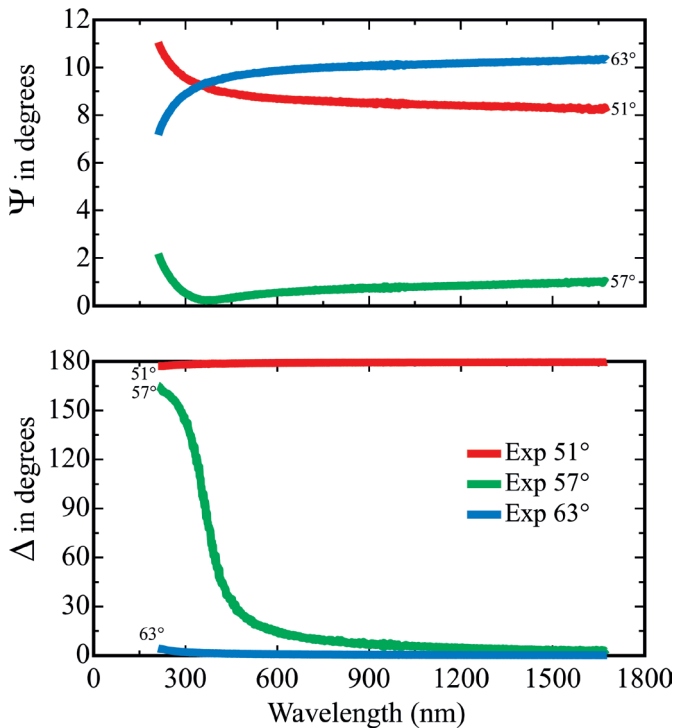


Figure 4.3. The values of Ψ and Δ for a dielectric substrate of N-BK7 glass with 1.3 nm of surface roughness. Three angles-of-incidence are shown.

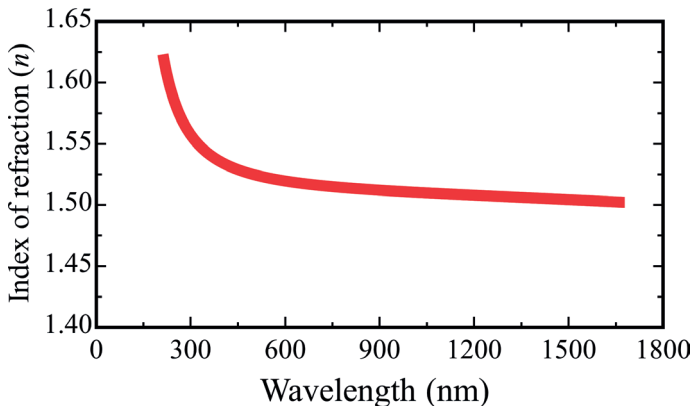


Figure 4.4. The values of the index of refraction, n , for a dielectric, N-BK7 glass.

From the definition of the “Brewster angle” (Equation 2.24), we see that for each value of the index of refraction, there is a corresponding Brewster angle. In Figure 4.4, we see that the values of the index of refraction for this sample are between about 1.5 and 1.63. The index of refraction for a Brewster angle of 51° and for a Brewster angle of 63° falls outside this range. However, the index of refraction for a Brewster angle of 57° is 1.54, and this occurs at a wavelength of about 366 nm for this sample. Accordingly, we could call this wavelength the Brewster wavelength (for an angle of incidence of 57°). We also note that the value of Ψ for this angle-of-incidence and at this wavelength is almost zero. If it were a pure substrate, Ψ would be equal to zero.

We can expect similar data behavior from other dielectric substrates such as fused silica, sapphire, calcium fluoride, and plastic materials. The Ψ curves will be relatively flat and their relative value will depend on the substrate index and the angle of incidence. If we remain in the transparent region of the dielectric, Δ will only show variation from 0° and 180° due to surface coatings.

4.1.2 METAL SUBSTRATES

Metals absorb light at all wavelengths. Thus, we can expect significantly different SE spectra compared to the dielectric substrates, which are transparent. The two primary differences are: (i) Ψ will not get close to zero, and (ii) Δ will not touch 0° or 180° . The absorption mechanism within metals generally causes the extinction coefficient, k , to rise toward longer wavelengths. This also leads to increasing Δ values toward longer wavelengths.

For typical Ψ and Δ spectra for metal substrates, we show those for cobalt in Figure 4.5. In contrast to the dielectrics, note that Ψ is considerably larger and Δ is in the middle of the range between 0° and 180° . We show four angles-of-incidence, all below the principal angle. It is less practical to collect data above the principal angle, which is usually between 80° and 90° .

The optical functions for cobalt are shown in Figure 4.6. Because, metals absorb all wavelengths of interest, we note that the extinction coefficient, k , is not zero, as was the case for dielectrics. As discussed above, k increases for longer wavelengths. For this metal, n is also increasing toward longer wavelengths; however, there is plenty of variation for different metals, so this is not a rule.

It is very difficult to obtain spectra for a pure metal substrate due to roughness, oxidation, or adventitious carbonaceous contamination from

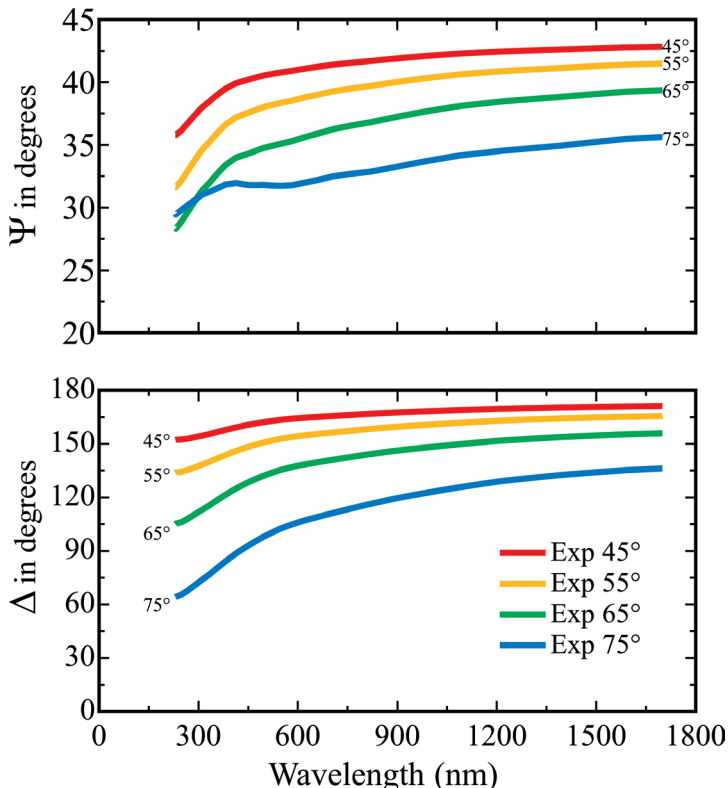


Figure 4.5. The values of Ψ and Δ for a cobalt substrate.

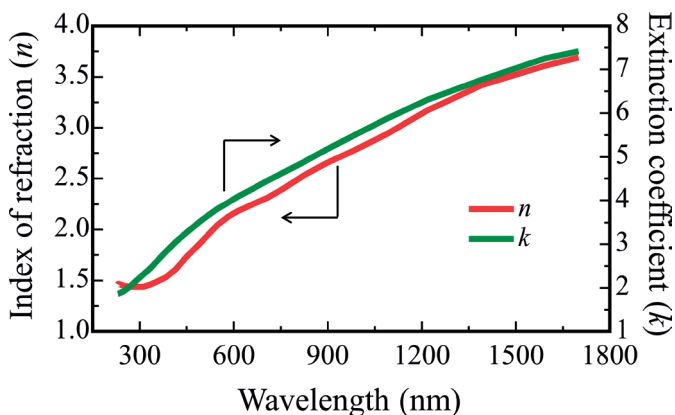


Figure 4.6. The values of the optical functions for cobalt.

the atmosphere. These very thin layers can contribute to the Ψ and Δ spectra, but we likely will not notice their effect, as they will slightly shift the values of Ψ and Δ . These thin layers are usually detected with another analytical technique such as Auger electron spectroscopy or scanning probe microscopy. The metal sample can then be modeled with these layers present, thus giving a better representation of the optical functions of the pure metal surface.

4.1.3 SEMICONDUCTOR SUBSTRATES

Semiconductor substrates contain the general features of both dielectrics and metals. Semiconductors have much lower bandgap energies than for dielectrics, so they will be absorbing at short wavelengths (above the bandgap) and transparent at longer wavelengths (below their bandgap). Thus, the semiconductor data curves will behave similar to dielectrics at long wavelengths and similar to metals at short wavelengths. Additionally, most semiconductor substrates are crystalline, which adds one more feature to the data for us to examine. The crystalline structure leads to much sharper absorption features at short wavelengths. These features are related to specific electronic transitions that occur within that semiconductor.

In Figure 4.7, we show Ψ and Δ spectra for a typical semiconductor substrate, single-crystal silicon. Note that for wavelengths greater than about 500 nm, the Ψ or Δ behavior is not all that different from a dielectric. Here, Δ remains close to 0° or 180° , except at 75° where there is a transition through the Brewster angle. The Ψ spectra is flat and smooth, with values approaching 0° when measured near the Brewster angle.

For wavelengths shorter than 500 nm, the behavior is more like that of an absorbing material. Here, Δ remains away from both 0° and 180° , while Ψ remains at larger values away from 0° . The sharper features at 270 nm and 360 nm are due to critical point energies within the crystalline silicon. They act as a “fingerprint” for the type of semiconductor. If we measured a GaAs substrate, we would see features at 240 nm, 390 nm, and 425 nm. GaAs becomes transparent above 880 nm and shows “dielectric” behavior at longer wavelengths. We can expect similar behavior from all semiconductor substrates.

In Figure 4.8, we show the optical functions of a single-crystal silicon. For wavelengths longer than about 500 nm, the extinction coefficient, k , is very small, and for wavelengths longer than 1100 nm, the extinction coefficient is exactly zero. On the other hand, the extinction coefficient is quite large for wavelengths below about 450 nm. Accordingly, this material

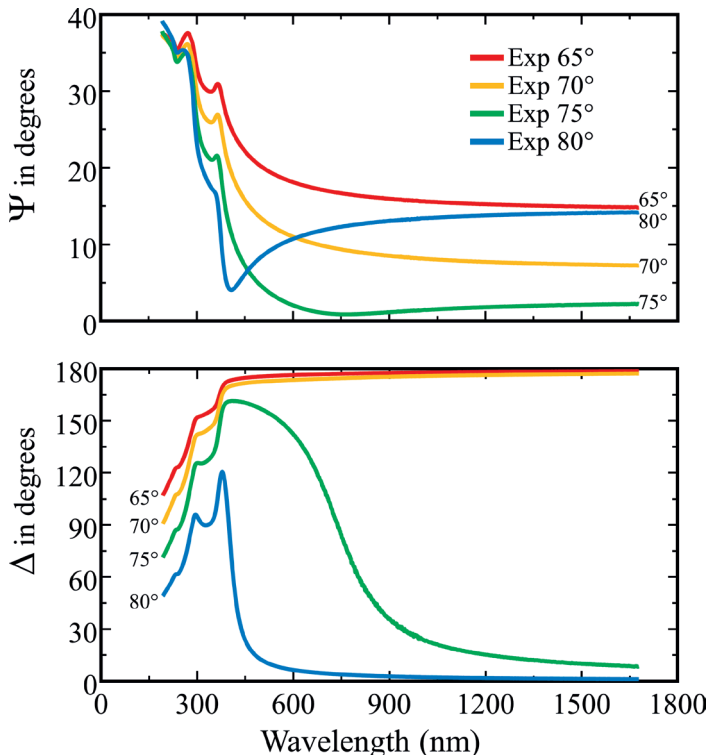


Figure 4.7. The values of Ψ and Δ for a typical semiconductor substrate, silicon.

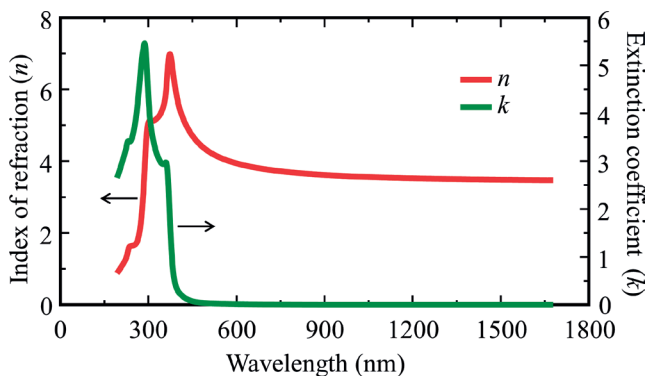


Figure 4.8. The values of the optical functions for a typical semiconductor, silicon.

has some features similar to a dielectric and some features characteristic of absorbing materials.

4.2 SPECTRA FOR FILMS ON A SUBSTRATE

The SE data from a sample which consists of a thin film on substrate will depend on the light interactions that reach the detector. Thus, we need to consider (i) transparent films, (ii) films that have an absorbing spectral region, and (iii) absorbing films. The absorbing films are easy to dismiss, as they behave exactly like absorbing substrates. That leaves transparent films and films with absorbing spectral regions.

4.2.1 TRANSPARENT THIN FILMS

To illustrate the spectra for a sample which consists of a transparent film on a substrate, we have chosen thermal oxide (SiO_2) on a single-crystal silicon substrate. As the film is transparent, light will travel through the film and return to the detector, as shown in Figure 4.9. The Ψ spectrum is shown in Figure 4.10. The thickness of this particular film is 1 μm , or 1000 nm. For comparison, we have included the Ψ spectrum for a bare silicon substrate.

We observe oscillations in the spectrum, going from a value near that of the bare substrate to near 90° (at least at longer wavelengths). The data oscillations are caused by constructive and destructive interference between the light reaching the detector. This is illustrated in Figure 4.11, where (a) destructive interference occurs when the light combines “out-of-phase” and (b) constructive interference occurs when the light combines “in-phase”. As the wavelength changes, it shifts the interference giving rise to the up-and-

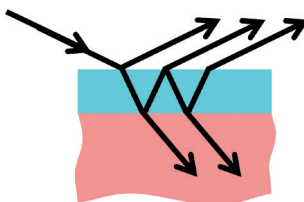


Figure 4.9. Reflection of light within a thin transparent film on substrate.

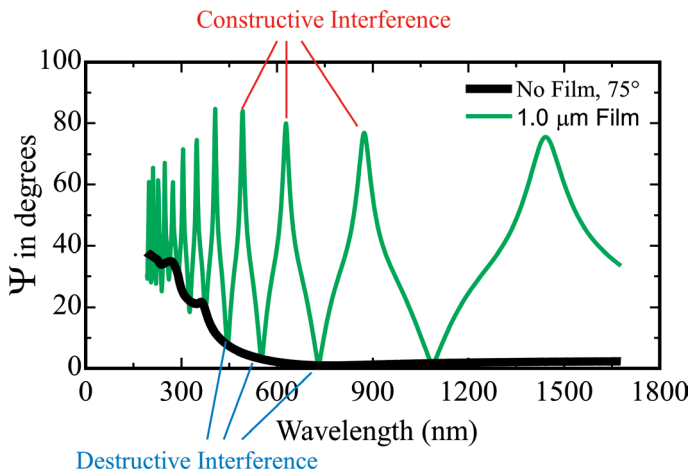


Figure 4.10. The Ψ spectrum for a transparent film on a substrate. For this particular example, we show a single-crystal silicon substrate with a 1 μm thermal oxide film. Also shown is the spectrum for the bare substrate. The peaks and valleys correspond to wavelengths where the detected light from the thin film exhibits constructive and destructive interference.

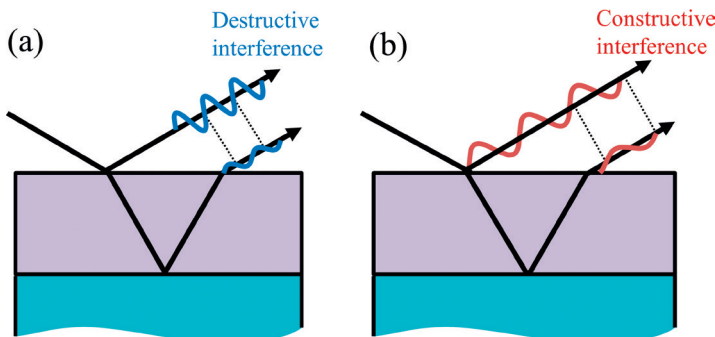


Figure 4.11. Destructive and constructive interference from within a thin film. Different wavelengths will produce different effects, depending on how the final light components “align” in-phase or out-of-phase as they recombine traveling to the detector.

down data fluctuations as shown in Figure 4.10. A few points in Figure 4.10 are marked to indicate the effect of constructive and destructive interference.

The data fluctuations are a direct indicator of film thickness as illustrated in Figure 4.12. If we were to make the film slightly thicker, the interference features (peaks and valleys) would move toward longer wavelengths. In

addition, the interference features would come closer together. Conversely, for thinner films, these features move toward shorter wavelengths and would move farther apart. In a given spectral range, thinner films have fewer interference features than thicker films. We also note that the interference features are closer together for shorter wavelength than for longer wavelength.

The large Ψ fluctuations of nearly 90° from Figures 4.10 and 4.12 were caused by the large optical contrast between silicon and silicon

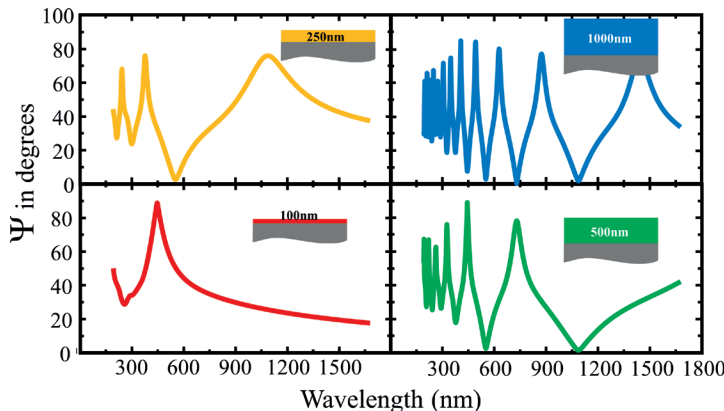


Figure 4.12. The Ψ spectrum for a series of SiO_2 coatings on crystalline Si with different film thicknesses. As the thickness increases, so do the number of interference features within the measurement wavelength range.

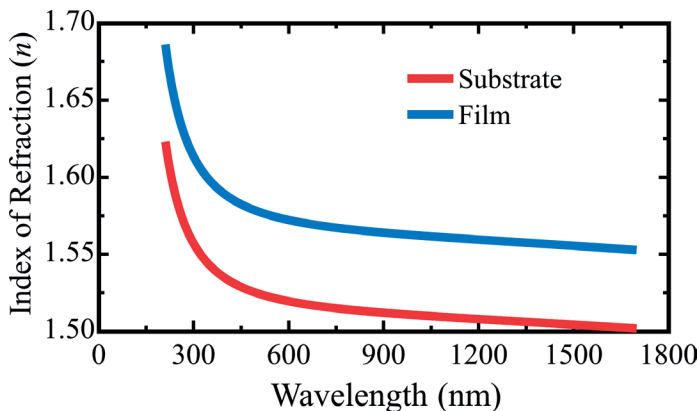


Figure 4.13. Comparison of the index of refraction for the thin film and glass substrate. This small index difference leads to smaller amplitude data fluctuations.

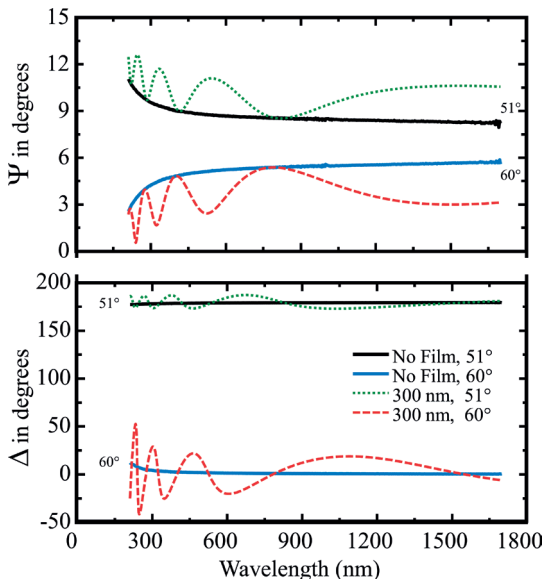


Figure 4.14. Ψ and Δ spectra for a coating on BK7 glass substrate. The coating has a slightly higher index of refraction than the substrate. This leads to interference oscillations as compared to the data from the bare substrate (also shown). Note the interference features for Ψ have one edge along the bare substrate curves—high or low edge depends on the angle of incidence. The Δ interference features fluctuate around the central curve of the bare substrate.

dioxide ($\Delta n \sim 2.5$). In contrast, a dielectric coating on a glass substrate will have smaller optical contrast, as shown in Figure 4.13. In Figure 4.14, we show the Ψ and Δ curves at two angles of incidence for a thin dielectric on glass. The fluctuations in Ψ are now closer to 3° . We also graph the bare substrate data for comparison. Note how the Ψ fluctuations are bounded by the substrate curves. This boundary can be either at the top or bottom of the interference features, depending on the angle of incidence and whether the film index is lower or higher than the substrate index. The Δ spectra also fluctuate, but as shown for the two angles (one below and one above the Brewster condition), Δ fluctuates around the bare substrate curve.

4.2.2 THIN FILMS WITH ABSORBING SPECTRAL REGIONS

Some films are transparent over a portion of the measured wavelengths and absorbing at other wavelengths. In the transparent region, we expect

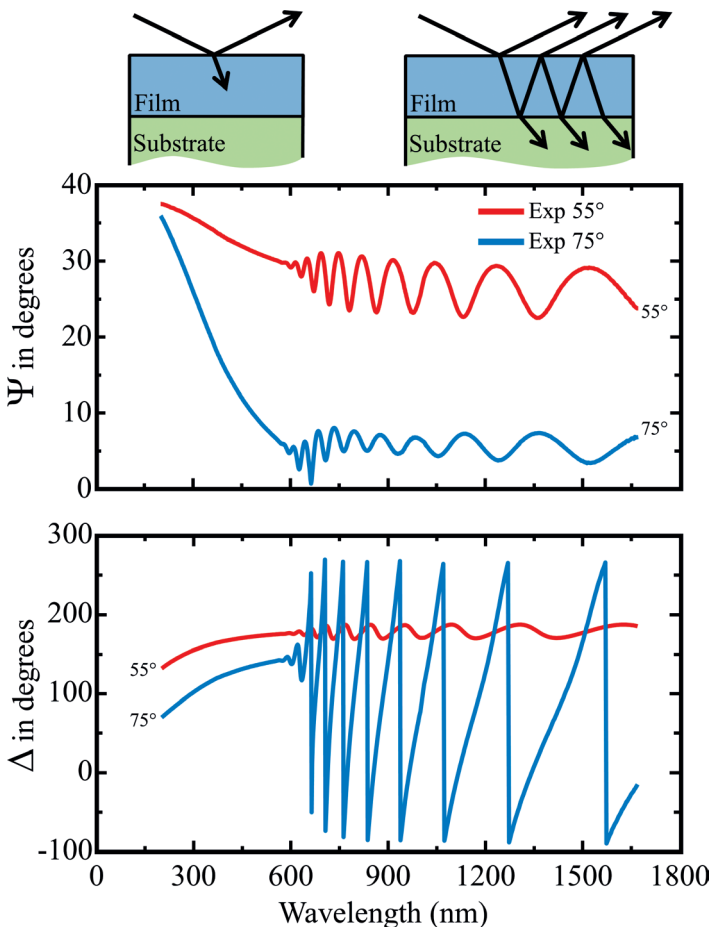


Figure 4.15. Ψ and Δ spectra from a semiabsorbing film show the interference features of a transparent film over the spectrum above 600 nm. However, absorption within the film prevents interference at shorter wavelengths. Thus, the data curves appear like an absorbing substrate at these wavelengths, as only light from the film surface reaches the detector.

the same behavior as with transparent films of the previous section—the Ψ and Δ curves should oscillate. It is important to measure some wavelengths in this region, as the film thickness can only be determined where the light can probe the film depth.

As the film becomes absorbing, the light traveling through the film is no longer able to return to the surface and reach our SE detector. The

data are now similar to the absorbing substrates discussed earlier. The Ψ spectra will be away from 0° and follow the shape of the optical functions. The Δ spectra will stay between 0° and 180° and will also follow the optical functions. If the material is amorphous, it is likely to have smooth absorbing features and thus we expect Ψ and Δ also to be smooth in this region. Figure 4.15 shows Ψ and Δ for an amorphous semiconductor film on a substrate. The data oscillate above 600 nm, where the thin film is transparent. The amplitude of these oscillations diminishes as light is more strongly absorbed until no light is able to return from the substrate interface. Here, the Ψ and Δ data are smooth and show only the surface of the thin film.

Now that we have considered the spectral shape for both transparent and absorbing materials, we will discuss the nature of the optical functions. Chapter 5 will introduce the general approaches to represent the optical functions of both transparent and absorbing materials.

CHAPTER 5

REPRESENTING OPTICAL FUNCTIONS

In the previous chapter, we illustrated the general shape of experimental data curves. The Ψ and Δ spectra describe how the polarization has been altered. We wish to extract material properties from the measurement. This requires model-based regression analysis, which we describe in Chapter 6. An important part of this process requires the user to estimate the sample structure. Specifically, each layer must be described by its thickness and optical constants. As the optical constants vary with wavelength, we also refer to the optical constant spectral shapes as the optical functions. In this chapter, we introduce the standard methods of representing optical functions.

Our choice of method for each material depends on the following questions:

1. Are the optical constants known?
2. Are they different from the reference values or expected to differ from sample to sample?
3. If values are unknown or expected to vary, is the material transparent or absorbing?

We introduce four common methods for representing the optical functions: tabulated lists, the Cauchy dispersion equation, oscillator models, and the b-spline.

5.1 TABULATED LIST

When the optical constants are known for a material, they can be listed directly for use in model calculations. The optical constants are entered

into a table consisting of columns for wavelength, values of n , and values of k . Table 5.1 is an example of a tabulated list. The first lines provide comments and instructions to the software concerning the list. Following this are rows listing the wavelength in nm, the value of n and the value of k . The list should cover the same wavelength range as the measured SE spectra, with allowances for minor extrapolation.

There are two common sources for tabulated lists. The first is to obtain published optical constants. The second is to measure a reference sample and save the values for future use. Example collections of published optical constant spectra include those by Palik and Adachi [17–20].

Tabulated lists are useful for two situations. First, they can be used when the optical constants are not expected to differ from the reference values. Second, they provide the general shape of optical functions for a material. This allows the user to get a preliminary calculation and then proceed to a dispersion model with knowledge of the shape of the optical function.

The values in the tabulated list cannot be conveniently adjusted. This form of the optical function is useful for materials which are extremely reproducible. The best applications of tabulated lists are for single-crystal

Table 5.1. Example of a tabulated list to represent the optical functions of GaAs

Gallium arsenide substrate		
Wavelength (nm)	n	k
210	1.3153	2.6163
215	1.3383	2.7205
220	1.3691	2.8515
225	1.4149	3.0071
230	1.4793	3.1894
235	1.5688	3.4146
240	1.7322	3.7145
245	2.0855	4.0432
250	2.6568	4.2026
255	3.2408	4.0501
260	3.6159	3.7094

materials. For example, a tabulated list of silicon optical constants can be used effectively from the ultraviolet to near infrared for any silicon wafer you may encounter, regardless of batch, crystal cut, or doping concentration. Tabulated lists are also useful for thin films which can be repeatedly prepared, such as thermal oxides of silicon and low-pressure chemical vapor deposition (LPCVD) silicon nitride. Tabulated Lists are less practical for polycrystalline materials as the optical constants depend on grain size, impurities, and so on.

There are tabulated lists for many metals in the literature. However, these should only be used as a starting point, since metal optical constants will vary with fabrication process and conditions. For example, it has been shown [44] that the optical functions of sputtered chromium depend on the pressure of the sputtering gas (usually argon). Thus, users should each create a metal reference for their own process.

Normally, it is expected that the analyst will determine the optical functions of a material of interest rather than use an existing tabulated list. The primary exceptions are the ubiquitous silicon and other semiconductors that can be readily obtained as single-crystal wafers. This leads us to the remaining types of optical function representations—all of which allow the optical functions to adjust to match the measured sample.

5.2 DISPERSION EQUATIONS

The primary disadvantage of tabulated lists is that they do not provide a method to vary the optical functions in a useful and efficient manner. Each individual value can be adjusted, but this introduces a maximum number of “free” parameters to describe the optical functions. This method is referred to as “point-by-point” or “wavelength-by-wavelength” fitting. It is very inefficient as neighboring wavelengths do not support each other. Rather, each wavelength is allowed to vary without knowledge of the optical constants at neighboring wavelengths. This often leads to noisy and possibly correlated results that are not unique and often wrong.

A better, more efficient approach is to use a dispersion equation. Dispersion refers to the variation of optical constants at different wavelengths. Thus, a dispersion equation relates to the wavelength-dependence of the optical functions. In this manner, neighboring wavelengths help support each other at arriving at a consistent answer to match the spectroscopic data curves.

We introduce here a variety of dispersion equations. Some are designed to work for transparent materials. Others describe both transparent and

absorbing optical functions. Some are empirical and were developed purely from the observation of the optical constant shapes, without physical meaning for this underlying shape. Others are rooted in a physical understanding of the material and the nature of its optical properties. Regardless, each provides the added benefits of (1) significantly reducing the number of free parameters, (2) maintaining smooth, continuous curves to describe the optical functions versus wavelength, and (3) allowing easy access to vary certain properties of the optical functions.

Before describing a few common dispersion equations, we consider the basic dispersion shape expected for transparent and absorbing materials, referred to as normal and anomalous dispersion, respectively.

5.2.1 NORMAL DISPERSION

For any transparent material, the index of refraction increases as the wavelength is decreased. This is referred to as normal dispersion. Even materials with absorbing regions must follow normal dispersion at the wavelengths where they are transparent. The optical functions of polyimide are shown in Figure 5.1. This material is transparent ($k = 0$) for wavelengths above 500 nm, and the index of refraction increases as the wavelength decreases down to 500 nm.

There are two common dispersion relations to describe the index of refraction of transparent materials: Sellmeier and Cauchy. Each can describe the normal dispersion of the index of refraction. However, the

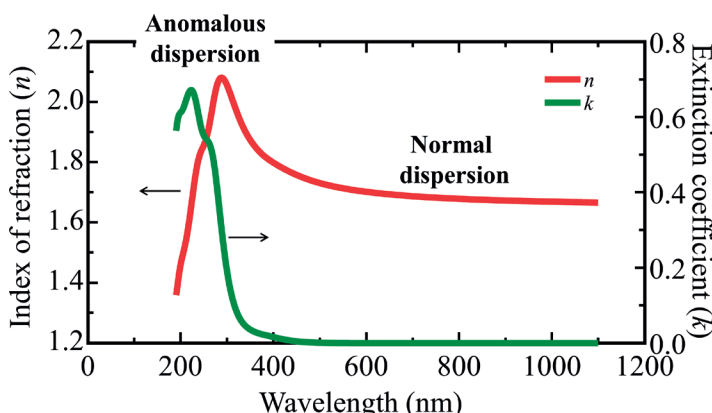


Figure 5.1. The optical functions for polyimide are shown with both normal and anomalous dispersion regions.

Cauchy equation (Section 5.3) is empirical and does not force the normal dispersion shape. Thus, it is possible to achieve a result where the index decreases toward shorter wavelengths, while the material is transparent. This result is not physically plausible and can be ruled incorrect.

5.2.2 ANOMALOUS DISPERSION

For wavelengths where a material is absorbing, the optical functions will follow anomalous dispersion. In general, the index will flip over near the peak in the extinction coefficient. Thus, the index decreases toward shorter wavelengths where the material is absorbing. This is also shown in Figure 5.1 for polyimide at wavelengths near 250 nm. The effect on the index depends on the strength and shape of the absorbing region. This is due to a physical tie between the real and imaginary optical functions referred to as Kramers-Kronig (KK) consistency (Section 5.4.1). There are many dispersion equations to describe the absorbing region of a material, including oscillator models (Section 5.4) and the b-spline (Section 5.5).

5.3 THE CAUCHY EQUATION—A DISPERSION EQUATION FOR TRANSPARENT REGIONS

In this section, we shall consider the wavelength range in which the film of interest is transparent. This is important for ellipsometry as light can penetrate the film and provide thickness information. When the index of the material is not known, or is expected to vary from sample-to-sample, we turn to a “dispersion” equation. For transparent wavelengths, it is common to use the “Cauchy Equation,”

$$n(\lambda) = A + \frac{B}{\lambda^2} + \frac{C}{\lambda^4} \quad (5.1)$$

where the index of refraction is described by three parameters (called the Cauchy coefficients) and the wavelength is given in units of microns. The optical function for the extinction coefficient is simple, that is, $k = 0$. The Cauchy coefficients are normally determined, along with the film thickness, during regression analysis of the ellipsometry data.

The general shape provided by the Cauchy equation is plotted in Figure 5.2. The value of the curve at longer wavelengths is determined

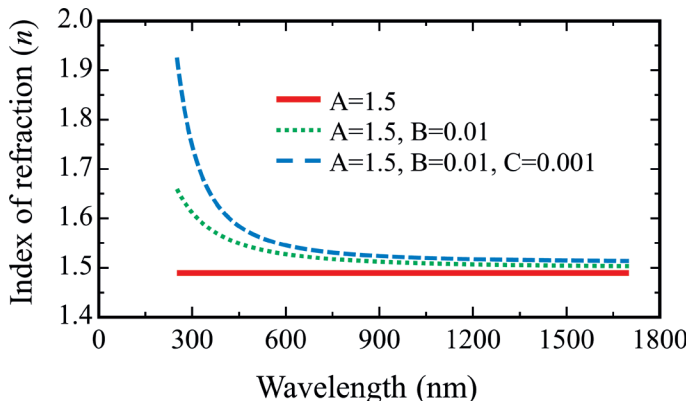


Figure 5.2. The optical function for n is shown as described by the Cauchy equation.

by the “A” parameter which is basically an “offset” for all wavelengths. Curvature is controlled by “B” and “C” parameters.

Because the Cauchy equation can be used anytime if a material is transparent, it is applicable to dielectrics, organics, and even semiconductors. If the material is absorbing at some wavelengths, the fit can be restricted to the transparent wavelength range. As discussed in the previous chapter, the transparent wavelength range can be estimated by looking for oscillations in the Ψ/Δ data curves.

Figure 5.3 shows the index using a Cauchy equation for a variety of dielectric materials. The corresponding Cauchy coefficients are listed in Table 5.2. The curvature tends to increase for materials with a larger index. The values of “B” are commonly between 0.002 and 0.02 for many transparent materials, while “C” remains near 0.000. It is important for the index to increase toward shorter wavelengths as required to maintain a “physical” shape when the material is transparent. This is not restricted by the Cauchy equation. If either “B” or “C” is a negative number, it is possible for the Cauchy equation to show an “unphysical” shape, where the index decreases toward short wavelengths. Thus, it is important to check the final shape of the index to ensure it follows normal dispersion (Section 5.2.1).

5.3.1 ADDING SLIGHT ABSORPTION IN THE UV

The Cauchy equation, by itself, assumes that $k = 0$. Some films which have slight absorption in the UV spectral region can still be described by

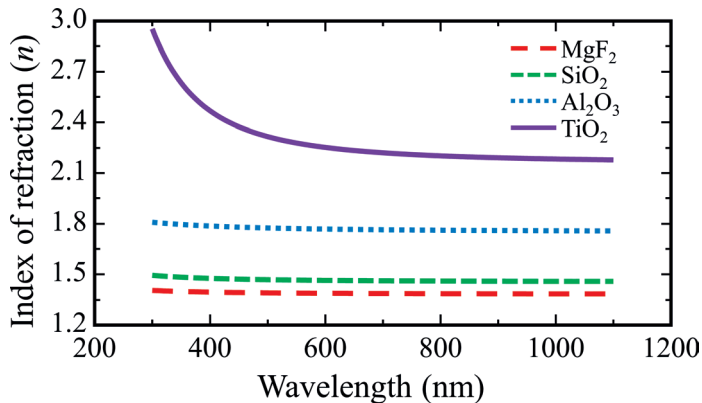


Figure 5.3. The optical function for n is shown for several dielectric materials as described by the Cauchy equation.

Table 5.2. Cauchy coefficients associated with each index curve shown in Figure 5.3

Material	A	B	C
MgF ₂	1.3831	0.00205	0.000000
SiO ₂	1.4544	0.00313	0.000036
Al ₂ O ₃	1.7528	0.00572	-0.000064
TiO ₂	2.1564	0.02182	0.004485

the Cauchy Equation, with slight modification. The index, $n(\lambda)$, is still described by the usual Cauchy equation, described in Equation 5.1. The extinction coefficient $k(\lambda)$ is described by the Urbach equation [45],

$$k(\lambda) = A_k e^{B_k(E - E_b)} \quad (5.2)$$

where E is the photon energy, and

$$E_b \approx \frac{1240}{\lambda_b} \quad (5.3)$$

The input parameters for the Urbach equation are A_k , B_k , and λ_b , which suggest, at first glance, a three-parameter equation. However, there are an infinite number of combinations of A_k and λ_b which result in the same

curve shape. Accordingly, during regression analysis, the value of λ_b is set by the analyst and the parameters A_k and B_k are allowed to vary. It is suggested that the value of λ_b be set to a value near the shortest wavelength in the spectral region. When the wavelength λ is equal to the assigned value of λ_b , the exponent is zero and $k(\lambda) = A_k$. Figure 5.4 shows the optical functions of a silicon nitride film described by the Cauchy equation along with Urbach absorption. The coefficient values are shown in Table 5.3.

While the Urbach absorption helps extend the useful wavelength range of the Cauchy, it should not be used when the material becomes significantly absorbing. In the next sections, we introduce models useful for both transparent and absorbing regions.

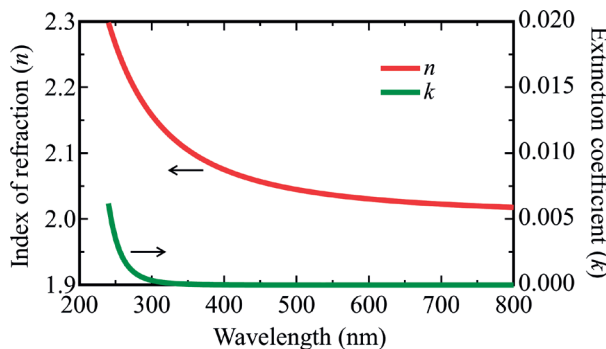


Figure 5.4. The optical functions for a silicon nitride film, described using the Cauchy equation for n with Urbach absorption to describe k .

Table 5.3. Cauchy and Urbach parameter values related to the optical functions plotted in Figure 5.4

Parameter	Value
A	2.0037
B	0.00831
C	0.000499
A_k	0.0039
B_k	2.7136
λ_b	248 nm

5.4 OSCILLATOR MODELS

We introduce here two common models for absorbing materials with unknown optical properties: oscillator model and the b-spline model. Our choice depends on the complexity of the optical functions. The oscillator model is most useful when there are a small number of absorption features. The b-spline is advantageous when describing more complex optical function shapes.

Let's consider the general shape of the optical constants in the absorbing region. There will be peaks in absorption at resonant frequencies where the material is most likely to absorb the incoming light of that wavelength. This is analogous to the resonance of a mechanical system such as a mass on a spring (Figure 5.5), which absorbs energy from the driving force when the driving force (the finger) is near the resonant frequency of the vibrating system.

For an optical system the incoming light provides the driving force and the material experiences a resonant vibration that absorbs this energy. At short UV to NIR wavelengths (very high frequencies) the electrons can absorb the light. If we slow down the frequency to mid IR wavelengths, lighter atoms can vibrate relative to the heavier atoms in a molecule.

There are many oscillator equations which can describe a resonant absorption. We introduce a few common oscillator functions here, but the equations for each (and others) are available in optics textbooks or handbooks [46, 47]. Rather than deal with the equations, we describe the shapes of the optical functions (see Section 2.2.2), either as the complex dielectric functions (ϵ_2 and ϵ_1) or the complex refractive index (n and k). The theory behind oscillator shapes is based on how the material reacts to incoming

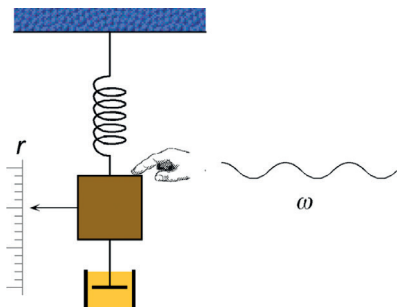


Figure 5.5. A mechanical oscillator, which is a forced harmonic oscillator with damping, is shown.

electromagnetic waves, thus it generally describes the complex dielectric function. Additionally, the response is frequency dependent, so it is common to show absorption features on a frequency scale (or photon-energy scale) rather than on a wavelength scale.

Oscillator models are beneficial for many reasons. First, they can describe both transparent and absorbing materials. Second, they maintain the physical tie between real and imaginary optical functions, referred to as KK consistency (Section 5.4.1). Third, they describe the optical functions with a greatly reduced number of free parameters.

A single Gaussian oscillator is shown in Figure 5.6. The dielectric function shape is described by four parameters. Three parameters describe the absorption shape (imaginary dielectric function, ϵ_2) and are analogous to the aforementioned vibrating oscillator. These parameters are similar for many oscillators we encounter: center energy (the resonant frequency), amplitude, and broadening. The fourth parameter (ϵ_1 offset) is used to shift the real component of the dielectric function.

This general shape is the basis for many simple oscillators, such as the Lorentz, Harmonic, and Gaussian. Their slight differences are easiest to visualize in comparison. Figure 5.7 shows ϵ_2 for both a Lorentz and

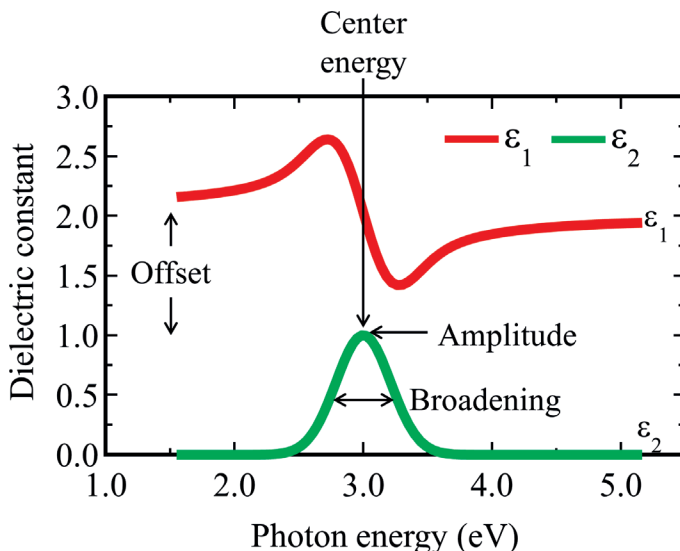


Figure 5.6. General shape for a Gaussian oscillator is shown. The imaginary dielectric function (ϵ_2) is described by the center energy, amplitude, and broadening of the resonant absorption. The real dielectric function is produced from KK transformation of the ϵ_2 curve, along with an offset added to ϵ_1 .

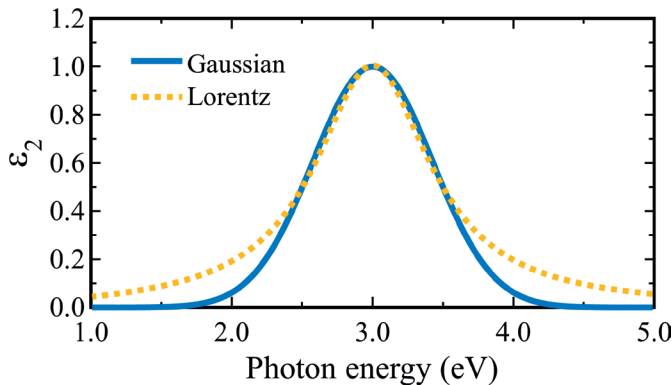


Figure 5.7. ϵ_2 versus photon energy plotted for a Gaussian oscillator and a Lorentz oscillator.

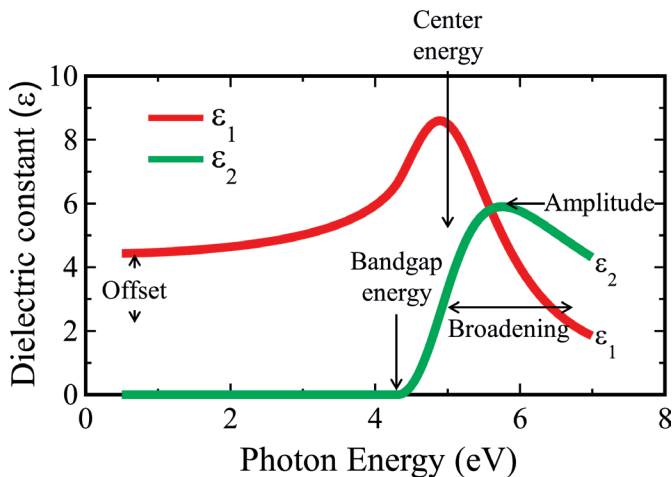


Figure 5.8. A Tauc-Lorentz oscillator describing the optical functions of Ta_2O_5 is shown.

Gaussian oscillator. Neither curve goes quite to zero on either side of the resonant absorption peak, but the Gaussian oscillator approaches zero much faster than the Lorentz oscillator.

Both Lorentz and Gaussian curves are nearly symmetric around the resonant absorption. A few asymmetric oscillators were developed for materials with a bandgap, where no absorption occurs at lower energies. These include the Tauc-Lorentz [48], which is commonly used for amorphous dielectrics and semiconductors. Figure 5.8 illustrates the

shape of a Tauc-Lorentz oscillator describing the dielectric function of a Ta_2O_5 film. The Tauc-Lorentz introduces an additional parameter, the “bandgap energy,” to the four traditional oscillator parameters introduced earlier. Adding the band gap term tilts the absorption to an asymmetric shape which moves much of the absorption to higher energies and shifts the absorption peak above the center energy within the equation. Regardless of the subtleties within the equation, it is very effective at describing the natural shape of amorphous materials with five simple free parameters.

5.4.1 KRAMERS-KRONIG RELATIONSHIP

The optical functions (ε_1 and ε_2) are not independent. They are physically connected by the KK relationship. If all the spectral values of ε_2 are known, then the values of ε_1 can be calculated by,

$$\varepsilon_1(E) = 1 + \frac{2}{\pi} P \int_0^{\infty} \frac{E' \varepsilon_2(E')}{E'^2 - E^2} dE' \quad (5.4)$$

where P is the principal part of the integration [7].

The key to this equation is the direct link between the real and imaginary optical functions. It forms the basis for each of the oscillator equations that we considered. The oscillator parameters are primarily used to describe the absorption shape. The KK integral allows calculation of the real part. An integral determines the area under a curve; thus the shape of ε_1 is tied to the area within the absorption shape. The integration covers all frequencies, yet our SE measurement collects but a small range of frequencies. Thus, the KK transform produces the general curve shape, but not the absolute magnitude of ε_1 . This is the reason that most oscillator models include an offset for the real part. The offset is often called either “ ε_1 -offset”, or “ ε_∞ ”, and represents the value of ε_1 far from the oscillator location, which corrects for missing ε_2 absorption not included in the integration.

Consider application of the KK transformation to a series of oscillators shown in Figure 5.9. The result is shown for ε_1 offsets of 1 and 2. The absorption is shown as “bumps” in the plot of ε_2 . Recall from Section 5.2.2 that anomalous dispersion says that the real part of the optical function will flip directions near the peak of the absorption. In Figure 5.9, each absorption “bump” produces a “wiggle” in the plot of ε_1 . They go together in that there is always a wiggle with every bump.

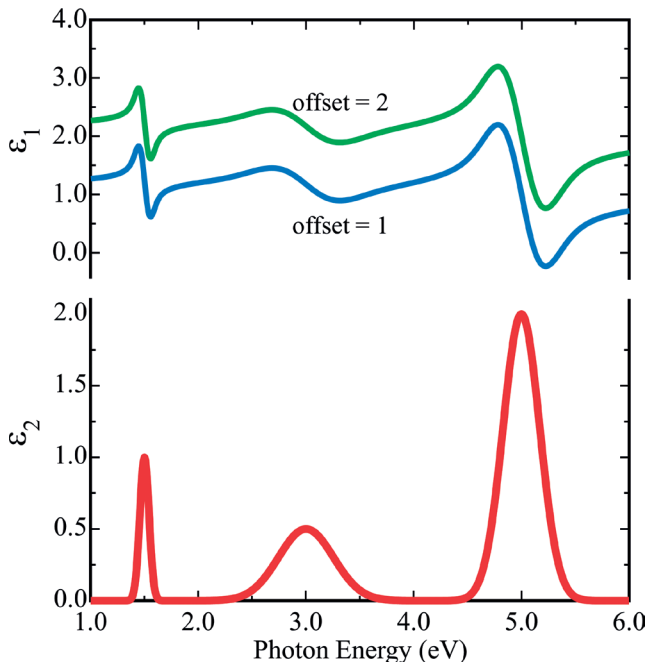


Figure 5.9. Optical functions for a material with three separate absorptions described by Gaussian oscillators. Each absorption “bump” has a corresponding “wiggle” in ϵ_1 . The general shape is determined from the KK transform, with an additional ϵ_1 offset (shown for two different values).

Looking closely at the dielectric function shapes of Figure 5.9, we can divide the curves into two distinct spectral regions. First, there are regions with little to no absorption ($\epsilon_2 \sim 0$). In this region, the ϵ_1 curve rises as we increase photon energy (normal dispersion, Section 5.2.1). Second, there are regions with strong absorption around the ϵ_2 peaks. These are the bumps that cause the ϵ_1 curve to flip-over or wiggle (anomalous dispersion, Section 5.2.2). Looking closely at the region of the absorption peak, the ϵ_1 curve has decreased about half-way near the ϵ_2 peak energy. The final shape of the ϵ_1 wiggle depends on the amplitude and broadening of the ϵ_2 bump, as shown by the variation of absorptions in Figure 5.9.

We have shown the absorption band using the dielectric function versus photon energy. In Figure 5.10, we show a Gaussian oscillator formatted as complex refractive index versus wavelength. Because wavelength is inversely related to photon energy, the wiggle of the index is

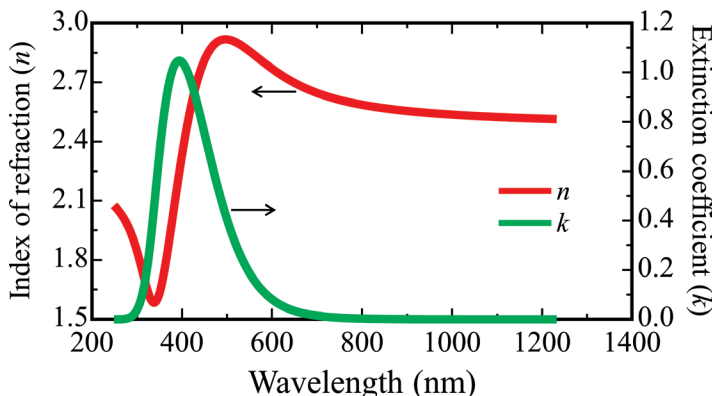


Figure 5.10. The optical functions, n and k , are shown versus wavelength for a Gaussian oscillator.

reversed compared to that shown for the dielectric function versus energy. Also, the bump in extinction coefficient is no longer symmetric.

5.5 B-SPLINE

A key benefit of “dispersion” equations is to describe the optical constants over a wide wavelength range with few free parameters. While we may measure 500 wavelengths, each of which has different n and k , their shape versus wavelength can often be represented by 5 to 10 parameters of a dispersion equation. It is nice if the dispersion equation is founded on an underlying “physics-based” model, such as many of the oscillator models of the previous section. However, it is often not necessary, or practical, to know the physics behind our material—we simply want a smooth, continuous curve that is described by a minimum of free parameters. One such example would be a curve given by a polynomial to the n^{th} degree, which is represented as:

$$p_n(\lambda) = a_n \lambda^n + a_{n-1} \lambda^{n-1} + \dots + a_1 \lambda + a_0 \quad (5.5)$$

You may see some similarities of the preceding curve to the Cauchy equation described earlier in the chapter. These equations are often empirical, which means they are designed to best match the known shape of optical constants. Polynomial equations may be adequate for narrow wavelength ranges or regions where the optical properties do not vary

significantly (such as the transparent region that is fit well by the Cauchy). However, they are not acceptable for wide wavelength regions with varying optical features (such as the absorbing region of most materials).

A better solution that adds significant flexibility is the use of a spline function. The spline divides the total wavelength range into intervals. Each interval is described by a simple function, such as a polynomial. With the spline, the interval size can be increased or decreased depending on how much variation is required over each wavelength range. There are many types of splines and they are designed to maintain continuous and smooth curves across the spectral range by matching values and derivatives where the segments are joined.

One special type of spline is called a basis-spline [49] (or b-spline). Rather than joining curves that are described for each segment, the b-spline sums individual basis functions to construct the final curve. Each individual basis function is constructed from polynomials, but now they are localized. This means that if the curve needs to vary at one specific wavelength, it will only be adjusted by the basis function that is in that region and avoid moving the optical functions at remote wavelengths. To visualize how this works, consider Figure 5.11. The “nodes” represent the amplitude applied to each individual basis function. The individual basis functions or “spline components” sum together to form the final b-spline curve. Notice that the final curve does not touch each control point (node). They simply adjust the general shape of the curve in a local region, but are summed with the edges of surrounding components to form the final shape. To increase control over the shape of the b-spline, the user

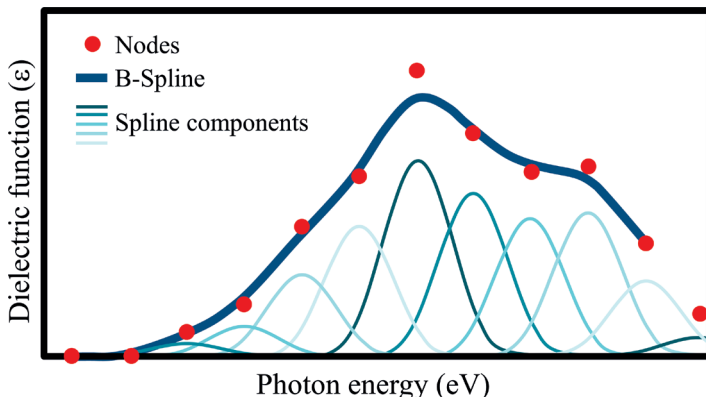


Figure 5.11. A b-spline curve is described by a series of nodes that adjust the amplitude of individual basis functions which are summed to form the final curve.

can increase the number of nodes within an energy range. If the optical functions are featureless, fewer nodes could be used to decrease the total number of “free parameters” describing the final shape.

In Figure 5.12, we show a b-spline representation of the dielectric functions of a phenyl-C₆₁-butyric acid methyl ester (PCBM) thin film. Here, there are two b-spline curves, one for the real dielectric function and one for the imaginary dielectric function. One of the key benefits of the b-spline curve is that it is amenable to the KK transformation. Thus, we can further simplify the b-spline description of a material by describing only the ϵ_2 function with a b-spline and then performing the KK transform to get the ϵ_1 shape.

This is represented in Figure 5.13 for PCBM, where now only the ϵ_2 curve is represented by a b-spline function. Recall that the KK transformation covers all frequencies and the final shape of ϵ_1 depends on the full integration. To add extra absorption outside of our measured spectral range that can be used within the integration, a few extra b-spline control points are allowed at higher photon energies.

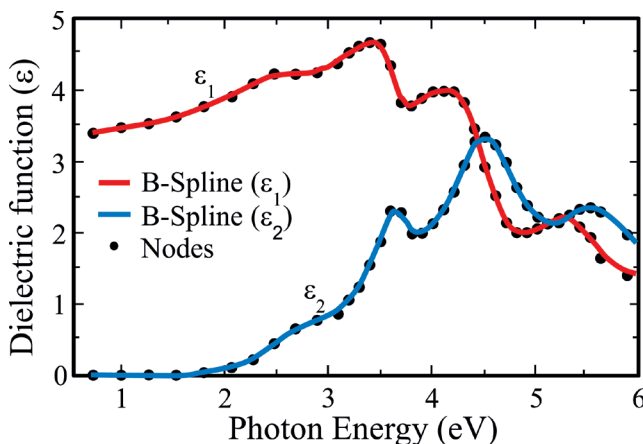


Figure 5.12. A b-spline is shown representing the optical functions for PCBM.

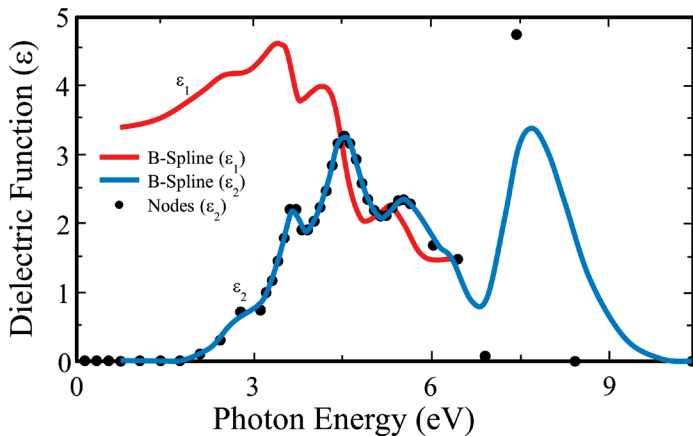


Figure 5.13. A KK consistent b-spline is shown representing the optical functions for PCBM.

CHAPTER 6

OPTICAL DATA ANALYSIS

Up to this point, we focused on the measurement of Ψ and Δ spectra. The goal, however, is to determine sample properties such as film thickness and optical functions. In this chapter, we consider the approaches used to obtain sample properties from the measured ellipsometry data, as illustrated in Figure 6.1.

We start by discussing the special case where optical functions of a bare substrate can be directly calculated from the experimental spectroscopic ellipsometry (SE) data. More commonly, our sample consists of one or more thin films on the substrate, which makes the determination of optical functions more involved.

Using the equations from Chapter 2, Ψ and Δ can be calculated for a given angle of incidence, layer thicknesses, and complex optical functions for each material. Some of these equations are transcendental, so they can't be inverted to represent the sample properties as a simple function of measured quantities. Rather, regression analysis methods are implemented as described in Section 6.3.

6.1 DIRECT CALCULATION: PSEUDO-OPTICAL CONSTANTS

If our sample is a bare substrate with a single, perfect interface between the material of interest and surrounding ambient, the measured values of Ψ and Δ for each wavelength can be directly inverted to give the complex optical functions:

$$\langle \tilde{\varepsilon} \rangle = \langle \tilde{N}^2 \rangle = \sin^2(\phi) \left[1 + \tan^2(\phi) \left(\frac{1-\rho}{1+\rho} \right) \right] \quad (6.1)$$

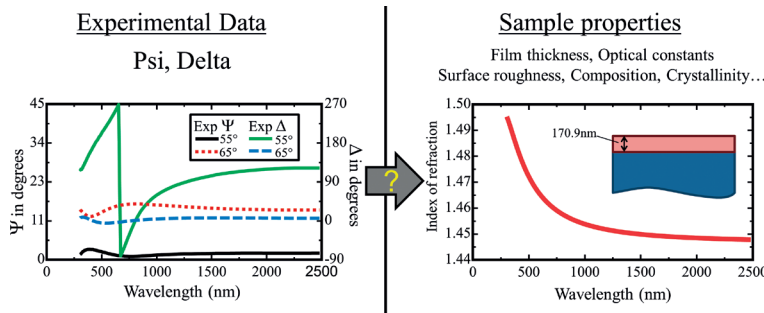


Figure 6.1. With ellipsometry, it is important to consider the methods to bridge from experimental measurements to desired sample quantities.

where ϕ is the angle of incidence, and ρ is given by Equation 2.32 (ρ contains the Ψ and Δ information). The assumption here is that the measurement comes from a single reflection at the surface. However, if there are any surface layers, regardless of how thin, the calculation will not produce the true optical functions. To distinguish between the true optical functions of a material and the direct-calculation values that may be influenced by the surface, we use triangle brackets around the optical functions and refer to these calculations as “pseudo” optical functions. The presence of even subnanometer surface roughness, oxidation, or contamination will produce pseudo-optical functions that vary from the actual optical functions.

Because most surfaces will not be pure, the direct calculation has limited use. However, it is applied to opaque metal surfaces to estimate the optical functions, even with the understanding that these surfaces may include roughness or oxidation. In this case, there is often not enough information from SE alone to fully characterize all unknown sample properties (complex optical function and surface layer). The calculated pseudo-optical functions are used to approximate the metal surface. The metal can then be coated with thin films and characterization of the films can use the pseudo optical functions for the metal.

An important test of the pseudo-substrate calculation is to compare results from multiple angles of incidence. In Figure 6.2, we show the pseudo optical functions calculated for an opaque metal surface. The Ψ and Δ curves for three angles of incidence all convert to the same pseudo-dielectric functions. This is not a guarantee the surface is coating-free. It merely indicates that any surface coatings are thin enough to appear similar when viewed from different angles. In essence, it also says that while our ellipsometric spectra look very different from each angle of incidence, they contain exactly the same sample information. With this in mind, it can be helpful to use the direct calculation on samples that are not bare substrates.

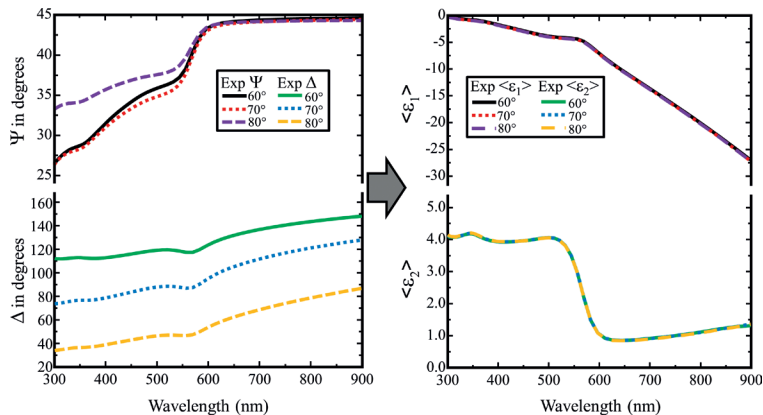


Figure 6.2. Ψ and Δ spectra were measured from an opaque metal film at three angles of incidence. These spectra are directly transformed to show pseudo-dielectric function curves corresponding with each angle. Because light is reflected from a single interface, the pseudo-dielectric function curves from the three angles overlap each other.

By varying the angle of incidence, the pseudo-optical functions can indicate if new sample information is available and whether the sample appears similar to a single surface reflection. If pseudo-optical functions from different angles lie on top of each other, there is no new information from different measurement angles. This also suggests that the sample appears to be similar to a single surface reflection. However, even a 20 nm thick surface layer can meet this requirement. We can also consider whether the pseudo-optical functions maintain a “physically plausible” result. Consider the SE data in Figure 6.3 from a multilayer SOI (semiconductor on insulator) stack. The pseudo-optical functions from two angles separate above 400 nm. In addition, the $\langle \epsilon_2 \rangle$ value goes negative, which is not physically plausible for ϵ_2 . Thus, the measured light did not come from a single surface reflection. Interestingly, the pseudo-optical functions do lie on top of each other for ultraviolet wavelengths (<350 nm). Here, the silicon film is strongly absorbing, and no light returns from the underlying interfaces. Even here there will be a native surface oxide that will affect the pseudo-optical functions.

6.2 DATA ANALYSIS—THE PROBLEM

The general purpose of ellipsometry characterization is to transform the measured quantities, Ψ and Δ , into sample properties such as optical functions and film thickness. For a substrate (i.e., no films), this transformation is straight forward, as discussed in Section 6.1. When a

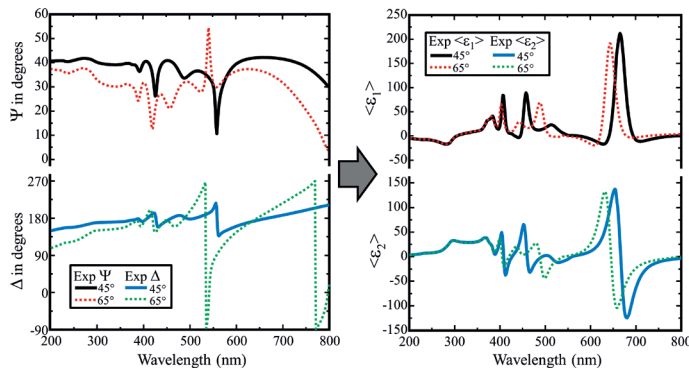


Figure 6.3. Ψ and Δ spectra from a multilayer SOI sample, along with the direct transformation to pseudo-dielectric functions. The pseudo-dielectric functions separate at longer wavelengths where light is detected from multiple interfaces within the thin film stack.

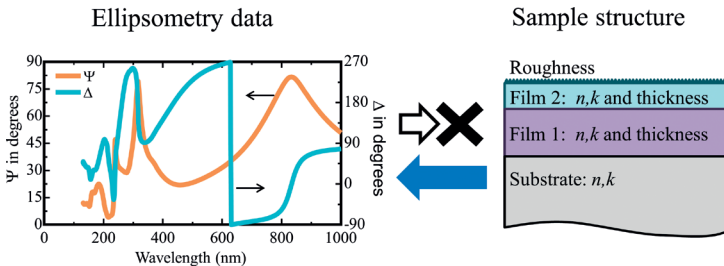


Figure 6.4. Demonstration of the “Inverse” problem, where sample properties cannot be directly calculated from measured ellipsometric quantities, but the ellipsometric quantities can be calculated for any given sample structure.

film is present, the Ψ and Δ can't be directly transformed into sample properties. However, we can transform the sample description into values of Ψ and Δ using the equations from Chapter 2. This is referred to as the inverse problem, as shown in Figure 6.4. Hence, to obtain optical functions and thickness from the measured ellipsometric quantities, we must use an approach that is more involved than simply plugging values into an equation and solving algebraically.

6.3 DATA ANALYSIS—THE APPROACH

Since we can transform our sample description into ellipsometric quantities, we shall do just that. Our goal is to find a unique set of sample

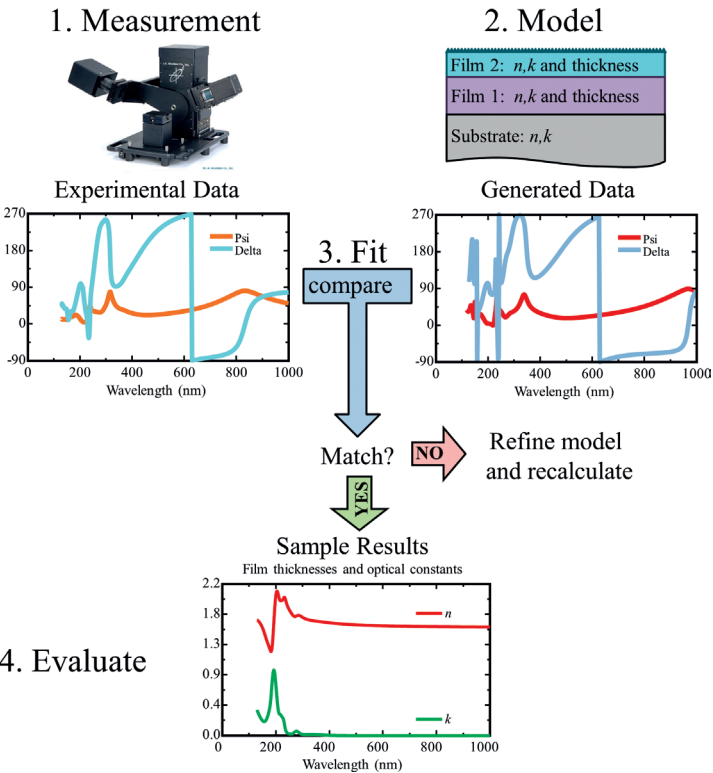


Figure 6.5. The typical flow for SE data analysis involves: (1) Measure the SE data, (2) describe sample with a model, (3) fit the experimental data and model-calculations by varying unknown model properties, and (4) evaluate results.

properties (thicknesses and optical functions) from which we calculate the same Ψ and Δ that we measure. This process can be divided into various steps, as illustrated in Figure 6.5. In general, (1) the experimental Ψ and Δ data are measured, (2) the sample is described by a model that allows calculation of corresponding “generated” data curves, (3) the model calculations are fit to the experimental data by adjusting any unknown sample properties, and (4) the results are evaluated. Each step is further detailed in the following sections.

6.3.1 MEASUREMENT

We start by measuring our sample to obtain Ψ and Δ data. The data are collected for each wavelength and angle of incidence combination.

Our primary goal is to collect adequate data to uniquely determine all unknown sample properties. It is okay to overdetermine the problem, so more wavelengths and angles are welcome. However, as we demonstrated in Section 6.2, increasing the number of angles does not necessarily lead to new information. Thus, our primary source of new information comes from additional wavelengths. This is the driving force behind modern ellipsometers with expanded wavelength ranges from ultraviolet to near infrared with 1,000 or more individual wavelengths. If there are too many unknown sample properties to determine uniquely, we may need to either divide the problem by measuring additional samples that provide supporting information or use additional characterization techniques to complement our SE measurements.

6.3.2 MODEL

Next, a model is constructed to describe our sample. The model consists of the structure of all materials the light may encounter. Each material must include a proposed thickness and optical functions to allow calculation of the ellipsometric response. The optical functions can be in any of the formats discussed in Chapter 5 (i.e., tabulated lists or dispersion equations). We start by entering all sample properties that we know—such as optical functions for our substrate and possibly even our thin films. Next, we need to provide initial estimates (our best guess) for the unknown sample properties. An example model is shown in Figure 6.6. With this initial sample description, the equations from Chapter 2 are used to calculate

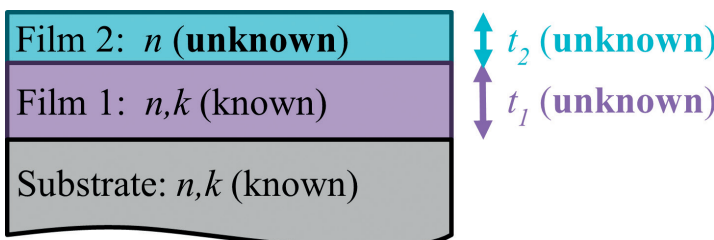


Figure 6.6. A model representing the measured sample with both fixed values (known properties) and fit parameters (unknown properties).

Ψ and Δ spectra. It is unlikely this initial estimate will produce a perfect match to the measured Ψ and Δ , but hopefully it will come close to the measured values. If not, we may need to reconsider our initial guesses, based on comparisons between the model-calculated and experimental data curves.

6.3.3 FIT

The sample properties that are not well known are identified as the “fit” parameters. The software will adjust these unknown sample properties in an attempt to find the best match between the model-calculated and experimental curves. This is called data fitting and involves regression analysis. A “goodness of fit” is used to quantify any discrepancies between the model-generated and experimental data curves. One such goodness of fit is the “Mean-Squared-Error” or simply “MSE,” and it provides a quantitative comparison between the generated and measured data curves. There are many formulations for MSE (also Chi-Square), but with each, a lower value represents a better match between the model and the experiment. The goal of the regression analysis is to minimize the MSE by adjusting the unknown sample properties. Once the minimum MSE is found, the fit will stop and present this answer to the user for evaluation.

To demonstrate the iterative Data Regression Analysis process, consider the experimental data of Figure 6.7. In this case, hundreds of wavelengths are measured at a single angle of incidence, with only a single unknown value to consider (film thickness). The initial thickness is estimated at 700 nm (basically, an educated guess), which produces the initial generated curve with similar overall shape but shifted to shorter wavelengths. The software will quantify the difference between this generated curve and the experimental curve, leading to an MSE over 500. The MSE contour for this case is shown in Figure 6.8. The contour is not known at time of fitting and is only convenient to graph for simple cases with one or two unknown parameters. As Figure 6.8 suggests, the MSE slopes down toward thicker films from this initial guess of 700 nm thickness. The algorithm to find minimum MSE follows the slope to adjust the estimated thickness to a larger value, leading to a lower MSE. This is repeated until the minimum MSE is found. This produces a final thickness value of 749.18 nm after nine iterations in our example.

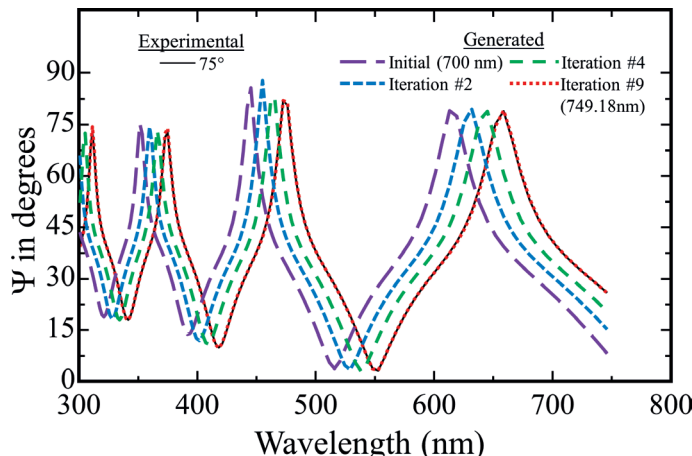


Figure 6.7. The curve generated from an initial thickness guess of 700 nm has a shape similar to the experimental data curve but is offset toward shorter wavelengths. An iterative data analysis algorithm searches for a minimum MSE value by adjusting the thickness guess. A few iterations are shown along with the final thickness result of 749.18 nm, which lies on top of the experimental data.

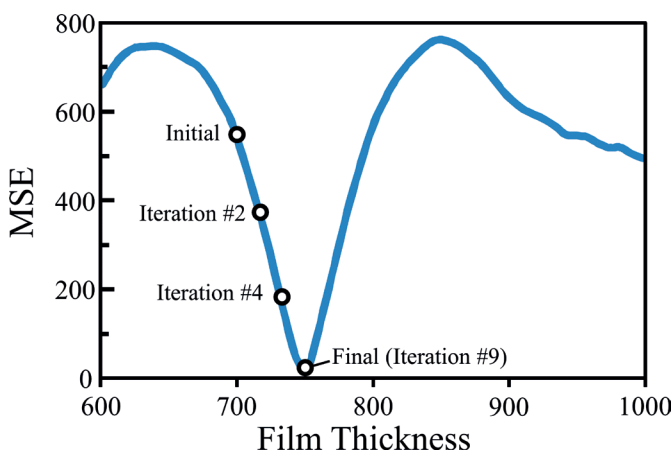


Figure 6.8. The MSE profile for the fit from Figure 6.7 versus thickness is shown. The initial guess has an MSE over 500. The slope of the MSE curve at this point shows that a thicker film will produce a lower MSE. The fit iterations progress toward the minimum MSE, which is reached for a thickness of 749.18 nm.

6.3.4 EVALUATION

After the regression process obtains the best fit, the analyst must then make an assessment of the results to decide whether the fit is reasonable. The first thing to consider is whether the fit was successful in finding the best MSE value. If the model-generated curves do not visually match the experimental data curves, then the fit may have failed to find a good solution. This is referred to as “chi-by-eye,” as the user makes a quick visual assessment of the fit results.

The final MSE is simply a minimum in the MSE shape with variation of the unknown parameter. However, it is possible for the regression algorithm to find a minimum that is not the best MSE. Consider the shape of the MSE in Figure 6.9. There are six separate MSE minima within this range of film thickness. The film thickness near 750 nm is the lowest MSE minimum, which we refer to as the global minimum. The other minima are referred to as local minima, and it is important to avoid results from these minima. For this case, all local MSE minima have a much higher MSE and should show visible differences between the model-generated and experimental curves. This will be the first clue that the analysis has fallen into a local minima. This graph shows the importance of estimating a good starting point for each parameter to allow the regression analysis algorithms to drop into the Global MSE minimum. Either

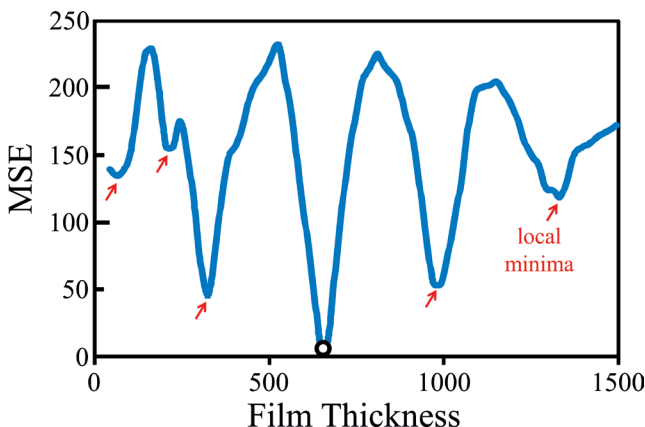


Figure 6.9. An MSE plot versus film thickness shows both the “best fit” MSE minimum (black circle) and many “local minima” that may stop a standard regression algorithm from proceeding but would not result in the best-fit result.

the user needs to start the model with guesses close to the final answer or sophisticated software methods need to be implemented to search for the Global Minimum.

Once the fit appears to have found the global minimum, there are other evaluation criteria to consider.

1. Is each “unknown” fit parameter uniquely determined? A good test for this criterion is to adjust the fit parameters away from their final solution and see if they reproducibly return to the same final values when the MSE is minimized.
2. What is the sensitivity to each fit parameter? This can be judged by the variation of the MSE as the fit parameter is adjusted from its minimum value. Are multiple fit parameters uncorrelated? This relates to whether we can uniquely discriminate the response from each fit parameter. If more than one fit parameter will adjust the calculated response in a similar manner, these parameters are correlated and neither set of parameters can be assumed to be correct.
3. Are the results physically plausible? This final consideration may be difficult to assess but becomes easier as the user becomes more experienced. For example, any determined optical functions should maintain Kramers-Kronig consistency (Section 5.4.1).

The uniqueness and sensitivity of our fit parameters can be estimated by studying the MSE profile. We saw in Figure 6.9 that multiple MSE minima may be found. However, only a single MSE minimum had a low value to suggest a good data fit; so the other minima could be dismissed. If multiple minima have similar MSE values, the result would not be unique.

The MSE minimum can also demonstrate parameter sensitivity. The faster the MSE rises on each side of the minimum, the more certain we can be in the obtained value of the identified fit parameter. As an example, we compare two MSE profiles in Figure 6.10. The MSE minimum is located at the same value for film thickness, but Model #1 is much more sensitive to the final fit result than Model #2. This is often the case when models become more complicated. It is common to introduce additional model complexity to improve the MSE. However, in doing so, we likely reduce our sensitivity to each of the fit parameters. Thus, a good rule-of-thumb is to use the minimum set of fit parameters that provides a good match to the data. For most cases, an MSE improvement of less than 10 to 20 percent may not warrant added model complexity. The simpler

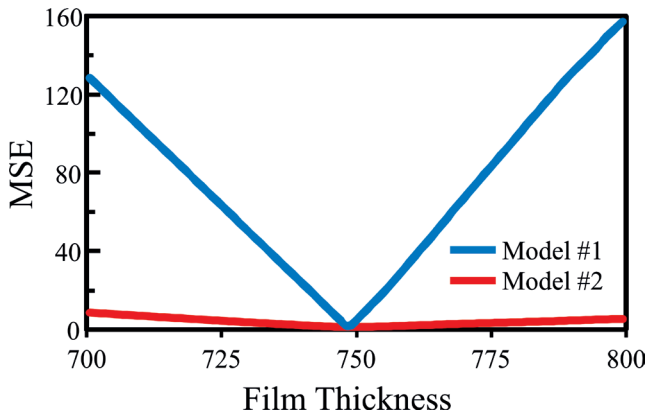


Figure 6.10. The MSE profile versus the fit parameter (in this case, film thickness) verifies how sensitive the data analysis will be to the fit parameter of interest. If the MSE rises quickly from the minimum value as the fit parameter varies, then the result has high sensitivity (e.g., Model #1). If the MSE stays nearly the same value around the minimum, it shows that other answers give similar results, which calls into question the uniqueness and sensitivity of the final answer (e.g., Model #2).

model still adequately matches the data and will have better sensitivity and uniqueness.

If the fit assessment indicates that the results are reasonable, then the values of the thickness and optical functions are accepted as the proper result of the regression analysis.

If the fit evaluation shows that the result is not a unique, sensitive description of the sample, it may be required to further extend the characterization of the sample. Following are three possibilities:

1. **More SE data:** It can be beneficial to measure more wavelengths or more angles of incidence, as all the data are used simultaneously to determine the unknown parameters. Even in the case of an overdetermined problem, the additional data can help reduce the statistical estimate of each unknown parameter.
2. **More samples:** When the measured data is inadequate to determine all unknown sample properties, it is often helpful to measure additional samples. For example, the problem can be divided by first measuring the bare substrate so that these properties can be

fixed when considering coated samples. If dealing with multilayers, it is common to also measure single-layer films to help get a good understanding of their optical functions and reduce the unknowns when considering the multiple layer thicknesses. In some cases, the uniqueness can be further enhanced by measuring multiple samples with the same thin films but with varying layer thicknesses. This works when the films maintain their same optical functions independent of film thickness, which is not always the case.

3. **Supporting characterization methods:** While SE is a great tool for characterizing thin films, it is not the only tool. The user should consider other characterization methods they have at their disposal.

In the remaining chapters, we will consider typical SE characterization examples including transparent films, very thin films, films with rough surface, films with absorbing regions, and more.

CHAPTER 7

TRANSPARENT THIN FILMS

The most common spectroscopic ellipsometry measurement is determination of thickness and refractive index from a transparent thin film. The film thickness can range from subnanometer to many microns. However, the optimum range for UV-vis-NIR spectroscopic ellipsometry to determine both thickness and index accurately is generally from 50 nm to 2 μm . If the layer is very thin (<10 to 20 nm), it is difficult to determine the index of refraction, as we discuss in Chapter 9. When films become many microns thick, the spectral features come very close together and can be affected by small nonidealities in either sample or measurement. Thus, although spectroscopic ellipsometry can successfully measure films up to 20 μm and thicker, it is only so with increasing difficulty and hence, other characterization methods may be preferred.

The approach outlined in this chapter can be applied to any transparent film. It can also be applied to films that are absorbing at some wavelengths if one simply restricts the wavelength region to where the film is transparent. We discuss how to identify the transparent wavelength region in Chapter 10, which also describes how to further analyze films that absorb at some wavelengths.

Many inorganic films, such as fluorides, oxides, nitrides, and carbides (Figure 7.1), are transparent for visible and near infrared (NIR) wavelengths. Many organic films are transparent over these same spectral regions. Semiconducting films may also be transparent if we restrict the wavelength range to longer, infrared wavelengths. When a material is transparent, it must exhibit normal dispersion (Section 5.2.1), where the index of refraction increases toward shorter wavelengths. This is true for all curves shown in Figure 7.1.

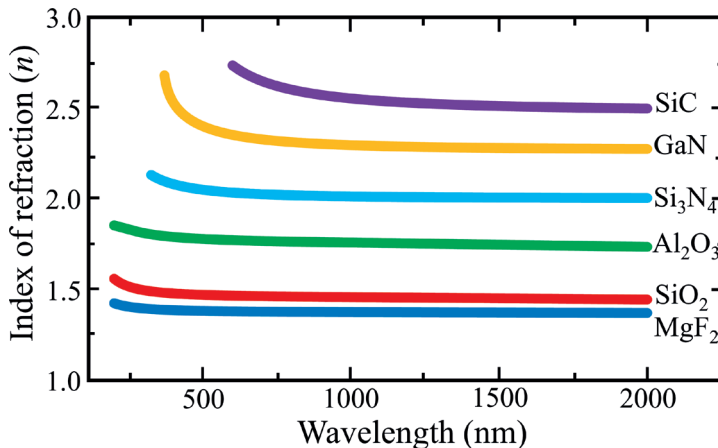


Figure 7.1. The indexes for various inorganic films are shown in their transparent spectral regions.

7.1 DATA FEATURES OF TRANSPARENT FILMS

For transparent films, the Ψ and Δ spectra are dominated by interference features from light traveling through the film and recombining with the surface reflection, as described in Section 4.2.1. This produces peaks and valleys in the spectral data. The interference oscillation shape depends on both film thickness and index, in addition to the substrate's optical properties. As film thickness increases, the oscillation positions shift toward longer wavelengths, as shown in Figure 7.2. As these interference features shift to longer wavelengths, additional features appear from shorter wavelengths that come increasingly close together. In this manner, the total number of oscillations in the spectral range of interest will increase as films become thicker, as demonstrated in Figure 4.12. Simply stated, the more peaks and valleys within the transparent spectral region, the larger the film thickness.

As the index of refraction increases, it also shifts the oscillation positions toward longer wavelengths, as shown in Figure 7.3. This occurs because increasing either the thickness or the index delays the light traveling through the film relative to the surface reflection. The increase in thickness directly affects the length of the light path, while increasing the index reduces the phase velocity. While both thickness and index shift the oscillation positions, only the index will also affect the Ψ oscillation amplitudes (also seen in Figure 7.3). Note how the increase in the index causes both a shift in the Ψ peaks to longer wavelength and a gradual

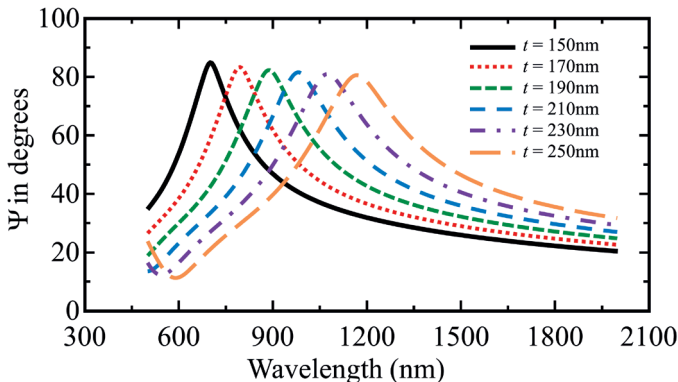


Figure 7.2. As film thickness increases, the interference features shift toward longer wavelengths. This is a result of longer path lengths within the film.

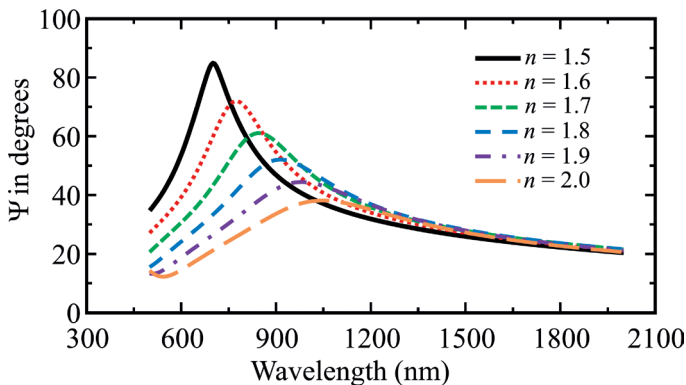


Figure 7.3. As the film index increases, the interference features shift toward longer wavelengths and with reduced Ψ peak amplitudes. This is a result of reduced phase velocity and reduced optical contrast between film and substrate.

decrease in the overall Ψ peak amplitude. The amplitude of the Ψ valley is not affected in this case, as the valleys were established by the silicon substrate optical constants. While the substrate formed the lower boundary for our curves in this case, it can also form the upper boundary depending on the angle of incidence and optical constants for both film and substrate. To judge whether the film is forming the peaks or valleys, you can simulate data from a bare substrate to compare with the experimental data and this will show the substrate boundary.

7.2 FITTING A TRANSPARENT FILM WITH KNOWN INDEX

If the optical functions are known for both the substrate and thin film, then the film thickness is the only unknown sample property. The interference features will guide us to the correct thickness result. The oscillation shapes and amplitudes should already be matched. As an example, consider Figure 7.4 where the Ψ spectrum from an SiO_2 coating on silicon is shown. There are five Ψ peaks in our measured spectrum. A curve was also generated for an initial SiO_2 thickness estimate of 150 nm. Note that 150 nm thickness produces only two Ψ peaks, so it is obvious that this estimate is too thin to describe the measured layer. If the regression process is started with the thickness seed value of 150 nm, the mean-squared-error (MSE) would fall into a local minimum rather than the global minimum and the regression process will fail. At this point, the user can refine the thickness estimate and generate another spectrum. The challenge for this type of analysis is to somehow choose an initial thickness estimate which is close enough to the correct value that the MSE falls into the global minimum. If the starting thickness is between 261 nm and 461 nm, the analysis will be successful and the best thickness fit will be determined to be 351 nm for the sample illustrated in Figure 7.4. Any value outside this range will result in the MSE falling into a local minimum, resulting in a failure of the regression process.

There are several methods for choosing an appropriate starting thickness. The first is brute force where the user repeatedly guesses

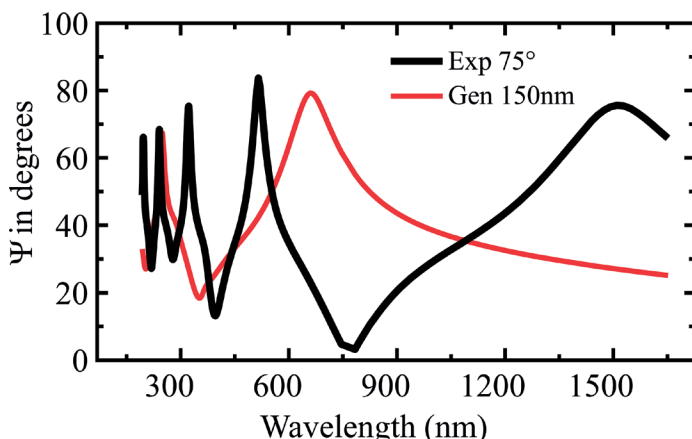


Figure 7.4. The measured Ψ spectrum for a thermal oxide on silicon is shown along with simulated data for a film thickness of 150 nm.

a thickness and then generates the data until the correct number of interference features is present. Some software allows the user to rapidly vary the thickness with a mechanical device (e.g., the scroll wheel on the mouse) while the generated data are continually updated to match the changing thickness value. A second method, often called a “global fit,” is to allow a computer algorithm to search a range of thickness values. In this case, the software repeatedly calculates the MSE with different thicknesses and reports the best MSE minimum found over the desired search range. With modern computing speeds, this can be done in a fraction of a second. Next, we consider the more common example of a transparent film where the index is unknown.

7.3 FITTING A TRANSPARENT FILM WITH AN UNKNOWN INDEX

When the optical functions of a transparent film are unknown, it is common to use the Cauchy dispersion relationship (Section 5.3) to describe the index of refraction. The simplest way to fit both the index and the thickness is to simply assume a value for the parameter and use the afore-described methods to find the best thickness fit. As discussed in Section 7.1, the film index will affect the overall oscillation amplitude and position of interference features. An incorrect “A” parameter, and thus incorrect index estimate, may prevent us from successfully fitting the data. However, we may be able to estimate the “A” parameter quite successfully. For most dielectric films, the value for the “A” parameter lies between 1.45 (silicon dioxide) and 2.2 (metal oxides or silicon nitride). Organic layers often have an “A” parameter near 1.6. Thus, the user may be able to estimate the “A” parameter quite successfully based on the material in question. When uncertain, it can also be practical to assume a value in the middle, for example, a value of 1.7. With the estimated Cauchy index, the thickness is varied, as described in Section 7.2, until the correct number of interference features is matched. Following the thickness fit, the “A” parameter is then allowed to vary until both the thickness and the “A” parameter are matched. Finally, the “B” and “C” parameters are included in the fit to obtain the best solution for a uniform film with no roughness.

In the event that this process is not successful, it may be necessary to obtain a better estimate of the correct index value. The following process illustrates how this is done.

Figure 7.5 illustrates this approach for any transparent film. We start by estimating the index of refraction, then estimating thickness, and finally

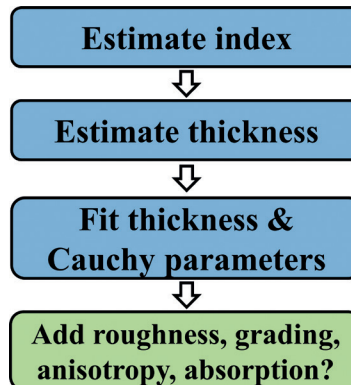


Figure 7.5. Advanced procedure is shown for fitting thickness and index of transparent thin film using the Cauchy dispersion relation.

fitting both thickness and Cauchy dispersion parameters. If the fit is not adequate, optional model complexity can be considered. We now discuss each step in further detail.

7.3.1 ESTIMATING THE INDEX

If our transparent film thickness is between about 50 nm and a couple of microns, there should be one or more interference oscillations which will provide information to allow us to estimate the proper index value. As previously discussed and shown in Figures 7.2 and 7.3, the index of refraction affects the data in two ways. First, the index determines the phase velocity for light within the film, which adjusts the position and number of interference features. Second, the index determines how much light reflects from each interface, which affects the Ψ oscillation amplitudes. Because the former effect also occurs as the thickness changes, these two are potentially correlated—doing the same thing. However, the latter effect is unique to the variation in the index and is used to determine uniquely both the thickness and the index by ellipsometry.

As an alternate method for predetermination of the seed value for the index of refraction, it is beneficial to first adjust the index to match the Ψ oscillation amplitudes. To do this, a nominal thickness estimate is required to demonstrate the interference features. Figure 7.6 shows an experimental measurement from the transparent film along with simulated curves for different film indexes. We have modified the thickness of each guess to visualize the effect on the interference Ψ peak amplitude with changing index.

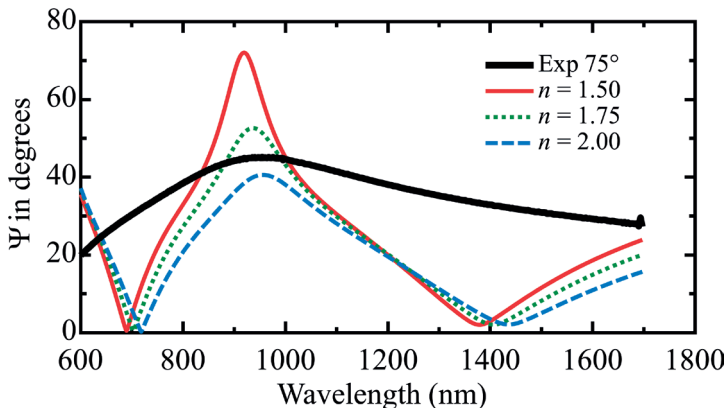


Figure 7.6. The index for this film on silicon can be estimated between 1.75 and 2.00 based on Ψ peak height.

The real curves would also shift the Ψ peaks to different wavelengths. From this simulation, it is clear that the measured film has an index between 1.75 and 2.00.

7.3.2 ESTIMATING FILM THICKNESS

Once you have the correct Ψ amplitudes, the thickness can be adjusted to match the position and number of interference features. For our example, we can estimate an index of 1.9 based on the Ψ peak amplitudes. Next, the thickness was adjusted to match the Ψ peak positions, as shown in Figure 7.7. Up to this point, we have not adjusted the index dispersion, which accounts for the increasing curve differences at shorter wavelengths. However, our goal in this step was not to perfectly match the data, but simply estimate the thickness close enough to fit into the global MSE minimum. We now fit the thickness, the Cauchy “A” and “B” parameters, and possibly the “C” parameter. Be careful not to find a false solution by choosing a physically implausible “B” or “C” parameter. The “B” and “C” parameters are typically near 0.00X to 0.0X and 0.0000X to 0.000X, respectively.

7.3.3 ADDITIONAL CONSIDERATIONS

It is possible to still have discrepancies between our model and experimental data curves after determining the thickness and refractive index as

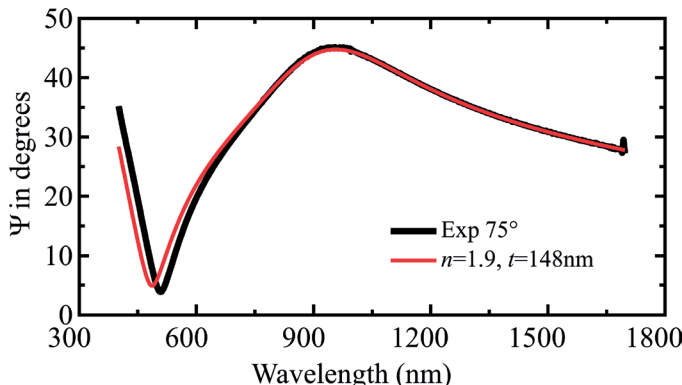


Figure 7.7. With estimated film index of 1.9, the thickness is adjusted to 148 nm to match the interference feature position.

described earlier. This is likely related to an incorrect assumption about our transparent film. We have assumed up to this point that the film is a uniform material with a constant index throughout and with perfectly smooth interfaces. Ellipsometry measurements are often highly sensitive to surface condition, so the data can be affected by even small amounts of roughness. We explore this in more detail in Chapter 8. In addition, ellipsometry data can be affected by depth-variations of the index, which we refer to as index gradients. Another possibility that generally occurs with polymer films and oriented microstructures is for the index to be anisotropic (different along different directions). If this is the case, separate Cauchy equations may be needed to describe the indexes parallel and perpendicular to the film surface. As the model becomes more complex, it is appropriate to monitor the MSE improvement. We expect MSE reductions that exceed 10 to 25 percent for each additional model complexity. If the MSE does not significantly improve, it is recommended to return to the simpler model. If all model complexities fail to provide adequate MSE improvement, the film may not be transparent as first suspected. We will consider thin films that absorb over certain spectral regions in Chapter 10. Now, let's consider a few examples of thin transparent films.

7.4 EXAMPLE: DIELECTRIC SiN_x FILM ON Si

Figure 7.8 shows data for a sample of silicon nitride where we desire to characterize the index (using Cauchy) and thickness of the film. In the previous

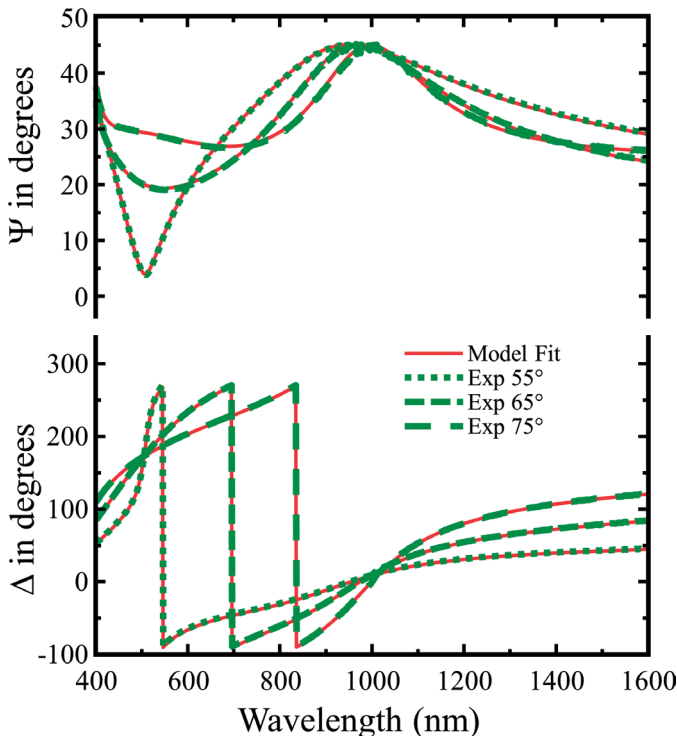


Figure 7.8. Data fits to both Ψ and Δ using a Cauchy dispersion relation for the SiN_x thin film.

example we illustrated two methods for this determination, both of which could be used in the present example. The thickness and Cauchy parameters can be determined either by starting with the Cauchy “A” parameter assumed to be 2.0 (typical of silicon nitride), doing a global fit for thickness, adding the “A” parameter into the fit, and finally including the “B” parameter. The alternate method of predetermining the value of the “A” parameter, discussed in Section 7.3.1, will also work. For this determination, we note that the experimental data in Figures 7.6 and 7.7 was a single angle of incidence selected from the example we will describe here—a SiN_x layer on silicon substrate. We have already demonstrated how the index of refraction was estimated near 1.9 and thickness near 148 nm. Now, we proceed by fitting all three angles over the wavelength range down to 400 nm. Our resultant MSE is near five and one can visually see a good match between the model-generated and experimental Ψ and Δ curves in Figure 7.8. Only two Cauchy parameters were required as adding the “C” parameter only reduced the MSE by about 4 percent. When there is insignificant MSE improvement, it is pref-

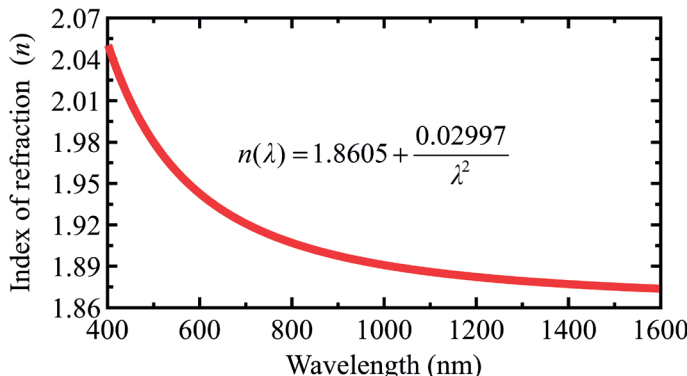


Figure 7.9. Cauchy index is shown for SiN_x .

erable to stay with fewer fit parameters. The final index as described by the Cauchy relation is shown in Figure 7.9 and follows normal dispersion, which is required when a film is transparent.

7.5 EXAMPLE: DIELECTRIC SiO_2 FILM ON GLASS

Our attention up to this point has been on coatings on silicon substrates. However, we now consider a thick oxide coating on a glass substrate. The first difference we notice occurs when we estimate the film index. Because glass has a very low index compared to silicon, the interference oscillation behavior is also very different. This behavior can also change depending on the angle of incidence that we consider, so the example here is just a representation of what you may see. Figure 7.10 shows the index variation for a series of films on fused silica substrate. The thickness for each simulated curve was adjusted such that the primary effect we witness is related only to the film index. As the index increases, the Ψ valleys have lower amplitudes. In this case, our bare substrate defines the upper boundary, while the film is responsible for the valleys. This is in contrast to our previous examples on silicon. Again, this may not be the case for all angles of incidence, but we have chosen to simulate at 70° , which is significantly above the Brewster angle for the glass substrate. We also stopped our simulation when the film reached an index of 2.1. Above an index of 2.1, the minimum Ψ valley starts to rise again, which may lead to some confusion during our estimation.

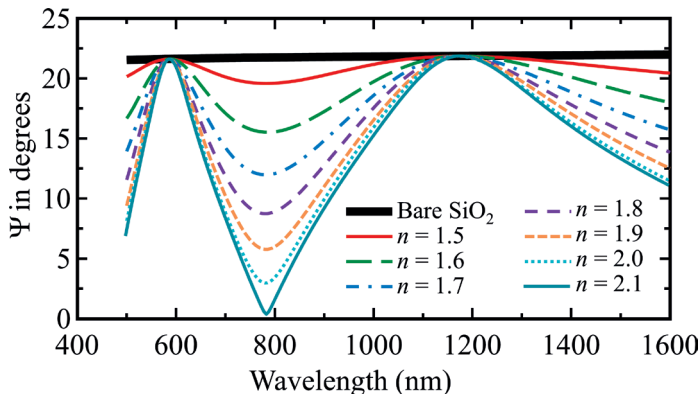


Figure 7.10. Index variation is shown for films on fused silica.

When multiple index values produce the same general Ψ amplitudes, the correct result can be ensured by considering the Δ curve. In all analyses, one should at least glance at the Δ curves.

Figure 7.11 shows the experimental data for both Ψ and Δ from a single angle for our SiO_2 coated glass. We have also generated a curve assuming bare glass. The bare glass is obviously defining our Ψ peaks. We adjusted our film index to a value just above 1.52, while the glass substrate index is near 1.50. This produces the correct Ψ oscillation amplitudes. Next, we adjusted the thickness to better match the number of interference oscillations. After fitting thickness and Cauchy parameters, we noticed a great match to Ψ , but the Δ curves were not well matched. The overall tilt of Δ is caused by a thin surface roughness layer. Adding less than 6 nm of surface roughness to the 3,824 nm thick SiO_2 layer produces our final fit result. We discuss surface roughness further in Chapter 8. The final refractive index for our film is compared to the substrate index and that of the roughness layer in Figure 7.12.

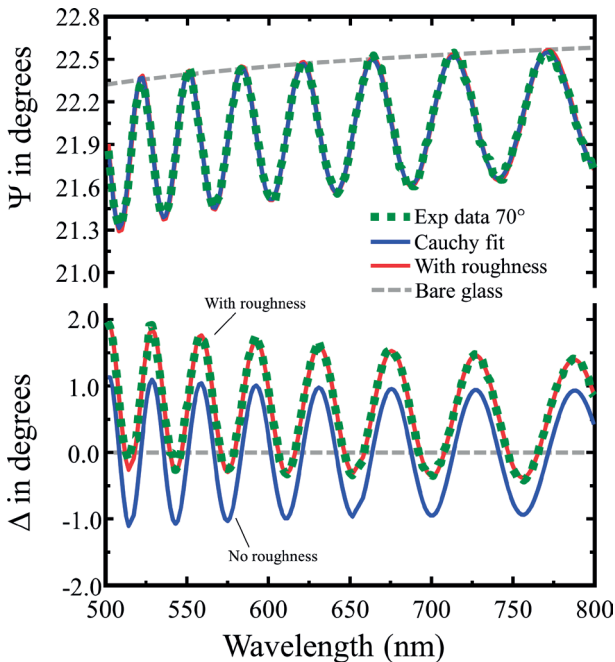


Figure 7.11. Data fit for SiO_2 coating on glass substrate. While Ψ curves are well matched with a single-layer model, the tilt in Δ spectra is only matched with the inclusion of a thin surface roughness layer.

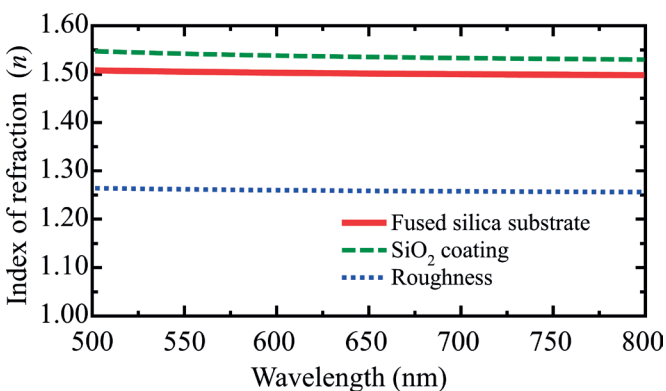


Figure 7.12. The index is shown for the glass substrate, our SiO_2 film as described by a 3-term Cauchy relation and the surface roughness layer as described by a 50-50 effective medium approximation.

CHAPTER 8

ROUGHNESS

As we model substrates and films, we assume that the interfaces are planar and parallel. For actual samples, the interfaces are not necessarily planar, but may have roughness. We distinguish between two types of roughness. When the spacing between the asperities (or the hill-to-valley distance) is greater than the wavelength of the light beam, we have macroscopic roughness. When the spacing between the asperities is less than the wavelength, we have microscopic roughness. These two situations are treated differently.

Roughness may be at the surface of the sample or at the interface between layers in the sample. It is not generally our intent to characterize the sample roughness. Rather, we wish to ensure that the roughness does not negatively impact the accuracy and precision of our film thickness and optical constant measurements.

8.1 MACROSCOPIC ROUGHNESS

Macroscopic roughness is illustrated in Figure 8.1. We note that the dimensions of the roughness (peak-to-peak distance and peak-to-valley distance) are much greater than the wavelength of the probing light beam.

When a collimated light beam is used, all incoming light rays are traveling in the same direction. The reflection of rays #1 and #2 occur from parallel regions on the surface, resulting in reflected rays traveling in the same direction. Both will go into the instrument detector. While ray #3 was also parallel to the other incoming rays before reaching the surface, the macroscopic roughness resulted in a different direction for the outgoing ray #3. Hence, this ray will not go into the instrument detector and will not impact the measurement. This particular aspect of macroscopic roughness simply causes much of the light to be scattered and not included in the measurement. Fortunately, ellipsometry is not concerned with the absolute

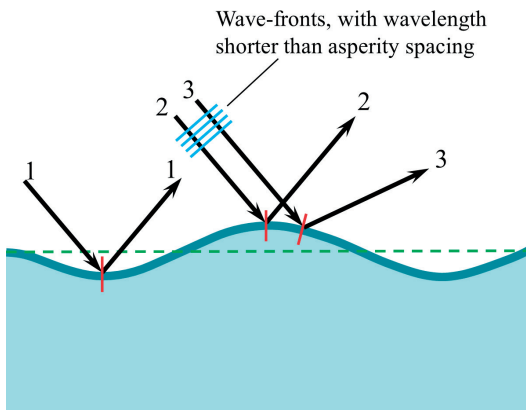


Figure 8.1. A representation of macroscopic roughness. Note that the wavelength of the light is much shorter than the roughness dimensions.

intensity of light, so any lost light can be ignored without affecting the accuracy of the ellipsometry measurement. The resulting ellipsometry data will only represent the surface region that reflected light into the detector.

Another aspect of macroscopic roughness is that when rays #1 and #2 enter the detector, ray #1 will have traveled a different distance than ray #2. This can result in a loss of coherence between the two beams, depending on the spatial separation between these rays. If this surface is a substrate, the data should not be affected, as each detected light ray “sees” the same sample. However, if the macroscopic rough surface is actually a thin film on the substrate, this may appear as a nonuniform thickness as each detected ray may experience different film thicknesses. The net effect from a nonuniform thickness is to round-off any sharp features in the ellipsometry spectra. Some ellipsometry software has a feature to model the effects of nonuniform film thickness.

8.2 MICROSCOPIC ROUGHNESS

A roughness with dimensions that are much less than the wavelength of the light probe is shown in Figure 8.2. Because the surface features are significantly smaller than the wavelength, they do not scatter the reflected light rays to different angles. Rather, we can expect to collect all of the reflected light in our detector. However, the rough surface will have an effect on our ellipsometry data.

The bulk material (below the bottom dashed line) has well defined optical constants. The ambient (above the top dashed line) also has well defined optical constants. The region between the two dashed lines may or may not have well defined optical constants; if it does, they will certainly not be the same as those of the bulk material or the ambient. We can consider the region bounded by the dashed lines to be (effectively) a film with well-defined optical constants that are different from both those of the bulk material and the ambient.

In this case, the presence of roughness at the surface has an effect similar to the presence of a thin film at the surface, where the thin film has optical constants somewhere between those of the regions above and below the interface. For this reason it is often adequate to model surface or interfacial roughness as a discrete thin film. This is shown schematically in Figure 8.3.

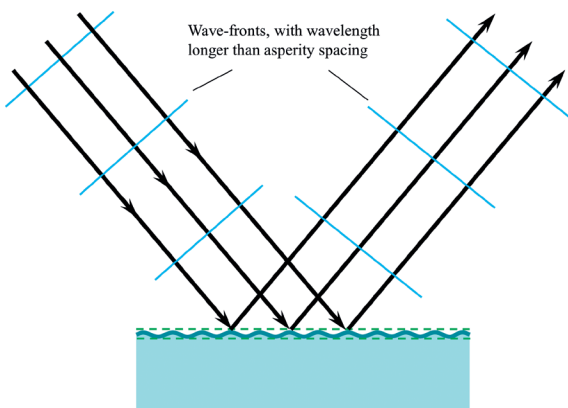


Figure 8.2. A representation of microscopic roughness is shown. Note that the wavelength of the light is much longer than the roughness dimensions.

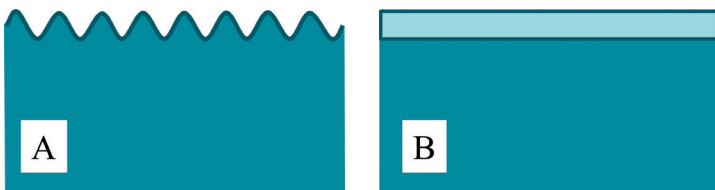


Figure 8.3. (A) A bulk material which has microscopic roughness. (B) A model of the material shown in (A) where the roughness is modeled as a thin layer whose index of refraction is intermediate between that of the bulk material and empty space.

8.3 EFFECTIVE MEDIUM APPROXIMATIONS

Next, we consider the common approach to modeling the rough surface. As suggested in Figure 8.3, we will treat this surface as a layer consisting of a mixture of the materials above and below the interface. We will assume that both materials mix together, but retain their own optical properties. The resulting mixture is called an effective medium approximation (EMA) as it approximates the new material based on the mixed constituents. The simplest EMA model consists of linear interpolation between the dielectric functions of the constituent materials:

$$\tilde{\epsilon}_{EMA} = f_A \tilde{\epsilon}_A + f_B \tilde{\epsilon}_B \quad (8.1)$$

where $\tilde{\epsilon}_{EMA}$ is the effective complex dielectric function of the composite material, $\tilde{\epsilon}_A$ and $\tilde{\epsilon}_B$ are the complex dielectric functions of the constituent materials, and f_A and f_B are the volume fractions of each constituent, the sum of which must equal unity. The linear EMA, while simple to calculate, is not particularly accurate. It is much more common to use the Bruggemann EMA, in which the effective dielectric function is obtained by solving the following equation:

$$f_A \frac{\tilde{\epsilon}_A - \tilde{\epsilon}_{EMA}}{\tilde{\epsilon}_A + 2\tilde{\epsilon}_{EMA}} + f_B \frac{\tilde{\epsilon}_B - \tilde{\epsilon}_{EMA}}{\tilde{\epsilon}_B + 2\tilde{\epsilon}_{EMA}} = 0. \quad (8.2)$$

For a thorough review of EMA modeling, consider the work of Aspnes, Theeten, and Hottier [50] and Losurdo and Hingerl [8].

8.4 ROUGH FILM EXAMPLE

Normally, the thickness of a roughness layer is less than about 100 Å. In Chapter 9, we will show that for films this thin, there is a strong correlation between the index of refraction and thickness. Thus, we face this same difficulty when modeling most rough surfaces. We may be highly sensitive to the thickness, but have little sensitivity to actual optical constants. With the EMA, we can vary the index of refraction by adjusting the volume fraction between the two constituents. When approximating roughness with an EMA, the optical constants are totally dependent on the fraction of the overlying and underlying material. However, for very thin roughness layers, it is inappropriate to try to determine both the relative fraction of the

two materials and the thickness. Accordingly, for convenience, the relative fraction is generally assumed to be half and half. With this assumption, the thickness can then be precisely determined.

The sensitivity to roughness also depends on the material we are encountering. Because roughness reduces the optical constants of any material toward that of the void ($n = 1, k = 0$), it has a much more pronounced effect when the roughness occurs on high-index or absorbing materials. The effect is much less pronounced on low-index films such as SiO_2 or MgF_2 .

Let's consider a single-layer coating of niobium oxide on glass. The total layer thickness is nearly 7,000 Å, and interference within this transparent layer produces the data oscillations versus wavelength. In Figure 8.4, we show only the 65° data, as the Ψ curves are suppressed at this angle and will allow easier visualization as the model is varied. First, we fit the data as a single-layer film using the Cauchy dispersion equation to describe the index of refraction. The index for this film is quite high for a dielectric layer ($n \sim 2.3$ to 2.4). This increases our sensitivity to roughness, as the lower-index surface mixed with void will have an index, $n \sim 1.6$. Both the model-fits without roughness and with roughness are shown compared to the experimental Ψ data. There is significant improvement (MSE decreases from 1.5 to 0.6) with the addition of a 30 Å thick roughness layer. Since this layer is very-thin, we do not try to fit the volume fraction parameter, but rather leave it fixed as a 50-50 mixture.

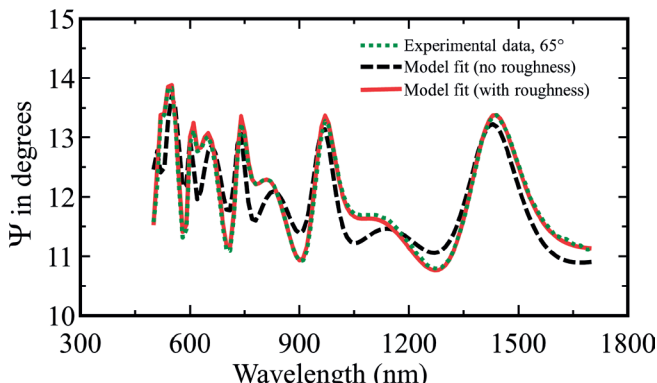


Figure 8.4. Experimental Ψ from a niobium oxide layer on BK7 glass, along with two model fits—one without roughness and the second with roughness. The MSE for the model-fit without roughness is 1.5; while the MSE reduces to 0.6 with the addition of a 30 Å roughness layer modeled using a 50-50 EMA approach.

CHAPTER 9

VERY THIN FILMS

One purpose of this book is to demonstrate the rather impressive capabilities of the spectroscopic ellipsometry (SE) technique. In this chapter, we focus on very thin films, that is, films which are thinner than 100 Å (or 10 nm). Examples in this category include self-assembled monolayers, adsorbed layers, native oxides, some gate dielectrics for microelectronic devices, metal layers in magnetic random access memory devices, and so on.

However, it is important to show both what the technique can and cannot do, and in this chapter we will identify each of these features.

The areas of consideration are:

- Determining film thickness when optical constants are known;
- Determining film optical constants of a very thin layer; and
- Distinguishing one film material from another.

We shall find that SE is very good in the first area while the second and third are much more difficult, if not impossible.

9.1 DETERMINING THICKNESS WITH KNOWN OPTICAL FUNCTIONS

For transparent films, it is possible to precisely measure the thickness of very thin films when the optical functions are known. Figure 9.1 shows ellipsometric spectra for a film-free silicon surface and for various thermal oxide thicknesses (up to 100 Å) on silicon. It would appear that in certain parts of the spectrum, we could easily distinguish between a 5 Å film and a 6 Å film. We note that this extreme sensitivity comes from the Δ values. The Ψ values for these very thin films show much less variation. This is to say that the phase shift between the p-waves and the s-waves is very

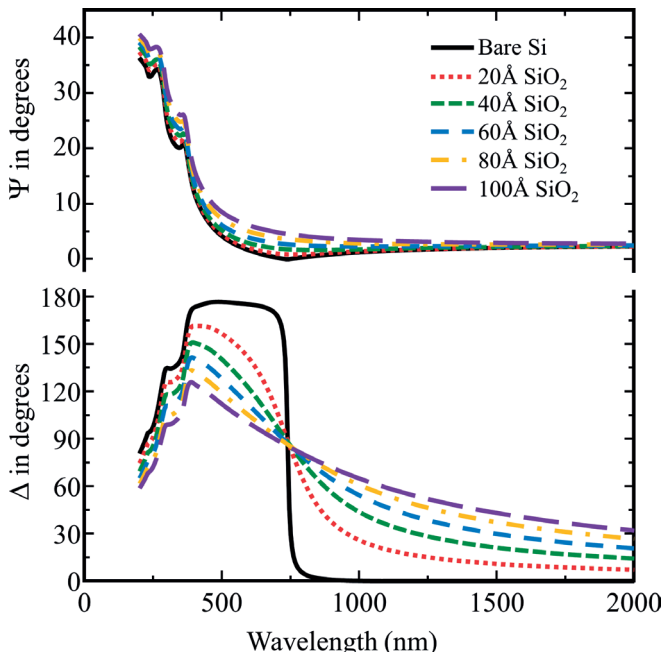


Figure 9.1. Ellipsometry spectra are graphed for film-free silicon and for oxide on silicon. Plots are shown for 20 Å, 40 Å, 60 Å, 80 Å, and 100 Å oxide films at a 75° angle-of-incidence.

sensitive to film thickness whereas the reflectance for either the p-waves or the s-waves is not very sensitive to film thickness.

With a modern spectroscopic ellipsometer, the thickness for a very thin oxide film can be measured repeatedly with a precision of .002 nm (1σ from 30 measurements). This is significantly smaller than the diameter of a hydrogen atom, which raises the question of how to interpret the precision of thickness at this level. In general, the measurement beam will cover a surface area measured in square millimeters and thus the ellipsometric response is averaged from the total interaction at the surface.

9.2 DETERMINING OPTICAL CONSTANTS OF A VERY THIN FILM

Although we are able to determine the thickness of a very thin film if we are willing to assume the optical constants of the film-material, we shall find that *it is very difficult to determine the optical constants of*

any transparent film which is thinner than about 100 Å. To understand the rationale behind this statement, let us consider a concept taken from single-wavelength ellipsometry. Consider a substrate of a single-crystal silicon with a film having an index, n . Let's first consider a wavelength of 632.8 nm and an angle of incidence of 70°. Figure 9.2 shows a series of Ψ - Δ trajectories where the data variation is shown for increasing film thickness. This is done for a series of different film indexes, n . The open circles indicate an increment of 50 Å each in film thickness.

From these trajectories, we see that most thickness sensitivity comes from the changes in Δ , while the index information (separation between curves) is related more to Ψ . For thicknesses of 300 Å, the trajectories are better separated and it is reasonable to determine both thickness and index if we can accurately measure Ψ and Δ . As the film gets thinner, the separation between different trajectories is less and less. For thicknesses less than 100 Å, the trajectories overlay one another and a slight uncertainty in Ψ will cause a large uncertainty in the index. Note that the majority of data change occurs in Δ , while Ψ is separating on a much smaller scale. Accordingly, one should not attempt to determine the index for very thin films.

The quandary, then, is how to proceed? Let us *assume* an index value and consider the consequences of being wrong. Keeping in mind that

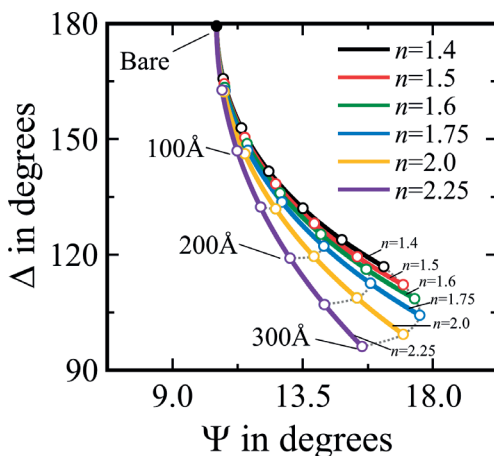


Figure 9.2. The first part of the Ψ - Δ trajectories for a single wavelength for transparent films on silicon with index of refraction of the films as indicated. These trajectories are for an angle-of-incidence of 70° and a wavelength of 632.8 nm.

most index values for dielectrics fall between 1.4 and 2.0, if we know the identity of the material we can often guess the index to within 10 percent. If we assume an index of 1.5, and if the truth were known and the value is 1.65, our answer to the value of thickness might be off by 10 percent. In other words, if we conclude that the thickness was 100 Å, the true value might be 90 Å, but it would not be 50 Å or 200 Å. Thus, we can precisely determine the thickness with the assumed index, but the accuracy of our thickness relies on the accuracy of our assumed index value.

Interestingly, we can improve the sensitivity to very thin layers by reducing the wavelength of our ellipsometry measurement. This can also be demonstrated using the Ψ - Δ trajectories in Figure 9.3, but now we compare curves for the same index ($n = 2$) and angle (70°) but for different probe wavelengths (200 nm, 600 nm, and 1800 nm). We intentionally chose wavelengths that were 3X apart to show that the sensitivity to thickness scales similarly with decreasing wavelength. Consider the sensitivity to thickness as we progress along the Ψ - Δ trajectory to that point from the bare substrate point. At 500 Å for the 1800 nm wavelength, we travel less distance than the length to the 200 Å point for the 600 nm wavelength. Similarly, the 500 Å point for $\lambda = 600$ nm is less distance along the trajectory than the 200 Å point for the 200 nm wavelength. Thus, we should be able to reduce our “cutoff” thickness where we can still obtain both the thickness and index by decreasing the wavelength. Following this logic, it would require a wavelength around 67 nm to get another 3X sensitivity improvement. Unfortunately, it is impractical to reduce the SE wavelength much below 150 to 200 nm. Since we are actually sensitive to the optical thickness

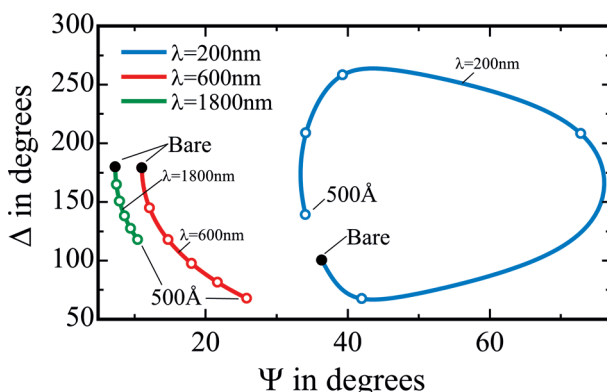


Figure 9.3. Ψ - Δ trajectories are plotted for the first 500 Å of a film with index of 2.0 at a 70° angle of incidence. Each open circle represents 100 Å increments along the trajectories.

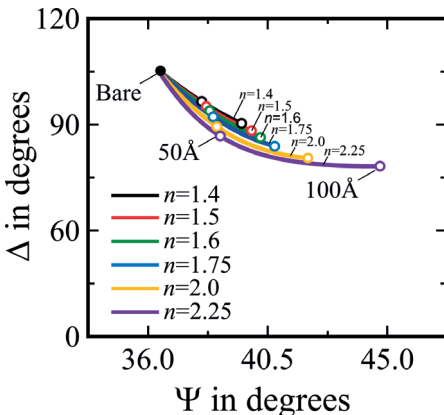


Figure 9.4. The first part of the Ψ - Δ trajectories for a single wavelength for transparent films on silicon with index of refraction of the films as indicated. These trajectories are for an angle-of-incidence of 70° and a wavelength of 200 nm.

(thickness–index product), this cutoff also depends on the index of the film. The cutoff thickness will be thinner for a higher index film.

In addition to sensitivity to the thickness, shorter wavelengths also produce improved discrimination between the curves for different index values. This is demonstrated in Figure 9.4 where the Ψ - Δ trajectories are repeated at a wavelength of 200 nm for only the first 100 Å thickness range. The Ψ and Δ range for this figure were set to match those of Figure 9.2 to allow easier comparison between the effects at 200 nm and 632 nm wavelengths. Not only will shorter wavelengths help us distinguish between the thickness and index for thinner layers, it is also more likely that the index will be higher at these short wavelengths for many materials, which also leads to better discrimination. Of course, we have not considered the effects of ultraviolet absorption on these trajectories—so there are still considerations that can affect these simple comparative simulations.

9.3 DISTINGUISHING ONE FILM MATERIAL FROM ANOTHER

Although we may have difficulty determining the index with good accuracy, it may still be possible for us to distinguish between different

materials. To illustrate this concept, let us consider a thin thermal oxide film on silicon. If we model this sample using thermal oxide film optical constants, the best-fit thickness is determined to be 96.5 Å. The measured and modeled values are shown in Figure 9.5. In this case, the mean squared error (MSE) is 1.85, implying a very good fit.

Now, suppose that this were an unknown film, and we guessed it was actually a Si_3N_4 layer, using index values from the literature. The measured and modeled values are shown in Figure 9.6. Now, the thickness value obtained is 76.6 Å with an MSE of 22.1. In this case, we could clearly see that the nitride model is inappropriate, whereas the oxide model fits nicely.

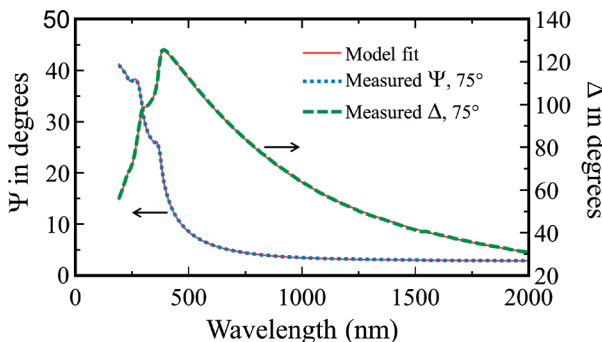


Figure 9.5. Experimental data along with modeled data for a thermal oxide on silicon, modeled with a tabulated list for the thermal oxide. The resulting thickness was 96.5 Å and the MSE was 1.85.

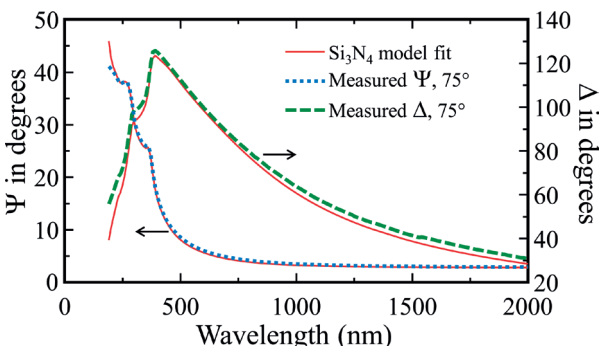


Figure 9.6. The same data as shown in Figure 9.5, modeled as a silicon nitride film, using a tabulated list for LPCVD Si_3N_4 . The resulting thickness is 76.6 Å and the MSE is 22.1.

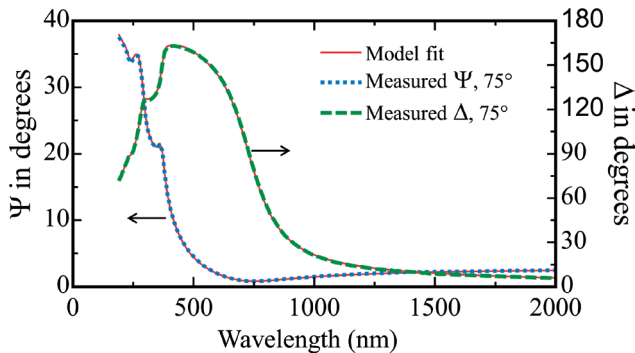


Figure 9.7. A native oxide film on silicon, modeled as SiO_2 , with tabular values for the index of refraction. The thickness value was determined to be 17 Å with an MSE of 2.4.

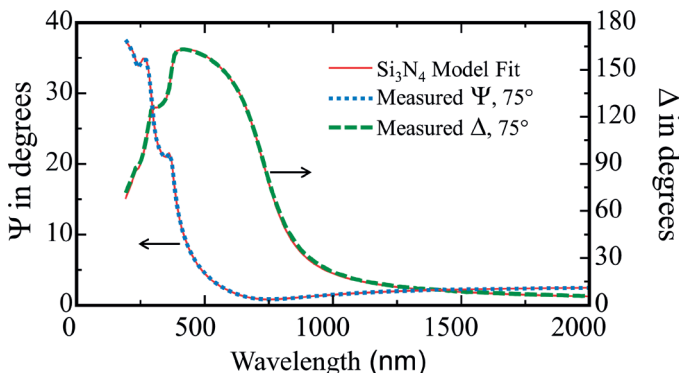


Figure 9.8. The same data as shown in Figure 9.7, modeled as a silicon nitride film, using a tabulated list for LPCVD Si_3N_4 . The resulting thickness is 13.6 Å and the MSE is 3.82.

If this were an unknown film, we could not say with all certainty that it is SiO_2 , since other materials may have similar optical functions, but we can say that it is *not* an Si_3N_4 layer. For unknown materials, it is much easier to make statements regarding what the material is *not*, rather than what the material is.

Next, let us consider a sample that is much thinner (a native oxide on silicon). When modeled as an oxide, using optical constants from the literature, the thickness fits to 17 Å with an MSE of 2.4. The measured values and modeled values are shown in Figure 9.7.

Let us consider the situation if this were an unknown film. Again, we approach the data with a guess that the film is Si_3N_4 . In Figure 9.8, the nitride model matches the experimental data quite well visually. In fact, the MSE is only slightly higher (3.82) with a resulting nitride thickness of 13.6 Å.

The point illustrated here is that for films which are thicker than 50 Å to 100 Å, many materials can be distinguished from each other. However, for very thin films even this becomes difficult to deduce.

In order to distinguish one material from another, it is necessary that they have optical constants which are significantly different. Accordingly it is much easier to distinguish a thin metal film from a thin dielectric film because of the different shape of their optical functions. On the other hand, most dielectrics have similar dispersion shapes (with different magnitudes). Accordingly, it is very difficult to distinguish a very thin film of one dielectric from a very thin film of another dielectric.

CHAPTER 10

THIN FILMS WITH ABSORBING SPECTRAL REGIONS

In Chapter 7, we discussed an important application of ellipsometry—measuring the thickness and index for thin transparent films. If we are only interested in film thickness, it is preferable to restrict the data analysis wavelengths where the film remains transparent. However, with the expanded wavelength range of modern ellipsometers we may now access interesting optical features where our films are absorbing, even for films that are traditionally transparent. Thus, an important process for modern ellipsometry data analysis is the determination of the thickness and optical functions for films that absorb at some wavelengths. Figure 10.1 shows the extinction coefficient spectra for a few materials that are transparent at longer wavelengths, but absorbing at shorter wavelengths. These include organic films, inorganic dielectrics, and even semiconductors.

The general data features for thin films that are transparent for some wavelengths and absorbing for other wavelengths was discussed in Section 4.2.2. As mentioned, we expect to see interference features when the film is transparent and these interference features will be damped or completely eliminated as the film becomes more absorbing. This is demonstrated in Figure 10.2. If the material is absorbing at all wavelengths, it produces a special challenge, which we will discuss in Chapter 11. Let us consider how to proceed with films that are both transparent and absorbing, depending on the wavelength range we consider.

Films that absorb are more challenging because there are additional unknown sample properties; the thickness, n and k . Also, we can no longer expect the index (n) to follow “normal” dispersion. Our general approach for data analysis is to divide the problem. We will first fit the transparent region, as covered in Chapter 7. To accomplish this, we need to determine at which wavelengths the film is absorbing and at which it is

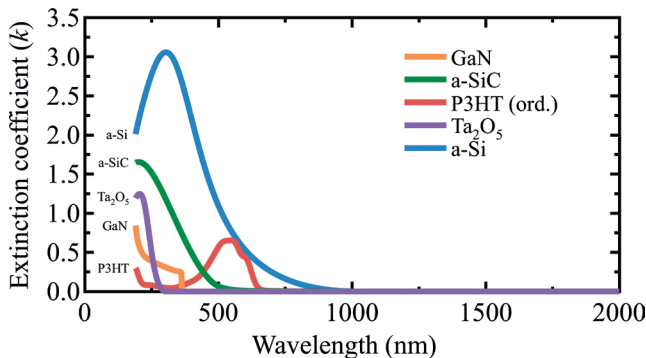


Figure 10.1. Example materials, which are transparent at longer wavelengths, but absorbing at shorter wavelengths, are graphed.

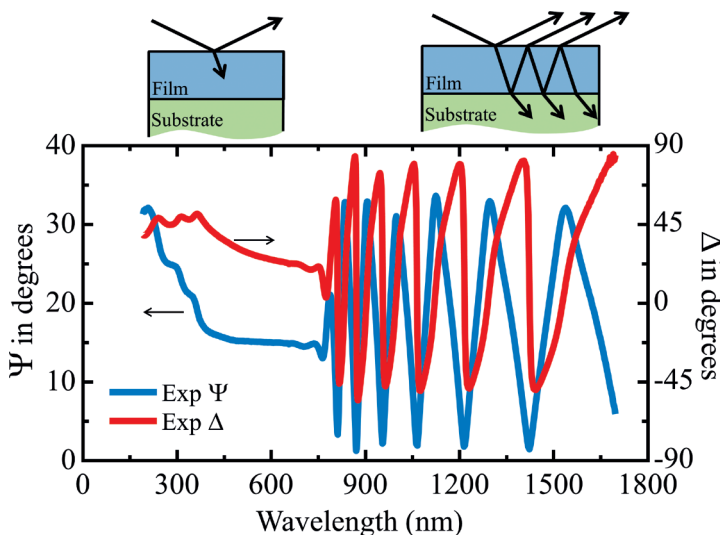


Figure 10.2. Ellipsometry spectra from a film that is transparent above and absorbing below 800 nm.

transparent. After we fit the transparent spectral region, we can fix the thickness and move to the absorbing spectral region. The thickness we determine is a physical property and is independent of the wavelength we use to probe the sample. Thus, we have reduced the total number of unknown sample properties and can determine complex optical functions more directly from our Ψ and Δ spectra. We step through this approach, as illustrated in Figure 10.3.

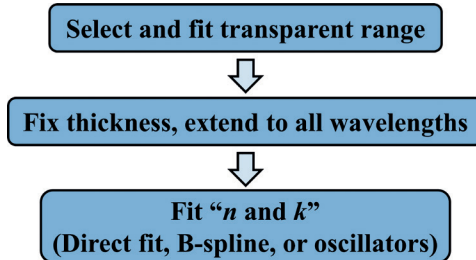


Figure 10.3. The general procedure for data analysis of a thin film with absorbing spectral regions is shown.

10.1 SELECTING THE TRANSPARENT WAVELENGTH REGION

The interference features will be damped and eventually eliminated as the film becomes more absorbing. If the film becomes fully absorbing, it can be much easier to identify the transparent and absorbing spectral regions. For example, consider the measured spectra for an amorphous semiconductor on a germanium substrate, shown in Figure 10.4. The interference features occur below 2.0 eV; however, their amplitudes start to dampen above 1.75 eV. The spectra versus photon energy were plotted to illustrate that the spacing of interference features is nearly constant when plotted on a frequency scale. The slight compression of interference features at higher energies (shorter wavelengths) is due to the natural increase in refractive index from normal dispersion. A dashed curve has been added to show the natural upper trajectory of the interference amplitude if the film remains transparent. At higher photon energies, the light is no longer able to penetrate the film and return to the surface, so no interference is present.

This visualization is not always as straight-forward as the case for amorphous dielectrics and semiconductors. For organics, bumps associated with small absorptions often appear in the visible and ultraviolet spectrum. Also, organic absorptions are often weaker and may not absorb the light entirely. Consider the data measured from an organic layer on silicon featured in Figure 10.5, where the interference features are more irregular. This is because the normal interference shape we see in the near infrared is modified by the organic absorptions in the ultraviolet and visible—many of which absorb only a fraction of the total light traveling through the film. Thus, we have a convolution of interference and

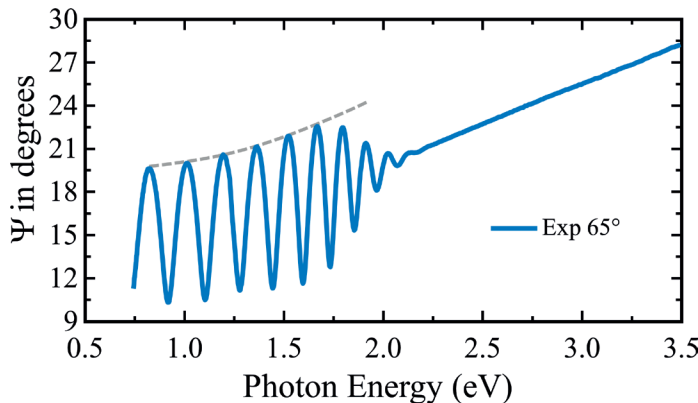


Figure 10.4. Graph of the transparent and absorbing spectral regions for an amorphous semiconductor film on a germanium substrate.

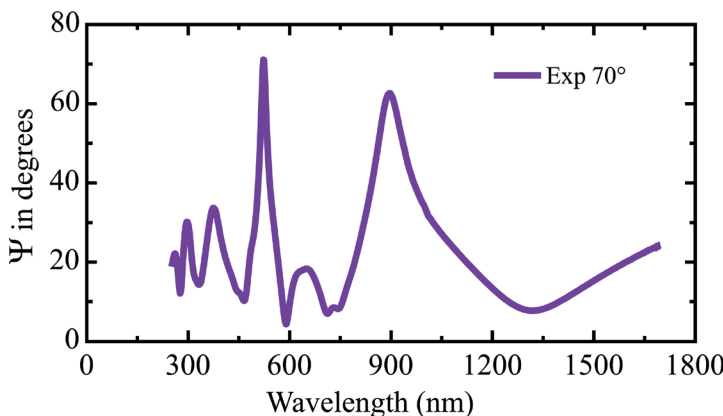


Figure 10.5. Visualizing the transparent and absorbing spectral regions for this organic layer on silicon is more complicated as small absorptions may not completely dampen the interference features.

absorption that produces the final spectral data shape. We would conclude that the transparent spectral region is above 850 nm where the interference features do not appear damped by any absorption.

After the transparent wavelength region is identified, the data can be analyzed using the procedure described in Chapter 7. The main goal is to determine an accurate thickness such that this value can be fixed when extending to wavelengths where the film is absorbing.

10.2 MODELS FOR THE ABSORBING REGION

The Cauchy is great for describing the index of refraction in the wavelength region where the film is transparent. However, it is not capable of handling the spectral region where the film absorbs, as the optical functions exhibit anomalous dispersion that causes the index to turn-over. For this wavelength region, there are three primary methods to describe the index of refraction: Direct fit for n and k , B-spline fit, or Oscillator Model fit. We will discuss each and then compare their merits and limitations.

10.2.1 DIRECT FIT FOR N AND K

One of the most common methods for the absorbing spectral region is to directly fit both n and k with the thickness fixed. The Direct Fit is also commonly referred to as the “Point-by-Point” Fit or “Wavelength-by-Wavelength” Fit. All parameters of the model must be fixed except the n and k values for the desired thin film. Then, the n and k values are allowed to vary independently at each wavelength. Even with a single angle of incidence, the two measured data (Ψ and Δ) are adequate to determine the best optical constants (n and k) that match. It is common to start the Direct Fit at the same wavelengths that were already fit using the Cauchy and this can be a good way to compare how the resulting optical constants are affected by data noise or lack of measurement sensitivity. This is demonstrated in Figure 10.6 for a 99 nm silicon oxynitride layer deposited on silicon. The Cauchy fit was used to determine the film thickness. Next, the thickness was fixed and the optical constants (n and k) were allowed to vary independently at all wavelengths. The measurement consisted of three angles of incidence, so there were a total of six data values at each wavelength to help determine our two unknowns. No constraints on the optical constant values were imposed, so that we can visualize the sensitivity to n and k on a wavelength-by-wavelength basis. Obviously any nonzero k values at wavelengths above 300 nm are incorrect and show our sensitivity to k is in the low third decimal place for the 100 nm thick layer. The downward tilt of k to negative values is actually due to an insufficient model assumption. If we had allowed 3 nm of roughness in our model, k would flatten and average to zero. We also see noise in n , which increases at longer wavelengths where sensitivity to this thin layer is reduced. Some of our issues could be resolved by placing constraints on the possible values. For example, we could constrain k to positive values or even force k to remain zero for wavelengths above 300 nm. However, if

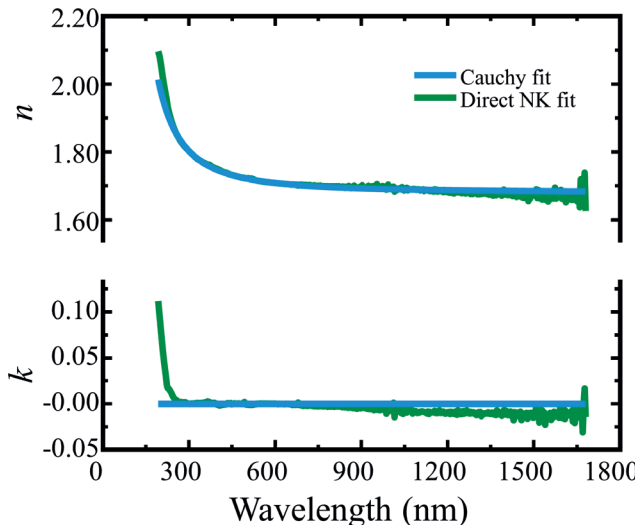


Figure 10.6. Optical functions from the Cauchy fit and Direct fit are shown for a 99 nm SiON film on a Si substrate.

we are only looking at the noise, we are missing the point of this strategy. Our goal was to extend our analysis to shorter wavelengths where the film absorbs and this was a success. Notice the increasing k values at wavelengths below 275 nm, which are produced from the Direct NK fit. The next two approaches will accomplish something similar, but will help retain smooth, noise-free curves throughout the spectrum.

10.2.2 B-SPLINE FIT

In Section 5.5, we introduced the b-spline function to describe both the real and imaginary optical functions. Once we have our thickness from the Cauchy fit, we could extend to absorbing wavelengths by using the b-spline. In fact, the b-spline could be used directly in the transparent range, without relying on the Cauchy, if we set it up correctly. This assumes we can control the b-spline to force a transparent region ($k = 0$). When extending into the absorbing wavelength range the primary concern is how close can the nodes be spaced. In general, we wish to have enough nodes to give the b-spline flexibility to match the actual shape of the optical dispersion but not so many that the shape follows the noise. To further reduce the total number of free parameters, we can force the two b-spline curves to maintain Kramers–Kronig (KK) consistency, as discussed in Chapter 5.

Our Example in Section 10.4 will show application of the b-spline for an organic photoresist on silicon.

10.2.3 OSCILLATOR MODEL FIT

In Section 5.4, we introduced the concept of oscillator models for describing both the real and imaginary optical functions. Again, we can use this approach to extend our fit after gaining thickness insight from the Cauchy fit. We could also start directly with the Oscillator model to get the thickness, as it significantly reduces the number of fit parameters such that we can fit both transparent and absorbing spectral regions while simultaneously allowing the thickness to vary. The main difficulty is how to construct an oscillator model that describes the correct shape for our optical functions. Figure 10.7 shows the general strategy used in this regard. One approach is to start with known reference material optical constants, such as tabulated values from a book or journal article. The second approach is to determine the shape by first fitting the data with the Cauchy and then using either the Direct fit or b-spline such that both absorbing and transparent regions are known for the sample. These optical constant values can then be used as a reference to build up the oscillator shapes.

When building the oscillator model, it is generally divided into two steps. First, the imaginary dielectric function is matched with an oscillator or a sum of oscillators. Next, the KK transformation should produce the appropriate real dielectric function shape. We may not have a perfect match strictly from the KK transformation, as additional absorption features may exist outside the spectral region that is accessible to the ellipsometry measurement. We then match the real dielectric function with a simple offset or via unbroadened poles outside the upper and lower

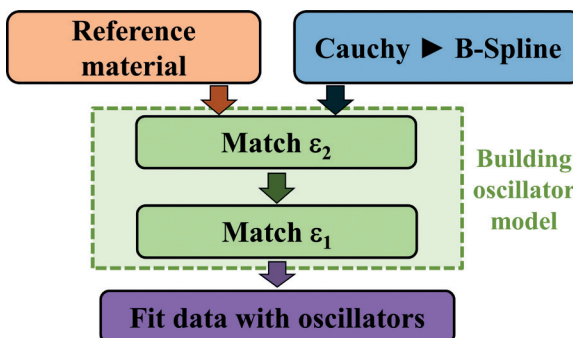


Figure 10.7. General procedure for oscillator modeling is shown.

measured energies. When finished, the oscillator model can then be used to fit the data—with each free value allowed to vary. In this way, it is common to also add the thickness as a fit parameter or even add roughness or index gradients simultaneously with the varied oscillator functions.

10.2.4 COMPARISON OF METHODS FOR FILMS WITH ABSORBING REGIONS

Each of the afore-described methods can be used to extend fits from the transparent spectral region into the absorbing spectral region. However, the choice of model depends on the type of material in question and on finding a balance between ease-of-use, robustness, and physically reliable descriptions. Table 10.1 lists advantages and disadvantages for each method.

As a general rule, it is common to choose the Direct NK fit or B-spline fit when many absorption features are present, such as with many organic films. The Oscillator Model fit is preferred for simpler absorption shapes such as we may find for amorphous dielectrics and semiconductors. We will consider two examples that represent different preferred methods.

10.3 EXAMPLE: AMORPHOUS Si ON GLASS, USING THE OSCILLATOR METHOD

Our first example is that of an amorphous silicon film on glass. This material is commonly used for many different applications—as a thin film photovoltaic, as thin film transistors in mobile displays, and even as a high-index optical coating. The silicon film is transparent in the near infrared, but strongly absorbs light in the visible and ultraviolet. Because the material is amorphous, the shape of the absorption is very broad without any sharp, individual features. A few oscillator dispersion models, Tauc-Lorentz (T-L) and Cody-Lorentz (C-L) [47, 48], were developed specifically to describe the shape of this absorption. Thus, the preferred model for this type of film is often an oscillator model. The Direct fit and B-spline approach may also work, but would result in a larger number of fit parameters and would not have the same physical origin as the T-L or C-L models.

Figure 10.8 shows the experimental data from three angles, along with the model-fits when a single T-L oscillator is used to describe the a-Si

Table 10.1. Comparison is given between different fit methods for films that absorb in some spectral regions

Method	Advantages	Disadvantages
Direct fit	<ul style="list-style-type: none"> Very easy to implement Can visualize parameter sensitivity 	<ul style="list-style-type: none"> Largest number of “fit” parameters Optical functions not constrained to “physically plausible” results
B-spline	<ul style="list-style-type: none"> Maintains smooth, continuous functions. Can enforce physical plausibility through KK With appropriate node resolution, can resolve even very fine dispersion features. 	<ul style="list-style-type: none"> Requires user to set appropriate node spacing required by material. May have large number of “fit” parameters, depending on node spacing. Software may not include b-spline
Oscillator	<ul style="list-style-type: none"> Maintains smooth, continuous functions. Enforces physical plausibility through KK Generally has a minimum number of “fit” parameters, which often allows the thickness and other model parameters to be simultaneously varied. Often is based on a “physical” description of optical properties. Once shape is developed for a material, very easy to use for similar materials by slightly varying the parameters. 	<ul style="list-style-type: none"> Typically require more steps to fit the data Depends on user to place the correct number of oscillators to match all absorption features present in the material.

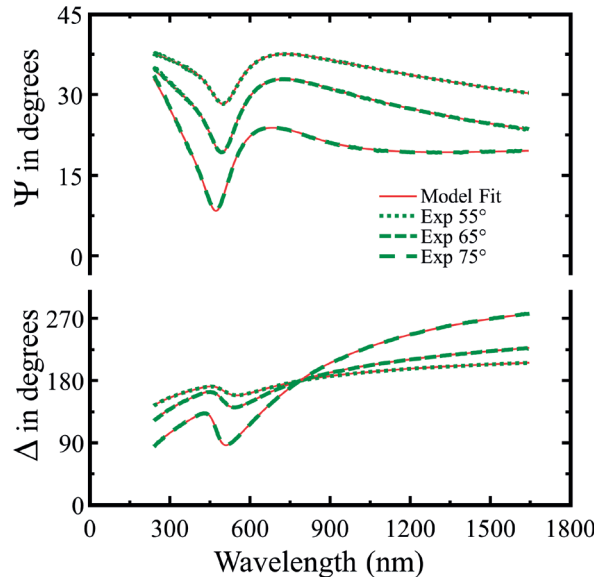


Figure 10.8. Data and fits are shown for an a-Si film on glass.

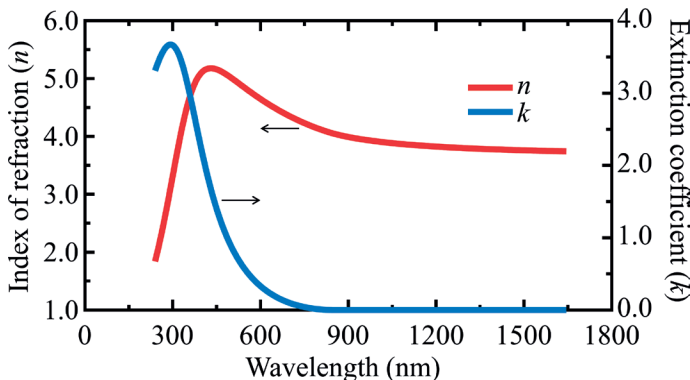


Figure 10.9. Optical functions for a-Si as determined using a T-L oscillator function.

optical functions. The resulting optical constants are shown in Figure 10.9. The resulting a-Si thickness was 47 nm with 2.6 nm of surface oxide. It is important that the oxide layer is added to the model, as the a-Si has a high index of refraction and ellipsometry is very sensitive to the surface conditions in this situation.

10.4 EXAMPLE: PHOTORESIST ON Si, USING THE B-SPLINE METHOD

In this example, we consider an organic layer on silicon. The organic layer is photosensitive, which means its properties will change when exposed to certain wavelengths of light. This is useful in the microelectronics industry, as the layer can be used to define lines and patterns. However, we must use care, when measuring with ellipsometry, that the measurement beam does not “expose” the photoresist layer and thus modify its properties. This may be accomplished by collecting the spectra very quickly and using very low amounts of ultraviolet radiation.

Figure 10.10 shows the measured spectra for the photoresist layer on silicon substrate. The interference features are present at wavelengths above 300 nm. They are damped significantly below 300 nm, but there are even small absorption features that affect our data curves at wavelengths up to 450 nm. For this reason, the Cauchy fit is only extended down to 450 nm to get accurate thickness. Because of the large number of absorption features, it is less common to approach this type of material

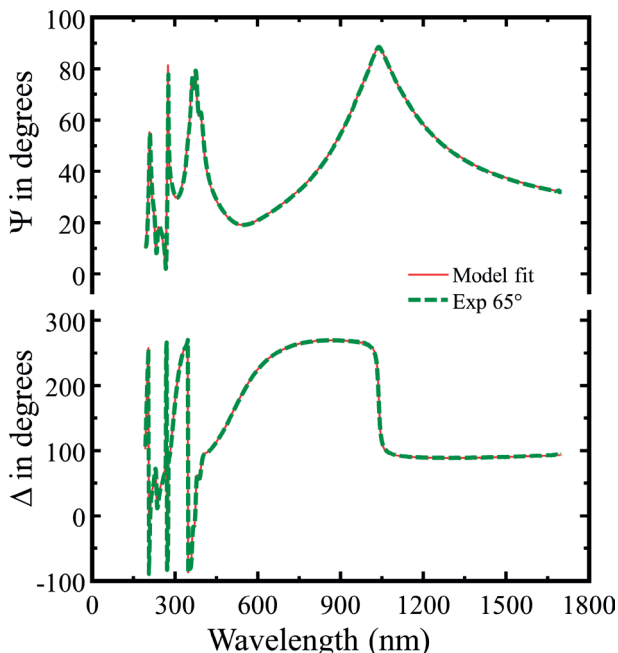


Figure 10.10. Data and fits are shown for a photoresist on Si.

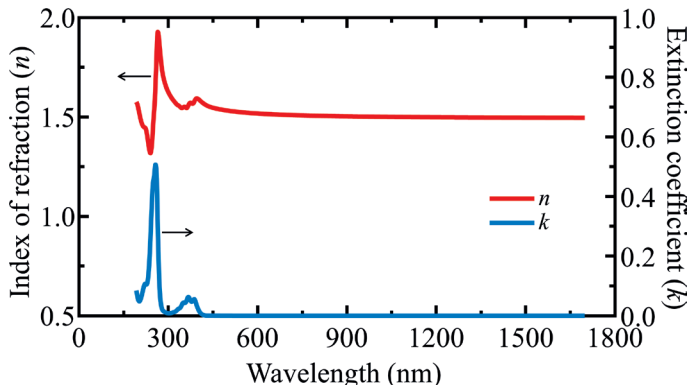


Figure 10.11. Optical functions are shown for the photoresist film.

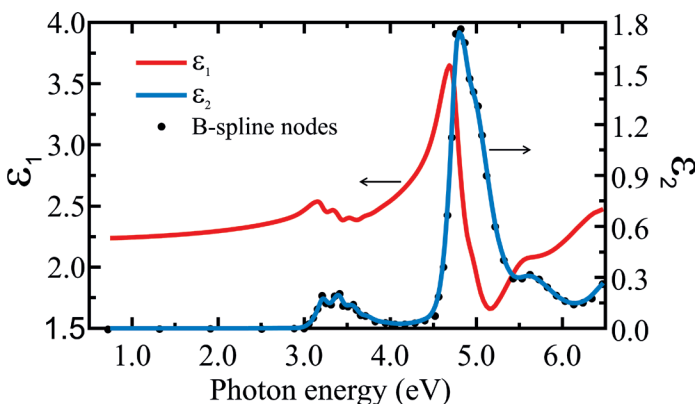


Figure 10.12. KK consistent B-spline model results are plotted for the photoresist.

with a summation of oscillators. Rather, the Direct fit or B-spline fit is preferred. Figure 10.11 shows the final photoresist optical constants which were obtained from a KK consistent b-spline layer. The final b-spline nodes and optical functions are shown in Figure 10.12.

CHAPTER 11

METALLIC FILMS

In this chapter, we consider films that absorb over the full measured spectrum. We assume that our spectroscopic ellipsometer has adequate wavelength range such that we can find a transparent region for any dielectric, organic, or semiconductor layer. However, metals absorb everywhere and present a unique challenge. Thus, we are not able to go to the transparent region to determine thickness using the methods of Chapters 7 and 10. We must solve for the thickness and both n and k simultaneously. This situation is only of concern when the metal film is thin enough for light to penetrate without being fully absorbed. Typically, this requires the metal layer to be thinner than 50 to 100 nm. Otherwise, there is no sensitivity to the metal thickness.

11.1 CHALLENGE OF ABSORBING FILMS

Simply said, the primary challenge of absorbing films is that we have more unknown sample properties than we have measured data parameters, as illustrated in Figure 11.1. We need to determine n , k , and thickness, but we only measure Ψ and Δ . Of course, we could try to add Ψ and Δ values from additional angles of incidence, but often the information from other angles contains nearly the same data content. If it is not uniquely different, the data from additional angles doesn't actually solve our problem.

11.2 STRATEGIES FOR ABSORBING FILMS

The strategies to overcome the challenge of absorbing films are divided into two categories. First, there are strategies that obtain extra measurement information. Second, there are strategies that attempt to reduce the number of unknown sample properties. Table 11.1 lists each of the potential methods, which are more fully reviewed in Hilfiker et al. [34, 35].

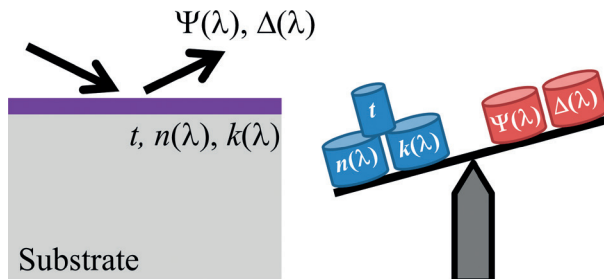


Figure 11.1. The basic challenge of absorbing films is that the number of unknown sample properties outweighs the number of measured data.

Table 11.1. Methods for absorbing films are listed based on their primary goal

Methods which reduce sample unknowns	Methods which increase the data content
<ul style="list-style-type: none"> • Opaque layer • Optical constant parameterization • Measure and fix thickness by other characterization methods 	<ul style="list-style-type: none"> • SE + T • Interference enhancement • Multisample analysis • In-situ SE

To test the merits of each absorbing-film method, it is helpful to consider “uniqueness graphs.” Here, the thickness is varied while all other fit parameters are allowed to fit. Then the mean squared error (MSE) profile is graphed, showing the best fit results from each thickness value (see Section 6.3.4). A flat MSE minimum demonstrates there is still strong correlation between the thickness and optical constants, which prevents a unique result. If the MSE profile dips to a single minimum value, then the correlation is broken by that method as only a single thickness result provides the best MSE. As shown in Figure 11.2, a comparison of absorbing-film methods shows that the direct fit of thickness and optical constants for a metal on silicon will not provide a unique answer as there are many thicknesses that provide essentially the same minimum MSE. Interference enhancement (IE, Section 11.2.4) also fails to provide a unique answer if a single angle of incidence is analyzed. However, interference enhancement with multiple angles of incidence does provide a unique result for thickness and optical constants of a thin metal layer. Another method which provides a unique result is to combine spectroscopic ellipsometry (SE) data with

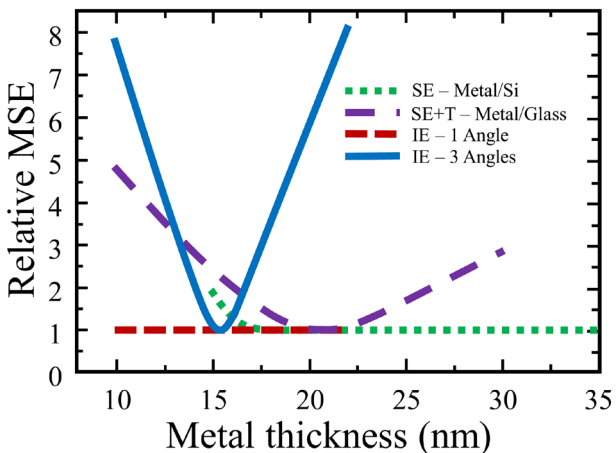


Figure 11.2. Comparison of methods for metal films is shown. Methods are successful if they provide a distinct MSE minimum for one thickness. The data are from different samples, which explains the different resulting thickness values.

intensity transmission data (SE + T, Section 11.2.3), as demonstrated for a metal layer on glass.

11.2.1 OPAQUE LAYER

One method to reduce the total number of sample properties is to measure an absorbing metal thick enough that no light can travel through the film. There is no longer sensitivity to the thickness and the measured Ψ and Δ can be directly used to determine the remaining unknowns: n and k . Of course, if determining layer thickness was the objective, this approach is not a direct solution. However, you can use the layer optical constants determined from the opaque metal to determine thickness of the thinner layers. This assumes that the optical constants for thinner layers will remain the same as the thicker opaque layers, which is not a very safe assumption for metals. The typical thickness where metals become opaque is around 50 to 100 nm.

11.2.2 OPTICAL CONSTANT PARAMETERIZATION

This method relies on a more efficient description of the n and k spectra by a dispersion equation. While this does reduce the number of fit parameters,

it does not reduce the number of unknown sample properties. The method can show some improvement to the overall problem, but is better when used in collaboration with other methods.

11.2.3 SE + TRANSMISSION

In this approach, the SE data is supplemented by a transmission intensity measurement as shown in Figure 11.3. The transmission intensity provides the extra data content to solve for all sample unknowns. However, this approach can only be used when the substrate is transparent and requires an accurate measure of the transmitted intensity over the same spectral range as the ellipsometry measurement.

11.2.4 INTERFERENCE ENHANCEMENT

This method has been developed extensively by McGahan, Johs, and Woollam [51]. In this approach, we actually make the sample more complicated (adding an additional layer) in order to gain the benefit of significant change in light interaction with the metal layer. The new layer must be a thick, transparent film—preferably between 100 nm and 1,000 nm. This produces new information content when the angle of incidence is changed, which then allows all sample unknowns to be determined—including the new layer thickness, as shown in Figure 11.4.

The drawback to this method is that an additional layer must be introduced into the sample processing. However, it really is the best approach when dealing with absorbing substrates, such as silicon wafers, where we can't access the transmission intensity data.

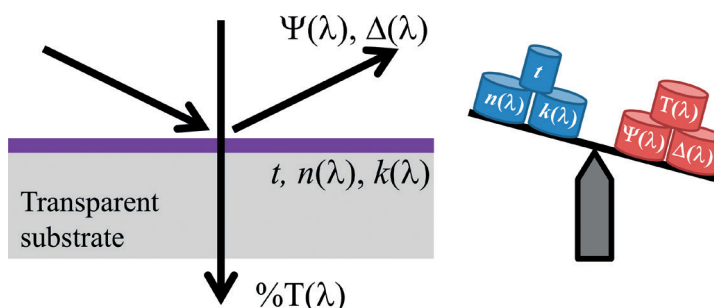


Figure 11.3. SE + T can be used to provide a unique solution for thickness and optical constants when the metal is deposited on a transparent substrate.

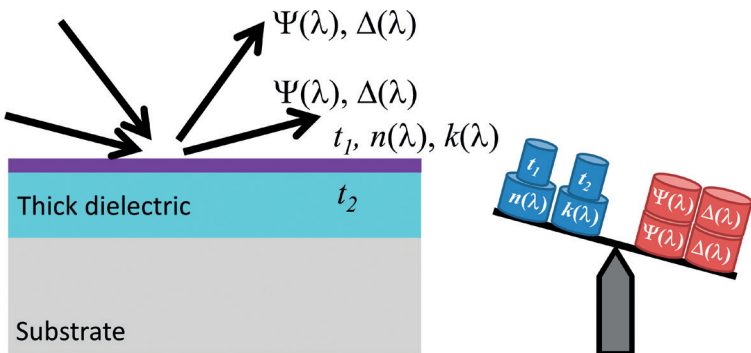


Figure 11.4. Interference enhancement method adds a thick transparent film below the metal to change the overall interaction of light with the metal layer for different angles of incidence. This can break the correlation and provide unique thickness and optical constants for the metal film.

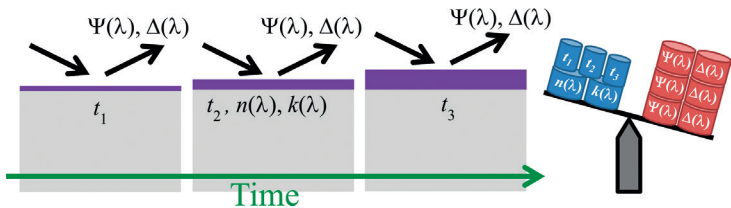


Figure 11.5. Multisample analysis, whether from multiple samples of varying thickness or directly from a dynamic measurement during film growth, can provide additional sample information to help solve for optical constants and each thickness.

11.2.5 MULTISAMPLE ANALYSIS OR IN SITU DATA

Multisample analysis has been developed extensively by Tompkins et al. [52], and in situ methods have been reviewed by Johs et al. [32] and Hilfiker [37]. Both multisample analysis and in situ measurements rely on a similar aspect to increase the data content. If we can measure multiple different thicknesses of the same material, we can use the additional measurement data to solve for all unknown sample properties. This is demonstrated in Figure 11.5 where three different film thicknesses are measured from the same material. While we now have three different thicknesses to determine, it is assumed that we only have one common set of optical constants that will describe all of the samples.

CHAPTER 12

MULTILAYER THIN FILM STACKS

There are many examples where multiple thin films are used in a stack and it is desired to determine the film properties without destroying the sample. Spectroscopic ellipsometry (SE) allows optical access to any and all layers that do not completely absorb the light. Thus, if we have a stack of transparent layers, the light will travel through all, returning to the surface with information from each of the various interfaces. This increases the complexity of our measured data, as the interference features depend on the dominating light components, which change on a wavelength-by-wavelength basis. For example, consider the ellipsometry spectra in Figure 12.1, which comes from a four-layer optical coating stack. The higher Ψ amplitude features occur when the interference is primarily due to the low-index film, while the lower Ψ amplitude features are due to the higher index layers in the stack. There is plenty of information contained in a multiangle SE measurement to determine all four layer thicknesses, along with the index for the two different transparent materials.

When some of the layers are absorbing, they will eliminate information from underlying layers. It is also common to have reduced sensitivity to layers that are lower in the stack than the films near the surface. Because of the increasing sample complexity and large possible number of unknown sample properties, there are two different methods of approach in order to simplify the data analysis. The first is to approach the layers one at a time. We will have two different strategies for dealing with this approach. The second method can be used when several of the layers in the stack have something in common. These methods could be called “coupling.”

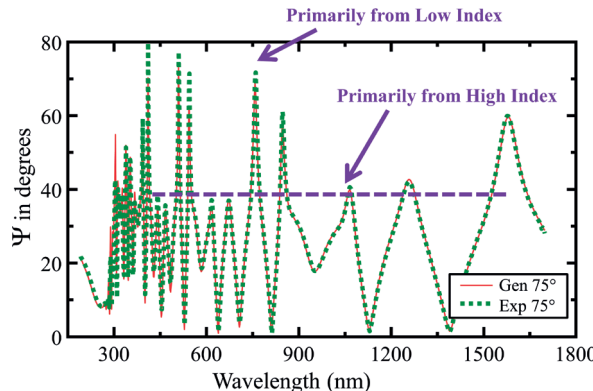


Figure 12.1. Measured spectra and model-generated fit from a four-layer optical coating stack consisting of high and low index dielectric layers.

12.1 MULTILAYER STRATEGIES

We consider four different strategies for multilayers. Each is designed to reduce the number of unknown parameters to provide unique fit results when tackling multilayer stacks. The four strategies include:

1. Divide and conquer
2. Consecutive layers
3. Coupled thicknesses
4. Coupled optical constants

The first strategy, which we have termed “Divide and conquer,” is all about getting information from single-layer films that can then be used when analyzing the multilayer structure. This is illustrated in Figure 12.2, where three single-layer films are first measured to determine their optical constants. Then, these optical constants can be fixed and only thicknesses for each layer needs to be determined when considering the multilayer.

One potential problem with “Divide and conquer” is that we hope the single-layer films will have the same optical constants when deposited directly on the substrate as they will within the multilayer stack. However, some layers are affected by the underlying material, which can cause changes in the film optical constants. In this case, “Consecutive Layers” may be preferred, where the stack is separated and measured after each layer is deposited, as shown in Figure 12.3.

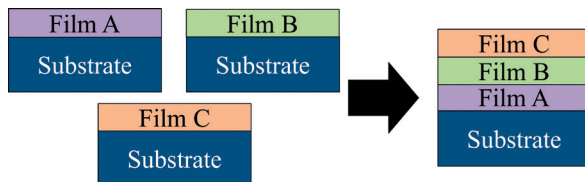


Figure 12.2. “Divide and conquer” approach to multilayer characterization is illustrated where the optical constants are first determined from single-layer films.

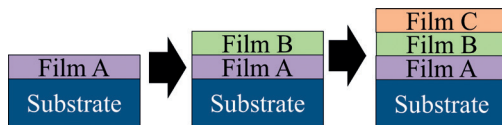


Figure 12.3. “Consecutive layers” approach to multilayers works by measuring each new layer as it is added to the overall stack.

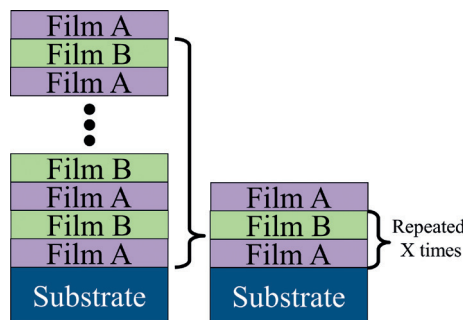


Figure 12.4. Consecutive films with the same thickness are simplified by using the same optical constants for each layer of the same material and assuming that the thickness for repeated layers that were designed and deposited is the same.

In addition to these two general approaches to divide up the layers and determine single layer optical constants, there are also approaches that involve the entire stack. Here, in a sample which might be called a “superlattice,” we can reduce the total number of unknowns by either coupling optical constants for “like” materials or coupling thicknesses. This is demonstrated in Figure 12.4 for a repeating stack structure with

two materials of repeated thicknesses. This method can still work to reduce unknown sample properties even when none of the layers repeat exact thicknesses. If we trust the deposition process to be stable, we may be able to couple different thicknesses using the ratio of time that was established to deposit each layer, at least for each different film type.

We now consider two examples of multilayer stacks.

12.2 EXAMPLE: TWO LAYER ORGANIC STACK, USING “DIVIDE AND CONQUER”

In this example, we have two organic layers on top of a silicon wafer. The underlying organic layer is used as a bottom antireflection coating layer, while the upper layer is a photoresist. As both layers are organic, their optical properties are quite similar at visible and near infrared wavelengths. In fact, if our spectroscopic ellipsometer was constrained to these wavelengths, there would not be adequate optical contrast to determine both layer thicknesses independently and we would only be able to assess the total stack thickness. However, the two organics are optically different in the ultraviolet, as shown in Figure 12.5, and we can use this spectral range to uniquely determine both layer thicknesses. In this case, we had previously determined each individual layer’s optical functions from single-layer coatings of the same material.

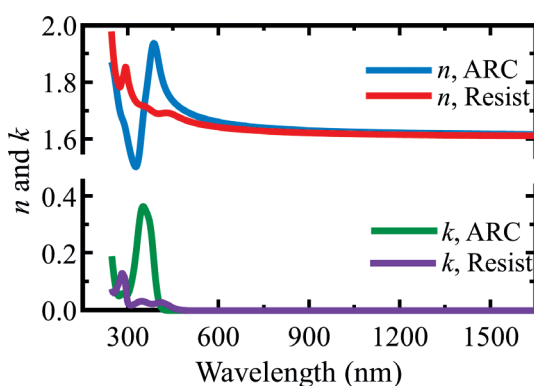


Figure 12.5. Optical functions for an antireflection coating and a photoresist, which are measured as a stack.

12.3 EXAMPLE: HIGH-LOW OPTICAL STACK, USING “COUPLING”

In this example, we consider a much more complicated multilayer stack consisting of high and low index coatings designed to enhance the reflection of light within a spectral window near 1,064 nm. The optical functions for both layers, shown in Figure 12.6, were determined from single-layer coatings and were modeled using dispersion equations. This allows the optical functions to be refined later if we are unable to fit the multilayer stack with only thicknesses.

The final multilayer consisted of 37 layers with a total thickness of over 4.5 μm with no two layer thicknesses the same. However, the deposition system is believed to be quite stable throughout this process, so we can significantly reduce the number of unknowns (37 thicknesses) by establishing ratios between each layer and the “base” layer for the high-index or low-index film. In this way, we are fitting only two thickness values that represent every layer thickness in the stack. Our results showed that while the high-index films were consistent with the designed thicknesses, the low-index films throughout the stack were about 2 percent thinner than designed. The Ψ spectra from two of our four total angles are shown in Figure 12.7. The measured spectra are significantly more complex due to all the interference features, which, with our model, requires an accurate description of all layers to reproduce.

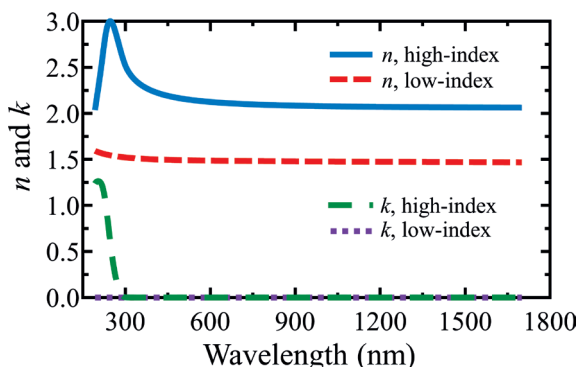


Figure 12.6. Optical functions for a high-index and a low-index film, which are used to construct a 37-layer optical coating stack.

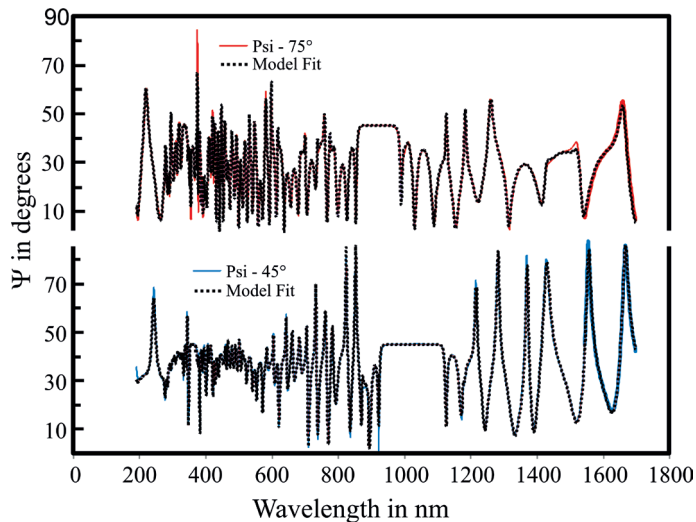


Figure 12.7. Measured spectra and corresponding model fits are shown from a 37-layer optical coating stack consisting of repeated high-index and low-index films.

REFERENCES

- [1] Azzam, R.M.A., and N.M. Bashara. 1977. *Ellipsometry and Polarized Light*. Amsterdam, Netherlands: Elsevier.
- [2] Röseler, A. 1990. *Infrared Spectroscopic Ellipsometry*. Berlin, Germany: Akademie-Verlag.
- [3] Tompkins, H.G. (1993) 2006. *A User's Guide to Ellipsometry*. Mineola, NY: Dover Publications. First edition published by Academic Press.
- [4] Tompkins, H.G., and W.A. McGahan. 1999. *Spectroscopic Ellipsometry and Reflectometry: A User's Guide*. New York: John Wiley & Sons, Inc.
- [5] Schubert, M. 2004. *Infrared Ellipsometry on Semiconductor Layer Structures: Phonons, Plasmons, and Polaritons*. Berlin, Germany: Springer.
- [6] Tompkins, H.G., and E.A. Irene, eds. 2005. *Handbook of Ellipsometry*. New York: William Andrew.
- [7] Fujiwara, H. 2007. *Spectroscopic Ellipsometry: Principles and Applications*. West Sussex, UK: John Wiley & Sons Inc.
- [8] Losurdo, M., and K. Hingerl, eds. 2013. *Ellipsometry at the Nanoscale*. Berlin, Germany: Springer-Verlag.
- [9] Hinrichs, K., and K.-J. Eichorn, eds. 2014. *Ellipsometry of Functional Organic Surfaces and Films*. Berlin, Germany: Springer-Verlag.
- [10] Boccara, A.C., C. Pickering, and J. Rivory, eds. January 11–14, 1993. “Proceedings of the 1st International Conference on Spectroscopic Ellipsometry.” In *Thin Solid Films*, Vols. 233–234. Paris, France.
- [11] Collins, R.W., D.E. Aspnes, and E.A. Irene, eds. 1998. “Proceedings of the Second International Conference on Spectroscopic Ellipsometry.” In *Thin Solid Films*, Vols. 313–314. May 12–15, 1997, Charleston, SC, USA.
- [12] Fried, M., K. Hingerl, and J. Humlíček, eds. 2004. “The 3rd International Conference on Spectroscopic Ellipsometry.” In *Thin Solid Films*, Vols. 455–456. July 6–11, 2003, Vienna, Austria.
- [13] Arwin, H., U. Beck, and M. Schubert, eds. 2008. “4th International Conference on Spectroscopic Ellipsometry.” In *Physica Status Solidi (a)*, Vol. 205, no. 4, pp. 709–948, (c), Vol. 5, pp. 1003–1442. June 11–15, 2007, Stockholm, Sweden: Weinheim: Wiley-VCH.
- [14] Tompkins, H.G., ed. 2011. “5th International Conference on Spectroscopic Ellipsometry—ICSE-V.” In *Thin Solid Films* 519. May 23–28, 2010, Albany, NY, USA.
- [15] Otani, Y., M. Tazawa, and S. Kawabata, eds. 2014. “6th International Conference on Spectroscopic Ellipsometry (ICSE-VI).” In *Thin Solid Films*, Vol. 571, Part 3. May 26–31, 2013, Kyoto, Japan.

- [16] Wooten, F. 1972. *Optical Properties of Solids*. New York: Academic Press.
- [17] Palik, E.D., ed. 1998. *Handbook of Optical Constants of Solids*. San Diego, CA: Academic Press.
- [18] Palik, E.D., ed. 1998. *Handbook of Optical Constants of Solids II*. San Diego, CA: Academic Press.
- [19] Palik, E.D., ed. 1998. *Handbook of Optical Constants of Solids III*. San Diego, CA: Academic Press.
- [20] Adachi, S. 1999. *Optical Constants of Crystalline and Amorphous Semiconductors*. Boston, MA: Kluwer Academic Publishers.
- [21] Yu, P.Y., and M. Cardona. 2010. *Fundamentals of Semiconductors: Physics and Materials Properties*. 4th ed. Berlin, Germany: Springer-Verlag.
- [22] Collins, R.W., I. An, and C. Chen. 2005. “Rotating Polarizer and Analyzer Ellipsometry.” In *Handbook of Ellipsometry*, eds. H.G. Tompkins and E.A. Irene. New York: William Andrew, pp. 329–429.
- [23] Collins, R.W., I. An, J. Lee, and J.A. Zapien. 2005. “Multichannel Ellipsometry.” In *Handbook of Ellipsometry*, eds. H.G. Tompkins and E.A. Irene. New York: William Andrew, pp. 481–564.
- [24] Jellison, G.E., Jr., and F.A. Modine. 2005. “Polarization Modulation Ellipsometry.” In *Handbook of Ellipsometry*, eds. H.G. Tompkins and E.A. Irene. Norwich, NY: William Andrew, pp. 433–479.
- [25] Chipman, R.A. 2010. “Polarimetry.” In *Handbook of Optics Volume I Geometrical and Physical Optics, Polarized Light, Components and Instruments*, eds. M. Bass and V.N. Mahajan. New York: McGraw Hill, pp. 15.1–46.
- [26] Born, M., and E. Wolf. 1999. *Principles of Optics*. 7th (expanded) ed. Cambridge, UK: Cambridge University Press.
- [27] Hecht, E. 2002. *Optics*. 4th ed. San Francisco, CA: Addison-Wesley.
- [28] Strong, J. 2004. *Concepts of Classical Optics*. Mineola, NY: Dover Publications.
- [29] Goldstein, D.H. 2011. *Polarized Light*. 3rd ed. Boca Raton, FL: CRC Press.
- [30] Woollam, J.A., B. Johs, C.M. Herzinger, J. Hilfiker, R. Synowicki, and C.L. Bungay. 1999. “Overview of Variable Angle Spectroscopic Ellipsometry (VASE), Part I: Basic Theory and Typical Applications.” In *SPIE Proceeding*, Vol. CR72, pp. 3–28.
- [31] Johs, B., J.A. Woollam, C.M. Herzinger, J. Hilfiker, R. Synowicki, and C.L. Bungay. 1999. “Overview of Variable Angle Spectroscopic Ellipsometry (VASE), Part II: Advanced Applications.” In *SPIE Proceeding*, Vol. CR72, pp. 29–58.
- [32] Johs, B., J. Hale, N.J. Ianno, C.M. Herzinger, T. Tiwald, and J.A. Woollam. 2001. “Recent Developments in Spectroscopic Ellipsometry for in Situ Applications.” In *SPIE Proceeding*, Vol. 4449, pp. 41–57.
- [33] Synowicki, R.A. 2008. “Suppression of Backside Reflections from Transparent Substrates.” *Physica Status Solidi (a)* 205, no. 4, pp. 1085–88.

- [34] Hilfiker, J.N., N. Singh, T. Tiwald, D. Convey, S.M. Smith, J.H. Baker, and H.G. Tompkins. 2008. “Survey of Methods to Characterize Thin Absorbing Films with Spectroscopic Ellipsometry.” *Thin Solid Films* 516, no. 22, pp. 7979–89. doi: <http://dx.doi.org/10.1016/j.tsf.2008.04.060>
- [35] Hilfiker, J.N., R.A. Synowicki, and H.G. Tompkins. April 2008. “Spectroscopic Ellipsometry Methods for Thin Absorbing Coatings.” *SVC Proceeding*, pp. 511–16.
- [36] Langereis, E., S.B.S. Heil, H.C.M. Knoops, W. Keuning, M.C.M. van de Sanden, and W.M.M. Kessels. 2009. “In Situ Spectroscopic Ellipsometry as a Versatile Tool for Studying Atomic Layer Deposition.” *Journal of Physics D: Applied Physics* 42, no. 7, p. 073001. doi: <http://dx.doi.org/10.1088/0022-3727/42/7/073001>
- [37] Hilfiker, J.N. 2011. ‘In Situ Spectroscopic Ellipsometry (SE) for Characterization of Thin Film Growth.’ In *In Situ Characterization of Thin Film Growth*, eds. G. Koster and G. Rijnders. Cambridge: Woodhead Publishing, pp. 99–151.
- [38] Darrigol, O. 2012. *A History of Optics from Greek Antiquity to the Nineteenth Century*. Oxford, UK: Oxford University Press.
- [39] Andriesse, C.D. 2005. *Huygens: The Man Behind the Principle*. Cambridge: Cambridge University Press.
- [40] Humlicek, J. 2005. “Polarized Light and Ellipsometry.” In *Handbook of Ellipsometry*, eds. H.G. Tompkins and E.A. Irene. New York: William Andrew, pp. 1–90.
- [41] Jellison, G.E., Jr. 2005. “Data Analysis for Spectroscopic Ellipsometry.” In *Handbook of Ellipsometry*, eds. H.G. Tompkins and E.A. Irene. New York: William Andrew, pp. 237–294.
- [42] Hamamatsu Photonics Catalog: Photomultiplier Tubes. 2000. http://www.chem.ucla.edu/~craigim/pdfmanuals/catalogs/Hamamatsu_PMT_Catalog-Handbook.pdf
- [43] Herzinger, C.M., B. Johs, W.A. McGahan, and J.A. Woollam. 1998. “Ellipsometric Determination of Optical Constants for Silicon and Thermally Grown Silicon Dioxide via a Multi-Sample, Multi-Wavelength, Multi-Angle Investigation.” *Journal of Applied Physics* 83, no. 6, pp. 3323–36. doi: <http://dx.doi.org/10.1063/1.367101>
- [44] Tompkins, H.G., J. Baker, and D. Convey. 2000. “Effect of Process Parameters on the Optical Constants of Thin Metal Films.” *Surface and Interface Analysis* 29, no. 3, pp. 227–31. doi: [http://dx.doi.org/10.1002/\(sici\)1096-9918\(200003\)29:3%3C227::aid-sia730%3E3.0.co;2-w](http://dx.doi.org/10.1002/(sici)1096-9918(200003)29:3%3C227::aid-sia730%3E3.0.co;2-w)
- [45] Urbach, F. 1953. “The Long-Wavelength Edge of Photographic Sensitivity and of the Electronic Absorption of Solids.” *Physical Review*, 92.
- [46] Wooten, F. 1972. *Optical Properties of Solids*. New York: Academic Press.
- [47] Collins, R.W., and A.S. Ferlauto. 2005. “Optical Physics of Materials.” In *Handbook of Ellipsometry*, eds. H.G. Tompkins and E.A. Irene. Norwich, NY: William Andrew, pp. 93–233.

- [48] Jellison, G.E., Jr., and F.A. Modine. 1996. “Parameterization of the Optical Functions of Amorphous Materials in the Interband Region.” *Applied Physics Letters* 69, p. 371. Erratum, *Applied Physics Letters* 69, p. 2137.
- [49] Johs, B., and J.S. Hale. 2008. “Dielectric Function Representation by B-Splines.” *Physica Status Solidi (a)* 205, no. 4, pp. 715–19. doi: <http://dx.doi.org/10.1002/pssa.200777754>
- [50] Aspnes, D.E., J.B. Theeten, and F. Hottier. 1979. “Investigation of Effective-Medium Models of Microscopic Surface Roughness by Spectroscopic Ellipsometry.” *Physical Review B* 20, no. 8, pp. 3292–302. doi: <http://dx.doi.org/10.1103/physrevb.20.3292>
- [51] McGahan, W.A., B. Johs, and J.A. Woollam. 1993. “Techniques for ellipsometric measurement of the thickness and optical constants of thin absorbing films.” *Thin Solid Films* 234, pp. 443–446.
- [52] Tompkins, H.G., S. Tasic, J. Baker, and D. Convey. 2000. “Spectroscopic Ellipsometry Measurements of Thin Metal Films.” *Surface and Interface Analysis* 29, no. 3, pp. 179–87. doi: [http://dx.doi.org/10.1002/\(sici\)1096-9918\(200003\)29:3%3C179::aid-sia701%3E3.0.co;2-0](http://dx.doi.org/10.1002/(sici)1096-9918(200003)29:3%3C179::aid-sia701%3E3.0.co;2-0)

INDEX

A

Absorbing films
challenges, 139
interference enhancement, 140,
142–143
methods, 140
multisample analysis/in situ data,
143
opaque layer, 141
optical constant
parameterization, 141–142
SE + transmission, 142
Absorption coefficient, 12
Angles of incidence, 45–57
Anomalous dispersion, 75

B

Basis-spline (B-spline), 84–87
Brewster angle, 20–24, 45–46
Brewster, David, 6
Broadband light, 33

C

Cauchy dispersion
equation, 75
dielectric materials, 76–78
fitting data, 105–107
transparent wavelengths, 75–76
UV absorption, 76–78
Characteristic Depth, 12–13
Circularly polarized light, 16–17
Compensators, 42–44
Complex dielectric function, 13

Complex refractive index, 10–13
Constructive interference, 9–10,
65–66

D

Data regression analysis process,
95
Delta, 27–28, 57
Destructive interference, 9–10, 66
Detectors, 34–35
Dielectric function, *See* Complex
dielectric function
Dielectrics
Substrates, 59–61
Films, 65–68, 101–112
Dispersion equation
anomalous dispersion, 75
Cauchy dispersion equation,
75–78
b-spline, 84–87
Gaussian, 80–84
Kramers-Kronig relation, 82–84
Lorentz, 80–81
oscillator models, 79–84
Tauc-Lorentz, 81–82, 134
normal dispersion, 74–75

E

Effective medium approximation
(EMA), 116
Electromagnetic wave
electric vibration, 5
interference, 9–10

- Maxwell's equations, 5, 7
 photon energy, 8–9
 wave equation, 7
 wavelength and frequency, 8–9
- E**
Ellipsometry
 Equations, 27–30
 historical aspects, 1
 Instrumentation, *See*
 Spectroscopic Ellipsometers
Parameters
 N, C, & S, 29
 Psi and Delta, 28
 spectra. *See* Spectrum
Elliptically polarized light, 17–18
EMA. *See* Effective medium approximations
Extinction coefficient, 11–12
- F**
Fitting Data, 92–96
Fourier coefficients, 50, 53
Fourier transform infrared (FTIR) spectroscopy, 37
Fresnel, Augustin-Jean, 6
Fresnel Equations, 19–20
- G**
Gaussian oscillator, 80–84
Gratings, 35
- I**
Index of refraction, 10–13
Infrared ellipsometers, 37
In situ ellipsometry, 47, 143
Intensity, 8
Interference, 9–10, 65–66
Interference Enhancement, 140, 142–143
- J**
Jones matrixes, 29–30
- K**
Kramers-Kronig (KK) consistency, 75
- L**
Laws of reflection, 14
Laws of refraction, 14
Light
 polarized light, 14–18
 reflectance and transmittance, 20, 26–27
 reflection and refraction, 14
 reflection and transmission
 Brewster angle, 20–24
 equations of Fresnel, 19–20
 Interaction with films, 18–30
 orientation, 18–19
 Stack calculations, 26
Light Source, 33
Linearly polarized light, 15–16
Lorentz oscillator, 80–81
- M**
Macroscopic roughness, 113–114
Maxwell's equation, 5, 7
Mean-squared-error (MSE), 95, 96
Metals
 Substrates, 61–63
 Films, 139–143
Microscopic roughness, 114–115
Model, 94
Monochromator, 35–36
Mueller matrixes, 30
Multi-sample analysis, 143
Multilayers, 145–150
- N**
N, C, & S, 29, 48–49
Normal dispersion, 74–75
- O**
Opaque layer, 141
Optical constant
 complex refractive index, 10–13
 complex dielectric function, 13
Optical constant parameterization, 141–142

- Optical data analysis
data analysis
“fit” parameters, 95–96
“inverse” problem, 91–92
evaluation, 97–100
measurement, 93–94
model, 94–95
SE data analysis, 93
- Pseudo-optical constants, 89–91
- Optical functions
- B-spline
 - KK consistent, 87
 - spline components, 85
 - dispersion equation
 - anomalous dispersion, 75
 - Cauchy dispersion equation, 75–78
 - Gaussian, 80–84
 - Kramers-Kronig relation, 82–84
 - Lorentz, 80–81
 - normal dispersion, 74–75
 - Oscillator Models, *See* Oscillator models
 - tabulated list, 71–73
- Oscillator models
- Gaussian oscillator, 80–84
 - Kramers-Kronig relationship, 82–84
 - Lorentz oscillator, 80–81
 - mechanical system, 79
 - Tauc-Lorentz oscillator, 81–82, 134
 - transparent and absorbing materials, 80
- P**
- Phase modulation ellipsometry (PME), 54–55
- Phenyl-C₆₁-butyric acid methyl ester (PCBM) thin film, 86
- Photon energy, 8–9
- PME. *See* Phase modulation ellipsometry
- Polarization state generator and detector (PSG/PSD), 32
- Polarization, manipulation
- reflection, 37–38
 - refraction, 39
 - total internal reflection, 38–39
 - transmission and absorption, 39–40
- Polarized light
- circularly, 16–17
 - elliptically, 17–18
 - linearly, 15–16
 - polarization, 15
 - unpolarized light, 15
- Polarizers, 40–41
- Prisms, 35
- Psi, 27–28, 57
- Pseudo-optical constants, 89–91
- PSG/PSD. *See* Polarization state generator and detector
- R**
- RCE. *See* Rotating compensator ellipsometry
- RPE/RAE. *See* rotating polarizer/ analyzer ellipsometry
- Refraction, 14
- Refractive Index, *See* Complex Refractive Index
- Reflectance and transmittance, 26
- Reflection and transmission
- Brewster angle, 20–24
 - equations of Fresnel, 19–20
 - Laws of, 14, 19–25
 - orientation, 18–19
 - Stack calculations, 26
 - with films, 25–26
- Rotating compensator ellipsometry (RCE), 51–53
- Rotating polarizer/analyzer ellipsometry (RPE/RAE), 49–51
- Roughness
- effective medium approximations, 116

- macroscopic, 113–114
 microscopic, 114–115
 rough film, 116–117
- RPE/RAE. *See* Rotating polarizer/analyzer ellipsometry
- S**
- Semiconductors
 Substrates, 63–65
 Films, 127, 134–136
- Semiconductor on insulator (SOI), 91, 92
- Silicon nitride film, 124
- Single-wavelength ellipsometry, 121
- SOI. *See* Semiconductor on insulator
- Source, *See* Light Source
- Spectroscopic ellipsometer
 compensators, 42–44
 detectors, 34–35
 dual rotating instruments, 53–54
 measurement angle
 angle errors, 45
 Brewster angle, 45
 Ex situ, 46–47
 In situ, 47–48
 measurement capabilities, 48–49
 phase modulation ellipsometry, 54–55
 phase modulators, 44–45
 polarization
 reflection, 37–38
 refraction, 39
 total internal reflection, 38–39
 transmission and absorption, 39–40
 polarization state generator and detector, 32
- polarizers, 40–41
- rotating compensator ellipsometry, 51–53
- rotating polarizer/analyzer ellipsometry (RPE/RAE), 49–51
- sources, 33–34
- spectrometers, monochromators, and interferometers, 35–37
- Spectrum**
 dielectric substrates, 59–61
 metal substrates, 61–63
 semiconductor substrates, 63–65
 single interface, 58
 thin films, absorbing spectral regions, 68–70
- transparent thin films
 constructive interference, 65
 destructive interference, 66
 oscillations, 65
 reflection of light, 65
 Ψ fluctuation, 67–68
 Ψ spectrum, 66
- T**
- Tauc-Lorentz oscillator, 81, 82
- Thermal oxide film optical constants, 124
- Thin films
 absorbing region models
 b-spline fit, 132–133, 135
 direct fit, 131–132, 135
 oscillator model fit, 133–135
 amorphous silicon film, on glass, 134, 136
 multilayer strategies
 “divide and conquer” approach, 147, 148
 coupling, 149–150
 optical constant determination
 mean squared error, 124
 nitride model, 126
 SE wavelength, 122
 silicon nitride film, 124
 single-wavelength ellipsometry, 121
 thermal oxide film optical constants, 124
 $\Psi\Delta$ trajectories, 122–123
- photoresist, on Si, 137–138
- thickness determination, known optical functions, 119–120

- transparent wavelength region, 129–130
- Total internal reflection (TIR), 43
- Transparent thin films
- data features of, 102–103
 - dielectric SiN_x film, on Si, 108–110
 - dielectric SiO_2 film, on glass, 110–112
- fitting with known index, 104–105
- fitting with unknown index
- film thickness estimation, 107
 - index estimation, 106–107
 - thickness and refractive index, 107
- W**
- Wave equation, 7
- Y**
- Young, Thomas, 6

OTHER TITLES IN OUR MATERIALS CHARACTERIZATION AND ANALYSIS COLLECTION

C. Richard Brundle, *Editor*

*Auger Electron Spectroscopy: Practical Application to Materials Analysis
and Characterization of Surfaces, Interfaces, and Thin Films*
by John Wolstenholme

A Practical Guide to Transmission Electron Microscopy: Fundamentals
by Zhiping Luo

*Secondary Ion Mass Spectrometry: Applications for Depth Profiling and
Surface Characterization* by Fred A. Stevie

Momentum Press is one of the leading book publishers in the field of engineering, mathematics, health, and applied sciences. Momentum Press offers over 30 collections, including Aerospace, Biomedical, Civil, Environmental, Nanomaterials, Geotechnical, and many others.

Momentum Press is actively seeking collection editors as well as authors. For more information about becoming an MP author or collection editor, please visit
<http://www.momentumpress.net/contact>

Announcing Digital Content Crafted by Librarians

Momentum Press offers digital content as authoritative treatments of advanced engineering topics by leaders in their field. Hosted on ebrary, MP provides practitioners, researchers, faculty, and students in engineering, science, and industry with innovative electronic content in sensors and controls engineering, advanced energy engineering, manufacturing, and materials science.

Momentum Press offers library-friendly terms:

- perpetual access for a one-time fee
- no subscriptions or access fees required
- unlimited concurrent usage permitted
- downloadable PDFs provided
- free MARC records included
- free trials

The **Momentum Press** digital library is very affordable, with no obligation to buy in future years.

For more information, please visit www.momentumpress.net/library or to set up a trial in the US, please contact mpsales@globalepress.com.

EBOOKS FOR THE ENGINEERING LIBRARY

*Create your own
Customized Content
Bundle — the more
books you buy,
the higher your
discount!*

THE CONTENT

- Manufacturing Engineering
- Mechanical & Chemical Engineering
- Materials Science & Engineering
- Civil & Environmental Engineering
- Electrical Engineering

THE TERMS

- Perpetual access for a one time fee
- No subscriptions or access fees
- Unlimited concurrent usage
- Downloadable PDFs
- Free MARC records

For further information, a free trial, or to order, contact:
sales@momentumpress.net



**MOMENTUM PRESS
ENGINEERING**

Spectroscopic Ellipsometry Practical Application to Thin Film Characterization

Harland G. Tompkins • James N. Hilfiker

Ellipsometry is an experimental technique for determining the thickness and optical properties of thin films. It is ideally suited for films ranging in thickness from sub-nanometer to several microns. Spectroscopic measurements have greatly expanded the capabilities of this technique and introduced its use into all areas where thin films are found: semiconductor devices, flat panel and mobile displays, optical coating stacks, biological and medical coatings, protective layers, and more.

While several scholarly books exist on the topic, this book provides a good introduction to the basic theory of the technique and its common applications. The target audience is not the ellipsometry scholar, but process engineers and students of materials science who are experts in their own fields and wish to use ellipsometry to measure thin film properties without becoming an expert in ellipsometry itself.

Harland G. Tompkins received his BS in physics from the University of Missouri and his PhD in physics from the University of Wisconsin–Milwaukee. He is a consultant for the J. A. Woollam Company in Lincoln, NE, as well as for other companies. He has written numerous journal articles in the reviewed technical literature, is the author of four books, and has edited two books.

James N. Hilfiker graduated from the Electrical Engineering Department of the University of Nebraska, where he studied under Professor John Woollam. He joined the J.A. Woollam Company upon graduation and has worked in their applications lab for 20 years. His research at the J.A. Woollam Company has focused on new applications of ellipsometry, including characterization of anisotropic materials, liquid crystal films, and, more recently, thin film photovoltaics. He has authored over 40 technical articles involving ellipsometry.

